# ELECTROMAGNETIC CRIMPING OF TERMINAL-WIRE INTERCONNECTIONS

A Thesis Submitted in Partial Fulfillment of the Requirements

for the Degree of

**DOCTOR OF PHILOSOPHY**

Submitted by

**Ashish Kumar Rajak**

**(Roll No. 136103016)**


Department of Mechanical Engineering

Indian Institute of Technology Guwahati

Guwahati – 781039, India

**March 2018**

Department of Mechanical Engineering,
Indian Institute of Technology Guwahati,
Guwahati – 781039,
India

# Declaration

I hereby certify that the information presented in the dissertation "**Electromagnetic Crimping of Terminal-Wire Interconnections**" is entirely my own account of research performed under the guidance of Dr. Sachin D. Kore. Any part of this work has not earlier been submitted for the award of any degree, diploma, associate-ship, fellowship or its equivalent to any University or Institution. I have not violated any copyright and plagiarism law. All text and figures are my own.

28-03-2018

**Ashish Kumar Rajak**
Roll No. 136103016
Department of Mechanical Engineering,
Indian Institute of Technology Guwahati,
Guwahati – 781039,
India

Department of Mechanical Engineering,
Indian Institute of Technology Guwahati,
Guwahati – 781039,
India

# Certificate

It is certified that the work contained in this thesis entitled "**Electromagnetic Crimping of Terminal-Wire Interconnections**" submitted by **Mr. Ashish Kumar Rajak** to the Indian Institute of Technology Guwahati for the award of the degree of Doctor of Philosophy has been carried out under my supervision in the Department of Mechanical Engineering, Indian Institute of Technology Guwahati. This work has not been submitted elsewhere for the award of any other degree or diploma.

28-03-2018

(**Dr. Sachin D. Kore**)
**Associate Professor**
Department of Mechanical Engineering,
Indian Institute of Technology Guwahati,
Guwahati – 781039,
India

To my parents

For their love, support, and patience.

# Acknowledgments

I would like to express my sincere gratitude towards many people who have helped me during the tenure of my Ph.D. work at IIT Guwahati. I take this opportunity to express my sincere appreciation to all of them for their support and help during various phases of my doctoral research work.

I wish to express my deepest gratitude to my supervisor, Dr. Sachin D. Kore for his valuable guidance, inspiration, and advice. I feel very privileged to have had the opportunity to learn from and work with him. I have been fortunate to have such advisor who gave me the freedom to explore on my own and at the same time the guidance to recover when my steps faltered. I would like to thank my doctoral committee members, Prof. S. Kanagaraj, Dr. S. N. Joshi and Prof. P. Roy Paily for their valuable suggestions and encouragement during the period of my research work.

I also like to express my heartful gratitude to the Director, the Deans Academic, Research and Development section, and other management of IIT Guwahati whose collective efforts has made this institute a place for world-class studies and education. I am thankful to all faculty and staff of Dept. of Mechanical Engineering for extending their co-operation regarding technical and official support for the successful completion of my research work.

I am thankful to my seniors Dr. Chandrahas Patel, J. K Doley, Vinod Yadav, Satish Kumar and Sibaji Garg for supporting and motivating to overcome any problems either in work and otherwise. I express my sincere thanks to my labmates Ramesh Kumar, Piyush Singh, Sagar Pawar, Getu Tilahun, Avnish Tiwari and Arpit Nagoi.

More important I want to thanks my best friends with whom I felt like home in a hostel for the past four years especially Tushar Semwal, Sunil Singh, Vishal Agrawal, Sonia Sharma, Shekhar Singh, Abhisekh Yadav, Manish Kushwaha, Kamlesh Birla, Yogendra Thakur, and Bidur for their unconditional love and support throughout my tenure. I want to thank Woldey G, Arvind Agarwal, Manish Dubey, Sundarlal Sanasam, Devarshi Kashyap, Hirak Basumatary and many other for making my life a memorable one at IIT Guwahati.

Most importantly, none of this would have been possible without the love and patience of my family. I want to thank my parents, brother, sister and jiju for being a constant source of love, concern, support and strength all these years.
Finally, I bow my head to the God almighty in deepest gratitude and seek blessings.

**Ashish Kumar Rajak**

# Abstract

Crimping of the terminal to wire strand is a crucial process for electrical power transmission connections. Poor crimping technique increases the resistance of current flow through terminal causing problems like power losses, spark, and heating in the joint. To overcome these problems caused by conventional crimping process a new method has been proposed using Electro-Magnetic (EM) forming process. The EM crimping process is a high-velocity metal crimping technique suitable for aluminum material as it increases its formability. EM crimping makes use of current pulse discharged from the capacitor, which passes through the coil generating very high EM force for the workpiece deformation. Initial experiments were carried out on finding the feasibility of electromagnetic terminal-wire crimping process and compared it with conventional terminal-wire crimping process. Work was extended to numerical and experimental approach. Numerical simulations were carried out on aluminum terminal over aluminum wire strands using three different types of helical coil cross-sections (CS) like circular, rectangular and trapezoidal, consisting of five number of turns. For the comparison CS area of the coil, and length was kept constant. Experiments were carried out using optimized value of discharge voltages to find the most suitable coil among the three coils for an effective crimping. Besides directly acting compression coils, field shapers are suitable tools for the manufacturing of electromagnetically crimped connections. A field-shaper is typically an axisymmetric component machined of an electrically conductive material in which the current density and the resulting field strength increases. Overall, the coil lifetime can be increased by a field-shaper since the mechanical loading of the coil can be significantly reduced. Also, the force between the field-shaper and the workpiece are considerably higher than the forces acting between field-shaper and the tool coil. So numerical and experiments were carried out on three different types of field-shapers (single step, double step, and tapered geometry) to find the most efficient field-shaper by varying discharge voltage. Tests like radial deformation, pull out, hardness over the CS and terminal surface, the contact resistance were carried over the crimped samples. Post-processing reveals that in a helical coil, trapezoidal CS geometry gives the maximum deformation as compared to rectangular and circular CS coil. While in field shapers, single step field-shaper was found to be more optimal design over double step and tapered field shaper, giving a uniform and higher deformation on the same discharge energy.

# List of Abbreviations and Symbols

**Abbreviations**

| | |
|---|---|
| CS | Cross-Section |
| EM | Electro-Magnetic |
| EMF | Electro-Magnetic Forming |
| FEM | Finite Element Method |
| BEM | Boundary Element Method |
| FS | Field-Shaper |
| SOD | Stand Off Distance |
| J-C | Johnson-Cook |

**Latin symbols**

| | |
|---|---|
| A | Johnson-Cook coefficient (Material constants- governing strength) |
| B | Johnson-Cook coefficient (Material constants-pre exponential factor) |
| $B_m$ | Magnetic field density |
| $B_1$ $B_2$ $B_3$ | Position of magnetic field in case of field shapers |
| C | Johnson-Cook coefficient (Material constants- strain rate factor) |
| $C_c$ | Capacitance of the circuit |
| d | Lattice spacing |
| $E_{mech}$ | Mechanical energy from discharge circuit |
| E(t) | Stored energy inside the capacitor |
| F | Load vector |
| $f$ | Lorentz force |
| $h$ | Airgap between the field shaper and workpiece |
| H | Magnetic field intensity |
| $H_r$ | Heat dissipation |
| T | Temperature |
| $i_t$ | Total current |
| $i_1$ | Current in the end zone |
| $i_2$ | Current in the working zone |
| $i_t$ | Total Current |
| $i_d$ | Double step field shaper current |
| $i_s$ | Single step field shaper current |
| $i_t$ | Tapered field shaper current |
| $I_1$ | Current passing through the forming machine |
| $I_2$ | Current induced over the workpiece |
| J | Total current density |
| $J_s$ | Source current density |
| $l$ | Coil length |
| $l_w$ | Length of the working zone |
| L | Inductance of the circuit |
| $L_1$ | Inductance of the coil attached |
| $L_2$ | Inductance of the workpiece |

| | |
|---|---|
| $L_c$ | Inductance of forming machine |
| $L_e$ | Equivalent system inductance |
| M | Mutual inductance |
| n | Strain hardening coefficient |
| N | Number of turns |
| P | Magnetic pressure |
| $r_w$ | Radius of the workpiece |
| R | Resistance of the circuit |
| $R_1$ | Resistance of the coil attached |
| $R_2$ | Resistance of the workpiece |
| $R_c$ | Resistance of forming machine |
| $R_e$ | Equivalent system resistance |
| $T_m$ | Melting temperature |
| $T_r$ | Room temperature |
| U(t) | Charging voltage over time |

**Greek symbols**

| | |
|---|---|
| $\beta_d$ | Damping coefficient |
| $\delta$ | Skin depth |
| $\sigma$ | Electrical conductivity |
| $\mu$ | Magnetic permeability in vacuum |
| $\mu_r$ | Relative permeability |
| $\omega$ | Current frequency |
| $\lambda$ | Wavelength |
| $\kappa$ | Williamson Hall constant |
| $\theta$ | Diffraction angle |
| $\beta$ | Peak width |
| $\eta$ | Strain induced |
| $\sigma$ | Stress |
| $\propto$ | Thermal coefficient |
| $\varepsilon$ | Plastic strain |
| $\dot{\varepsilon}$ | Plastic strain rate |
| $\varepsilon_e$ | Electrical permittivity |
| $\rho$ | Total charge density |
| $\emptyset$ | Electric scalar potential |
| $\Gamma$ | Surface of the coil |
| $\Gamma_c$ | Region of coil connected to external current supply |
| $\gamma$ | Slope angle of field shaper |

# Contents

# List of Figures

# List of Tables

# Chapter 1

## 1 Introduction

### 1.1 Terminal–Wire Crimping

Terminal-wire crimping is a process where the cable is stripped, and the strands of wire are placed into a metal terminal. The terminal is then compressed around the wire strands to ensure good electrical connectivity and mechanical strength across joints as shown in Figure 1.1. Crimping of wires to achieve a durable joint is one of the most critical challenges for electricity boards, automobiles, aviation, satellite, and communication. Modern automobiles contain several thousand crimp joints (Bergmann et al., 2013).

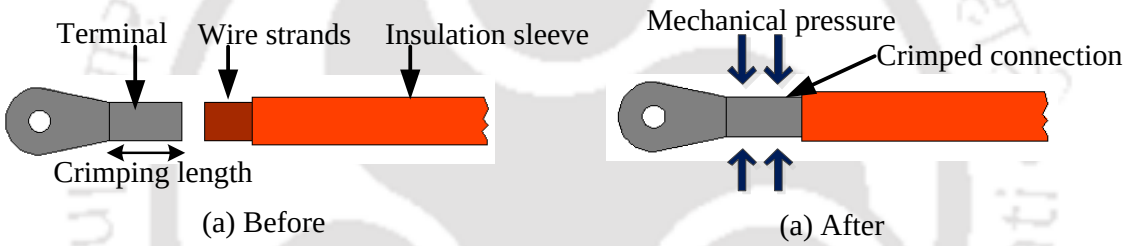


Figure 1.1 Illustration of an electrical crimp connection

There is a vast range of terminal crimping tools available to the industrial user. Still, producing a reliable, efficient, and long-lasting joint is a major challenge. Terminal-wire crimping machines are classified into three types, which are manual crimping tool, battery-powered tool and hydraulic tool as shown in Figure 1.2.

**a. Manual crimping tool**

Handheld tools are portable, inexpensive, and efficient. They typically have interchangeable die-sets. In manual crimping process, the wires are placed inside the terminal and squeezed with the help of lever mechanism manually. The manual crimping tool is a most widely used crimping tool for compression of the aluminium terminal.

**b. Battery powered tool**

To achieve a consistent crimping force over the terminal, battery-powered crimping tools are preferred. Battery powered tool uses an electronic control with lock function to

monitor complete compression of the terminal and retracting of the dies when the crimping is complete. It is ergonomically designed to reduce operator fatigue for use at the bench, on the line or in the field.

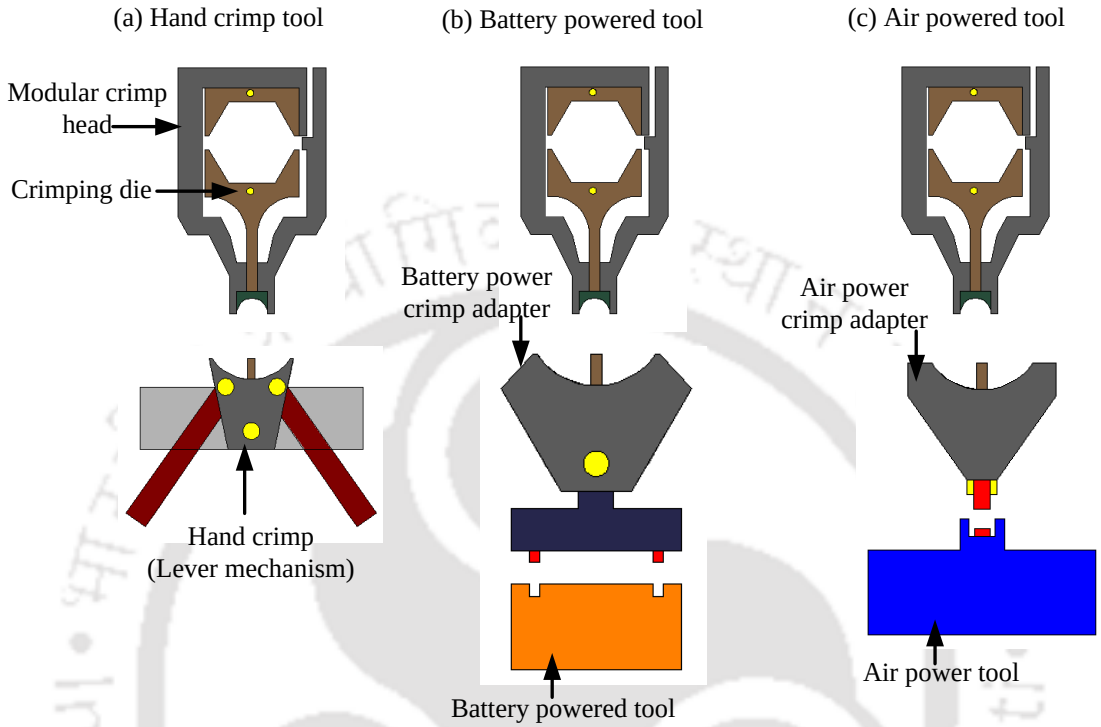


Figure 1.2 Different type of terminal-wire crimping tools

### c. Air powered tool

Mostly these tools are used to crimp on site, to achieve better output. Air powered tool can produce number of connections compared to manual and battery powered tool, but is expensive and require a careful handling to avoid leakage issues. Like battery powered tool it also has a manual return that brings the dies back to starting position by making use of pneumatic pressure. Careful adjustment of pressure is essential in the pneumatic crimping tool as less pressure leads to reduced deformation of the terminal while excessive pressure leads to over compression of terminal leading to cracks and failure of terminals.

Crimped terminals are exposed to various types of vibrations, different electrical environment, temperature gradient and the least concerned area even though most of the 60 % electrical failures take place in connector junctions (Gissila, 2013). Compression of the terminal over the wire strands using conventional crimping tool deteriorates the

material due to relaxation or partial release. Crimping of larger diameter terminals is always a problem due to spring back of material in industries when carried out using conventional crimping tool due to reduced strength and poor surface finish, which results in damaging and making cracks in crimp terminals (Rhodes, 1946). To overcome these problems caused by conventional crimping process a new contactless method has been proposed in this thesis using high strain rate Electromagnetic (EM) forming process. In comparison to other widely used joining techniques, like conventional mechanical crimping, EM crimping shows interesting characteristics which result in uniform forming pressure distribution (Weddeling et al., 2015). The advantage of EM process also includes no contact, low mould cost, no lubrication and less spring back making it a highly suitable tool for materials that are difficult to form (Psyk et al., 2011).

## 1.2 High Strain-Rate Metal Forming Process

Compared to the conventional metal forming process, high strain rate metal forming process are different as the workpiece is accelerated to a very high kinetic energy, resulting in plastic deformation of the material. Typically, a strain rate of $10^3$ $s^{-1}$ is achieved in this kind of processes. Some examples where high strain rate forming process are achieved are explosive forming, electrohydraulic forming, and EM forming. Due to the increased formability and reduced spring-back phenomena, in recent years, these methods are getting adapted in the industries.

### a. Explosive forming

The explosive metal forming process is a high strain rate forming process used since last 100 years, in which chemical energy of explosives is used. Specially used for the manufacturing of aerospace components like complex corrugated panels, exhaust tubes of engines and fuel filters. In this process, the explosive is placed at some standoff distance from the workpiece as shown in Figure 1.3. Shock waves of very high-intensity pressure waves are generated and strike the workpiece. The deformed workpiece takes the shape of the die. Some commonly used explosives are trinitrotoluene, cyclonite, and pentolite. Explosive forming requires long setup preparation time, and it is suitable for the production of unique, low volume products (Hustad and Lindland, 2014).

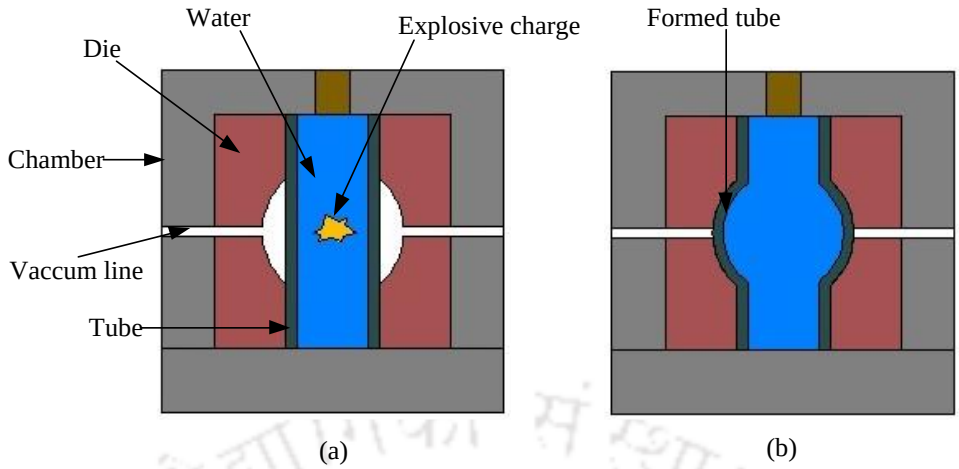


Figure 1.3 Explosive forming process

**b. Electrohydraulic forming**

The electrohydraulic forming process is a complicated process in which a very high voltage electric current is passed through a liquid. Electrical energy stored in a capacitor bank is rapidly discharged through the electrode in a liquid filled chamber, in which a high-temperature plasma channel is generated between the tips of the electrode (Gillard et al., 2013). The shockwave inside the liquid is initiated and propagate towards the tube at a high velocity, which deforms the tube into the shape of the die as shown in Figure 1.4.

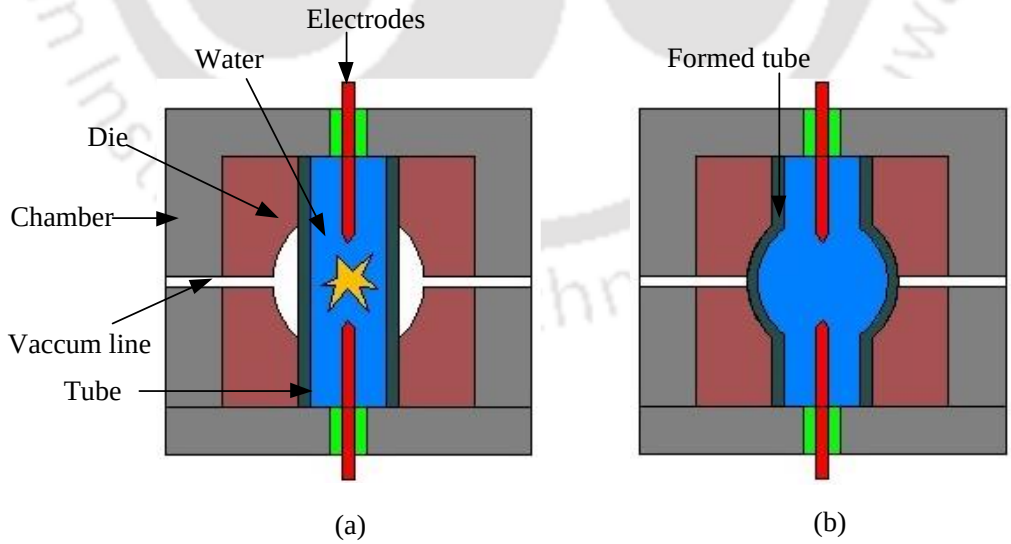


Figure 1.4 Electrohydraulic forming process

### c. Electromagnetic forming

In electromagnetic (EM) forming process, a metal workpiece is accelerated into a die or can be free formed by a transient magnetic pressure. EM crimping process is a high energy system that can discharge its energy within a very short period. The system consists of a capacitor bank ($C_c$), an inductor ($L$) and a resistor ($R$) which is connected in series with the coil as shown Figure 1.5. The circuit parameters like $R$, $L$, and $C_c$ are selected such that it operates in an over-damped condition (Mamalis et al., 2004). A transient magnetic field is produced by passing a sinusoidal damped electric current through the coil. The transient magnetic field generated by the coil induces an eddy current in the workpiece. The magnetic field of the workpiece is of opposite nature as produced by the coil. The opposing Lorentz forces between the two magnetic fields cause the acceleration of the workpieces away from each other. Depending on the geometrical configuration and process parameter, crimp joint is obtained.

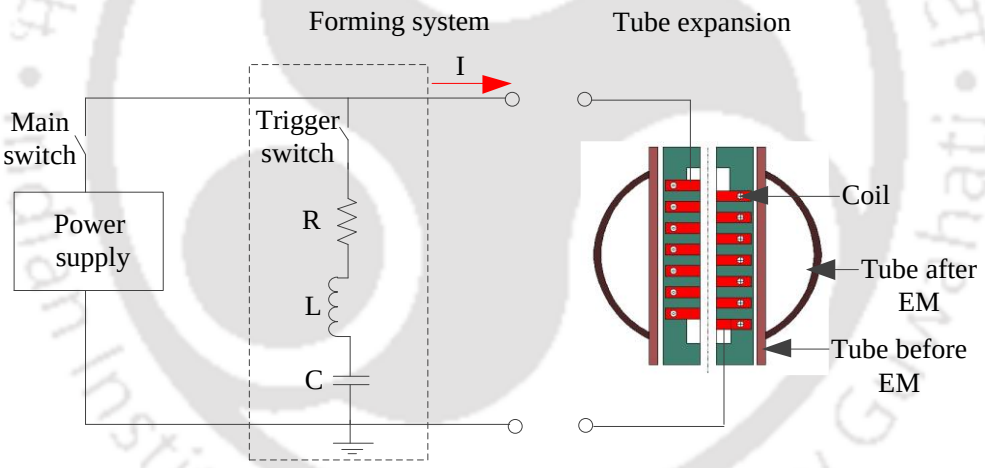


Figure 1.5 Schematic diagram of EM tube expansion process

For EM forming process, strain rate effect on the flow stress ($\sigma$) can be incorporated into the constitutive model for the material by including a strain rate ($\varepsilon$) term and strain rate sensitivity ($m$) exponent into the power hardening law of the material as shown in equation (1.1):

$$\sigma = K\varepsilon^{n}\dot{\varepsilon}^{m} \tag{1.1}$$

where $K$ is the strength coefficient, and n is the strain hardening exponent. The values $K$, $n$ and $m$ are the material parameters which depend on the material alloying elements.

For high strain rate process, for materials like aluminium, increase in the final flow stress is 50 % larger than the conventional quasi-static process. The value strain rate sensitivity ($m$) increases with the inertial effect. It was reported that inertial effect increases ductility that is not present in quasi-static deformation (Santinho and Martins, 2014). Spring-back of material it is the elastic recovery of the material after the stress is removed. Higher deformation velocity in high strain rate forming process leads to a reduction in spring-back phenomena (Padmanabhan, 1997).

Advantages of this process compared to conventional mechanical crimping processes are:

- When the material is deformed, it is stretched both plastically and elastically. After the removal of the deforming force, the elastic part of the strain is recovered causing a change in the shape of the product which is called spring-back phenomena. Spring-back has a significant effect on the product accuracy. It reduces the strength of mechanically joined products. Electromagnetically formed products show less spring-back compared to conventional formed products, thus creating products with a better accuracy.
- The workpiece forming velocities are much higher compared to conventional forming processes. Forming at high velocities, the failure strain is significantly increased and an increased formability can be obtained.
- In tube compression process, wrinkling is caused by the non-uniform compression. Forming at high velocities reduces wrinkling. The tendency for wrinkling gets reduced as the discharge energy of the capacitor bank increases. In other words, high velocities tend to suppress wrinkling.

Some other advantages of EM terminal-wire crimping process are:

- A workpiece surface finish can be executed before forming since there is no mechanical contact during the process.
- The system requires low maintenance and short setup times.
- A significant amount of energy is released very quickly.
- The workpiece surface does not need to be machined to tight tolerances before crimping.

- The process is environmentally friendly.
- Improved surface roughness due to contactless process.
- Improved surface hardness due to EM peening effect.

## 1.3 Motivation

Crimping is the most used technique in the terminal - wire interconnections in different fields like automotive, aerospace, power transmission sectors, battery units and many more. Even after many research in this area for years some important problems like spring back of the terminal, higher contact resistance, non-uniform deformation of the terminal, flash out of material, cracks over the terminal, poor durability, etc. are yet to be resolved. Its working principle is not however mastered, and the leading parameters involved in the crimping operations are yet to be defined properly.

The modern vehicles are equipped with highly sophisticated equipment which controls some essential safety features like airbags, seat belts, etc. thus increasing the necessity of the durable and reliable interconnections. In power sectors with the increase in demand in power consumption with the increase in population, it is important to transmit power from source to the consumer with minimum losses. Either a medium or high power transmission lines, it is reported that 60 % of the electrical failures take place in the connector junctions. These failures cannot be related to a specific kind of problems; there are multiple parameters which need to be mastered to avoid this type of circumstances.

There are industrial units which work on optimizing the crimping tool for making effective dies for crimping, taking into the prospect of different materials like copper, aluminium, steel or coated tin, but the problem remains the same. Still, the design of tools which are available till now for an effective terminal-wire crimping is a contact die-terminal crimping process. There are very few research papers on an aspect of crimp. The most of being about tool design, modelling using finite element analysis using 2D or 3D modelling taking into account of punch surface friction coefficient, and presented results of the influence of the tool surface finishing, crimp height to achieve required terminal deformation on the wire strands.

After carrying out the literature review, it was found that there can be one effective way of crimping that can resolve all these problems which are faced till decades using EM forming process. This process can effectively tackle all these issues very efficient and effective manner. None of the research work was carried out on electrical cable crimping using EM forming process. Because of the advantage of this process like contactless high strain rate forming process, EM forming can play a significant role in wire crimping in the years to come to make high durable electrical connections.

## 1.4 Objectives

The objectives of this dissertation are to provide an alternative method to conventional crimping process. Some of the objectives are summarised as follows:

- Acquiring a deep understanding of conventional and EM terminal-wire crimping process and making a comparison of both mechanical and electrical parameters.
- Numerical simulation for understanding the physics of EM crimping process and using its result for carrying out experiments on the different terminal profile. With an objective to improve the mechanical and electrical properties.
- Extending the numerical simulation work, on finding the suitable helical coil by comparing different types of cross-section profile, to get maximum deformation and contact length at lower energies level. Results to be used for carrying out experiments on the optimised helical coil geometry and discharge voltages to minimise the errors.
- Design and implementation of different types of field-shaper to increase the coil working life. Numerical simulations to find a suitable design for field-shapers for efficient terminal compression over the wire strands at lower energies. Numerical simulation results to be used for the fabrication of field-shapers to carry out experiments.

Overall, the objective is to develop a new technique for terminal-wire crimping process, which can provide required mechanical strength with lesser resistance at the contact interface to minimize the power losses and failure rates, so that it can benefit the industries

to produce reliable, efficient and long lasting crimp joint where cable connections are used in large numbers.

## 1.5 Organization of the Thesis

The thesis consist of six chapters, which are organized as follows:

- The current chapter provides the introduction along with the primary objectives and organization of the thesis.
- Chapter 2 presents a review of the literature on conventional terminal-wire crimping process, and the work carried out using experimental and numerical studies on EM forming process followed by the field shapers, and the important equations involved in the process. The inference from the literature review and detailed objectives of the present thesis have been outlined.
- Chapter 3 presents EM terminal-wire crimping which is carried out with different parameters and compared with conventional crimping process. With an aim to develop a new method for terminal-wire crimping that can be an alternative option for existing conventional terminal-wire crimping method in terms uniform terminal deformation, minimum electrical resistance, high pullout strength, good surface finish, increased hardness number and improved thermal property.
- In chapter 4, the simulation was carried out in the EM module of LS-DYNA software. Simulations were carried out to find suitable coil dimensions which act as a crimping tool in this process and to find the required discharge voltage for uniform deformation of the aluminium terminal over the copper wire strands. Results of the simulations were used to fabricate the coil. Experiments were carried out on the plain and threaded terminal for comparison. Results like terminal deformation, contact resistance, cross-section analysis, hardness along the terminal thickness and pull-out test were carried out and discussed in detail.
- Chapter 5 deals with the numerical simulations on three different types of helical coils with different cross-section (CS) geometry keeping the cross-section area constant carried out using LS-DYNA software. For comparison number of turns and the total length of coil remains same so that the total inductance of the coil

remains same of all the three cases. Results of the simulations were used to fabricate the coil for carrying out the experiments.

- In Chapter 6 the effects of three field-shaper geometry, like a single-step, a double-step and a tapered on the EM terminal- wire crimping were studied. As, no numerical and experimental comparison of three types of field-shaper with geometries like single-step, double-step, and tapered field-shaper has been reported yet. The comparison was carried out by keeping the total field-shaper length and effective working area of the field-shaper constant. As the slit in the field-shaper plays an essential role because it affects the performance, so slit width was also kept constant. The simulation on EM terminal-terminal-wire crimping process was carried out on LS-DYNA software, and the experimental work was carried out by comparing the results obtained from the simulations.
- Conclusions and scope of future work are presented in Chapter 7 followed by references and list of publications.

# Chapter 2

## 2 Literature Review

### 2.1 Introduction

Application of electromagnetic (EM) processing like welding, forming, crimping and cladding came into existence between 1960 and 1970, with a great interest in the research field. This process restricted to providing principles involving in this process. But in recent years due to the development of promising efficient tools in the area of EM forming process, a new scope has emerged which is slowly finding its place in the industries (Siddiqui, 2009). The EM forming process is a non-contact, high-speed forming technique, using a very high magnitude of force which is created by the pure EM interaction taking place between the tool coil and the conductive workpiece. Compared to other existing conventional quasi-static forming process, EM forming process shows many advantages. The EM forming process has potentially improved the formability of aluminium alloys, such as increased forming limit, reduced spring-back and wrinkling, and thus, it has recently attracted much attention in the field of modern manufacturing industry (Psyk et al., 2011).

Many researchers have worked till now in the area of EM crimping showing the advantages of this process over the conventional crimping process. In EM crimping, typically it uses a ring-shaped coil placed over the tubular workpiece. The forces generated by the two opposite magnetic fields result in a repelling force between the coil and the tube. As a consequence, the tube collapses onto the internal workpiece, creating a crimp joint. This process was used to develop form-fit crimp joints with a single groove and a double groove design, which subjects to an axial load (Faes et al., 2012). Weddeling et al. reported that the strength of the crimped connections could drastically increase compared to existing conventional process by using EM crimping process. The EM crimp connections can lead to strength high enough to cause failure in the base material and not in the joining zone (Weddeling et al., 2015).

This EM crimping process also demonstrated the capability of compressing high strength steel tubes by merely using a helical coil, showing the tremendous amount of pressure it

can generate for deformation, also increasing the forming limit which is not possible by any other existing process (Vivek et al., 2011).

Usually, connector terminals are loaded only to 50 % of their rating. The primary cause of failures takes place due to heat-related problems because of internal arching, which severely affects the connector terminals resistance stability and durability (Zhmurkin et al., 2008). Power cables either overhead or underground are the most essential and they are critical part of electricity transmission. Transmission through overhead wire sometimes causes wildfires causing a problem in the distribution in the power lines, which results in thermal expansion of connector terminal leading to loosening the strength constraining the wire strands and eventually failure (Tohidi et al., 2017). Most hand operated and hydraulic compressors with electric motors are used for crimping of terminals and cables. However, this equipment uses non-uniform pressure in the circumferential direction for crimping. So, the crimping part of the terminal with the inner wire will often have many defects (Prin et al., 2002). When the terminal connects to electrical equipment, a low crimping force causes the terminal to separate from the inner wire, and a low wire density in the terminal often leads to fire due to overheating. Moreover, compressed defect causes wear due to high temperature and electrical corrosion, which shortens the lifespan of the connection terminal. Therefore, these defects drive up manufacturing costs of the complete product. In particular, overheating in the terminal crimping not only interrupts the current supply resulting in a decrease in manufacturing production efficiency but also causes sparks on electrical equipment, thereby threatening workers safety. However, the development of crimping process for producing the high- durability terminal has been carried out by very few researchers (Shim et al., 2016).

Therefore, it is crucial to develop a new technique for wire crimping which can provide required mechanical strength with minimal resistance at the contact interface, which will minimize the power losses and failure rates. So, that it can benefit the industries to produce reliable, efficient and long lasting crimp joint where cable connections are used in large numbers. In this literature review Chapter, concisely literature survey is carried on conventional terminal-wire crimping process and the problems which are faced by using the traditional crimping tools. Work carried out by researchers and industry on

experimental and numerical studies on EM tube forming and crimping followed by the field-shaper is reviewed. At the end of this chapter important equations involved in EM forming is discussed followed by the research plan in the form of flowchart.

## 2.2 Conventional Wire Crimping Process

Electrical connectors play a vital role in the control system. The numbers, types, and complexity of electrical network systems in a commercial vehicle are continuously increasing, and the number of electrical contact points increases as well. Within this circumstance, the demand for lifespan and reliability of electrical components are increasing. The electrical connections are often a weak point in the electrical systems (Williams et al., 2015).

Crimping of terminal is one of the fastest and most reliable interconnection methods. However, if the terminals are not crimped properly onto the wire strands, it severely affects the integrity of the electrical connectivity and mechanical strength. Compression using conventional crimping tool deteriorates the material due to relaxation or partial release. Nevertheless, a specific care should be considered. Faulty crimps can lead to considerable damages and in the worst case can cause a fire (Soulinaris et al., 2014). Some important and most widely used applications of terminal-wire interconnections are shown in Figure 2.1 (a) overhead power transmission, (b) underground power transmission, (c) connectors connected to bus bars for high voltage application, (d) industries circuit connection for high power transmission, (e) battery connection of in aerospace application, (f) crimped connections in a cockpit of jet plane, (g) electrical power transmission of an automobile, (h) battery connections and, (i) power transmission system in buildings.

A proper terminal-wire crimping mechanism which can properly execute a crimp connection to make electrical reliable and mechanically strong connections in a single operation is still a significant challenge in the electrical industry. Crimping tool is a critical part for a quality crimp. Crimping takes advantage of the properties of metals to achieve electrically and mechanically sound connections. Metals used in crimp connectors, like copper, brass, aluminium, or bronze, are both ductile and malleable.

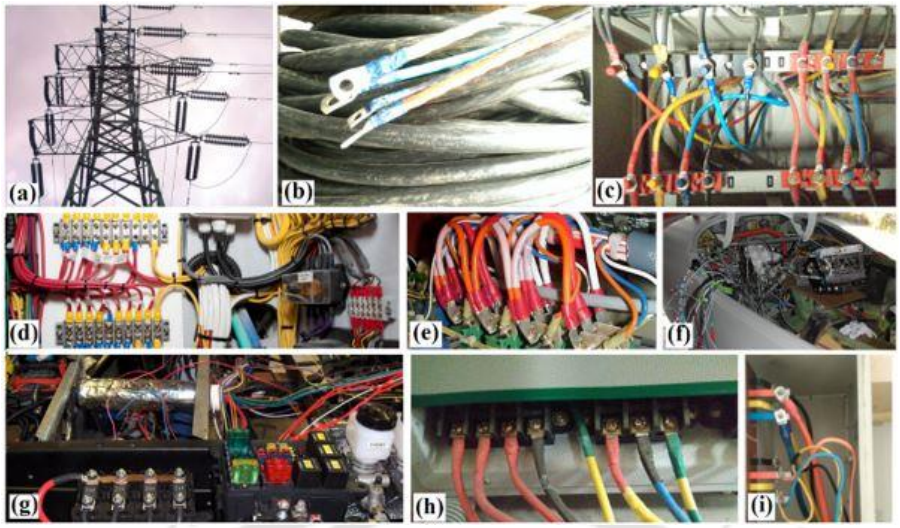


Figure 2.1 Different application of connector terminals

A metals ductility is the degree to which it can deform under tension, while malleability is a measure of how metal deforms under compression. Crimping involves applying significant compressive forces onto the crimp connector terminal and the wire, so the malleability of each element is an important factor in crimp quality. But ductility plays a role too as both connector and wire undergo significant stretching during the crimping process. As more pressure applies to the connection, metal in the wire strands begins to stretch and flow which loosens and increases contact resistance (Prin et al., 2002).

There are many terminal-wire crimping tools patents (Hashimoto and Kaneko, 2005; Katou, 2017; Mc Caughey, 1973; Theiler, 1980). But in every patent, there is one standard part that is a “crimping die”, which deforms or squeezes the terminal onto the wire strands to take the shape of the crimping dies when force is applied by using a lever or electrical motorised. Traditional crimping tools not only leaves the marks of the dies over the terminal surface but excessive pressure sometimes leads to the crack formation leading to mechanical fracture.

A properly executed crimp connection is electrically safe, reliable and mechanically robust. Some critical challenges which are faced by cable industries are:

- Improper deformation of wire strands resulting in voids.
- Excessive pressure leads to crack over the terminal.
- The improper pressure of the crimping tool leads to flash and burrs.

- An excessive pressure is leading to fractures over the terminal.
- Non-uniform deformation of the terminal.
- Uneven deformation of wires and a high percentage of voids which affects the pull force results and electrical performance.

As shown in Figure 2.2, executed crimp cross-section showing defects consisting of wire strands and terminal. The most important problem faced by wire crimping industry is the spring back of terminal on tool relaxation which generates a gap between wire strands and terminal contact interface. This increases resistivity and high amount of losses in wiring system (Weddeling et al., 2015).

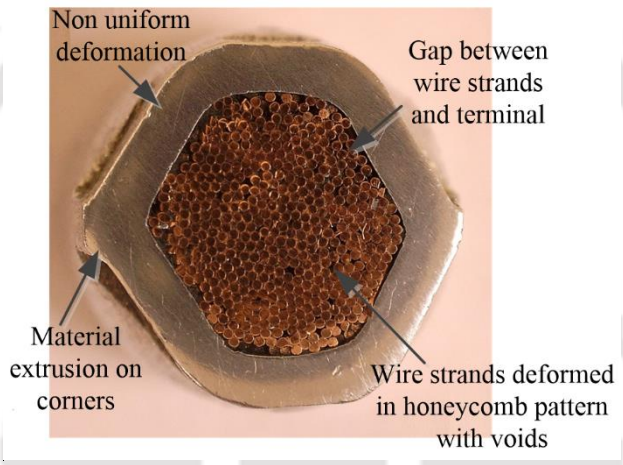


Figure 2.2 Cross-section of terminal crimped over the copper wire strands

As such electrical connector terminals work at different operating circumstances such as vibration, temperature gradient and different electrical environments that cause fretting corrosion/wear and relaxation of the contact forces. The most common failure mechanisms are surface film formation due to unsealed terminals, relaxation of the contact force due to high temperatures and wear or fretting corrosion due to mechanical or thermal micromotions. Vibrations are often the parameters which limit the lifespan of electrical contacts, but how large the damages become depends among other things on the electrical environments; current, voltage and inductance (Shim et al., 2016).

Therefore, it is essential to develop a new technique for wire crimping which can provide required mechanical strength with minor resistance at the contact interface to minimise the power losses and failure rates. So, that it can benefit the industries to produce reliable,

efficient and long lasting crimp joint. In comparison to conventional crimping tools which are most widely used in industries, EM crimping shows many advantageous like uniform pressure distribution, contactless process, low mold cost, lesser spring back of the material, minimum wrinkling, improved formability, no lubrication, few seconds for process completion, no tool deterioration, improved hardening due to shock pressure waves and good repeatability (Golovashchenko, 2007; Psyk et al., 2011).

## 2.3 Different Types of EM Forming process

In EM forming process different applications of forming can be achieved by making use of varying coil and workpiece arrangements. Figure 2.3 below shows compression of the tube, expansion of tubes and sheet metal forming for the different type of coil variant in EM forming process.

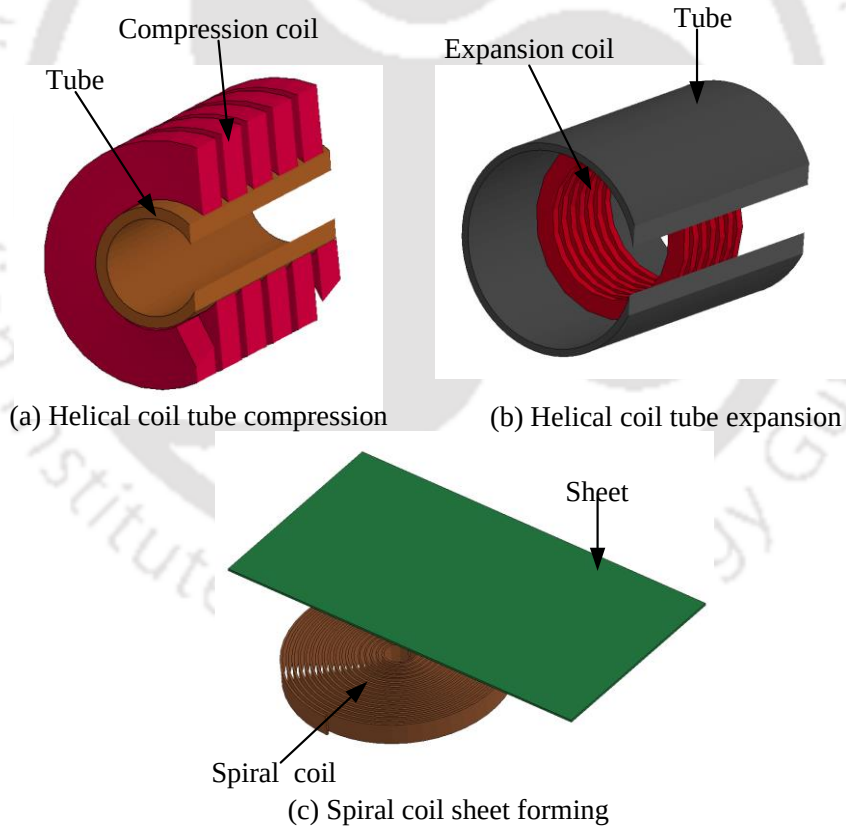


(a) Helical coil tube compression (b) Helical coil tube expansion

(c) Spiral coil sheet forming

Figure 2.3 Different types of EM forming process

**a) Tube forming**

The EM forming process is being used widely for axisymmetric components, which are used extensively in industrial applications. In EM forming of the tube, the cylindrical tube is uniformly expanded or compresses by the application of magnetic pressure (Haiping and Chunfeng, 2009).

**b) Sheet metal forming**

In EM sheet forming process workpiece is a flat sheet. It is the simplest one where rigid flat spiral pancake coil, is placed below the metal sheet which needs to be formed on the application of magnetic pressure. The deformed sheet can take the shape of the die or can be a free bulged. By this means, there is a drastic improvement in forming limit of metal sheet, which is not possible by the conventional quasi-static process (Doley and Kore, 2017).

**c) Hybrid system**

In hybrid systems, the conventional forming operation is replaced with EM effects. In hybrid process, one or more coils are installed to obtain the deformation of the sheet inside a die which consists of complex geometry. Deformation is achieved by making use of localized force using tailoring the coil to get required magnetic pressure in the desired location, which is not possible by any other conventional process (Vivek et al., 2013).

## 2.4 Experimental Work Carried Out on EM Forming

### 2.4.1 Tube Forming

An EM tube forming is a high-speed forming process by using Lorentz force created by the pulsed magnetic system to deform conductive material without any mechanical contact. In EM tube expansion process the coil is placed inside the axisymmetric metal workpiece as shown in Figure 2.4. Upon discharging the capacitor, time-varying currents flows through the coil and generates a transient magnetic field, which induced an eddy current in the workpiece and generates an opposing transient magnetic field. The interaction of these two magnetic fields created large repulsive Lorentz body forces to drive a rapid plastic deformation of workpiece. The repulsive Lorentz force developed

due to the interaction between the coil and the workpiece can easily overcome the yield strength of the workpiece causing permanent deformation.

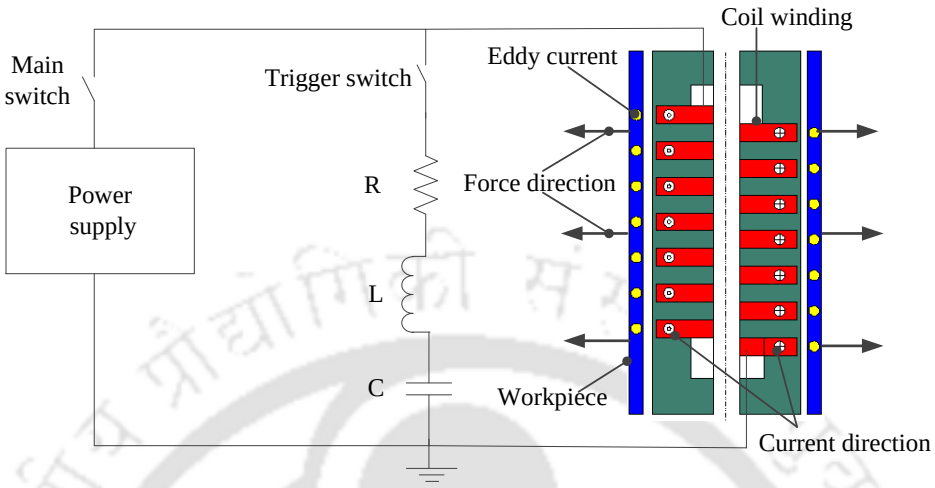


Figure 2.4 Schematic diagram of EM forming process

The metal forming process occurs within microseconds, and because of the large forces, portions of the workpiece undergo high acceleration. Some important research work carried out in the field of EM tube expansion is discussed.

Lee et al. studied the distribution of magnetic pressure as the relative coil workpiece axial position is varied. A 14 kJ EMF system and aluminium as the tube material were used to carry out the experiments. They stated that a variety of tube shapes could be produced due to the change in magnetic pressure distribution as the relative coil-workpiece axial position is varied (Lee, 2015). Various effect of coil parameters like the number of turns, height to diameter ratio and the cross-section geometry were studied. After carrying out many experiments, Song et al. concluded that the two main factors contributing the magnetic intensity between workpiece and coil are coil parameters and relative position of coil and workpiece (Song et al., 2004).

Zhang et al. found that magnetic field intensity between the workpiece and the coil is proportional to magnetic inductance developed between the coil and the workpiece (Zhang et al., 1995). Authors Kim et al. found similar results obtained by Zhang et al. like the magnetic field intensity in the space between the workpiece and coil is proportional to magnetic inductance developed between the coil and the workpiece (Kim and Shang, 2012). The Lorentz force distribution can be adjusted by changing the relative position of

coil and workpiece, which affects the shape of the workpiece deformation as shown in Figure 2.5 (a) tube length is larger than coil length, (b) tube length is equal to coil length and, (c) tube length is shorter than coil length.

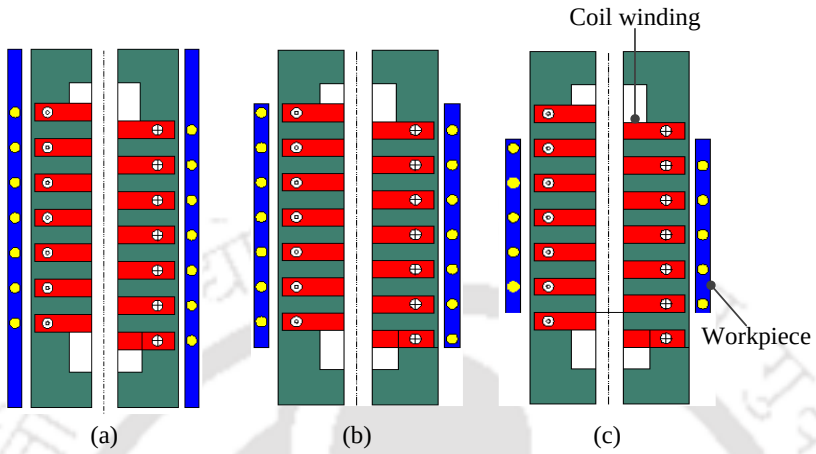


Figure 2.5 Sketch of the experimental installation of the workpiece

Suzuki et al. performed experiments on EM tube bulging. The tube bulging can be seen in Figure 2.6 for different coil and workpiece axial position. They concluded that with the help of a combination of coil geometry and charged energy in the capacitor bank, an approximate prediction of the final shape of bulged could be possible (Suzuki et al., 1987).

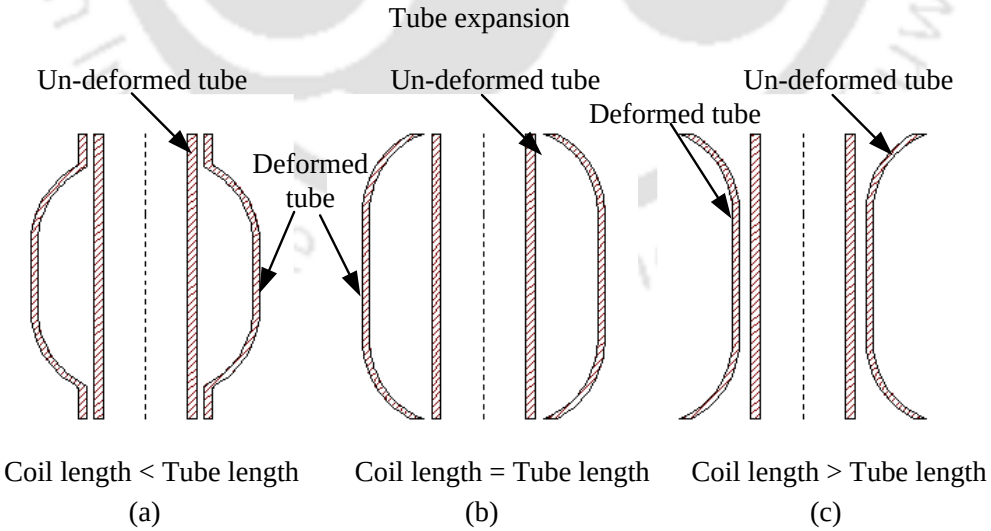


Figure 2.6 Typical shapes of bulged tubes

The EM process in the ring expansion was comprehensively studied by Huang et al. at various discharge voltage as shown in Figure 2.7. The formability and the hardness of the aluminium alloy ring at different discharge voltages were investigated. They found that the hardness of the ring increases with the increase of the discharge voltage. Especially, the hardness has a drastic rise when the discharge voltage changes from 5 kV to 6 kV and the hardness changes irregularly when the discharge voltage is higher than 8 kV. An increase of 46 % hardness value was achieved compared to the ring without expansion (Huang et al., 2014).

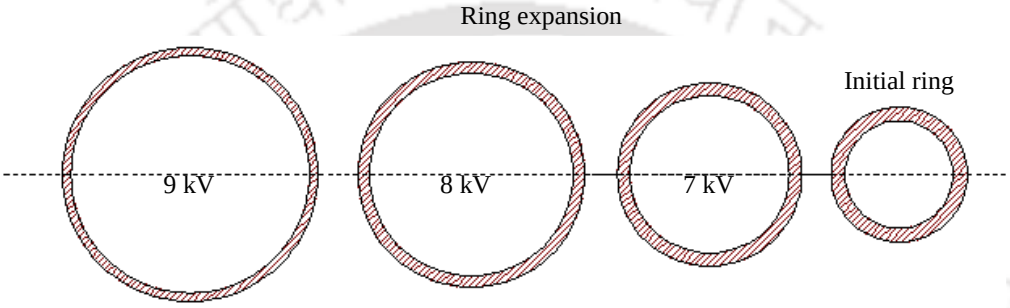


Figure 2.7 Initial ring and the expanded rings with different discharge voltages

### 2.4.2 Electromagnetic Crimping

EM crimping is a forming process mostly used to join or connect extruded metal tubes to achieve lightweight frame structures. It is not necessary to use an additional material such as screws, rivets, adhesives or auxiliary wire. With EM crimping process a high-quality joint can be achieved or manufactured to get interference fit, form fits or a combination of these two types.

The physics in the process remains the same as discussed in EM tube forming. The only change is the placement of the coil over the workpiece (or tube) as shown in Figure 2.8. A metal tube is placed coaxially inside a solenoid coil, which is connected to a capacitor by a high voltage switch. The capacitor is charged to an initial voltage, and when the switch is closed to complete the circuit, a sinusoidal damped current is produced. This current generates a transient alternating magnetic field about the coil; consequently, this field induces an eddy current in the flyer tube (Faraday's Law). The current in the coil and the workpiece flow in opposite directions obeying Lenz's law and repel each other (Weddeling et al., 2015).

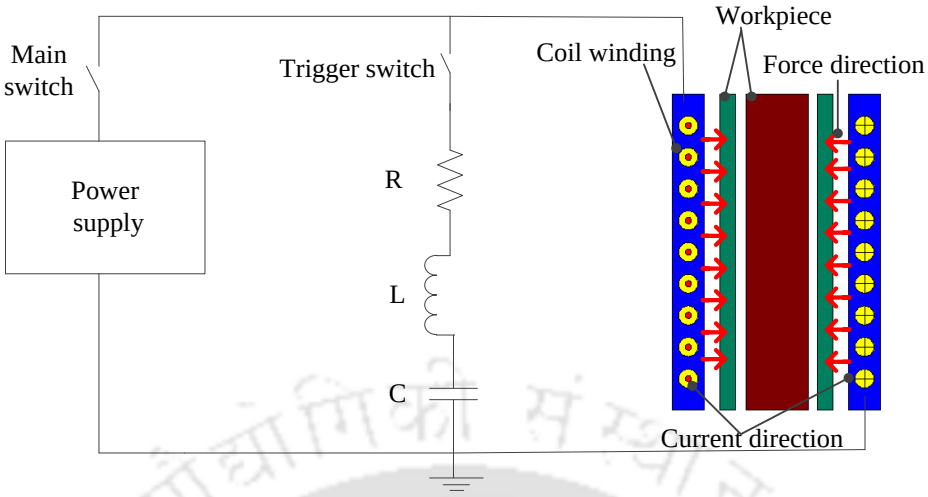


Figure 2.8 Schematic diagram of an EM crimping process

The EM forming process which is used most frequently in the industry is joining by EM compression of the tubular workpieces. Joints manufactured by EM forming can be classified into two categories and also shown in Figure 2.9.

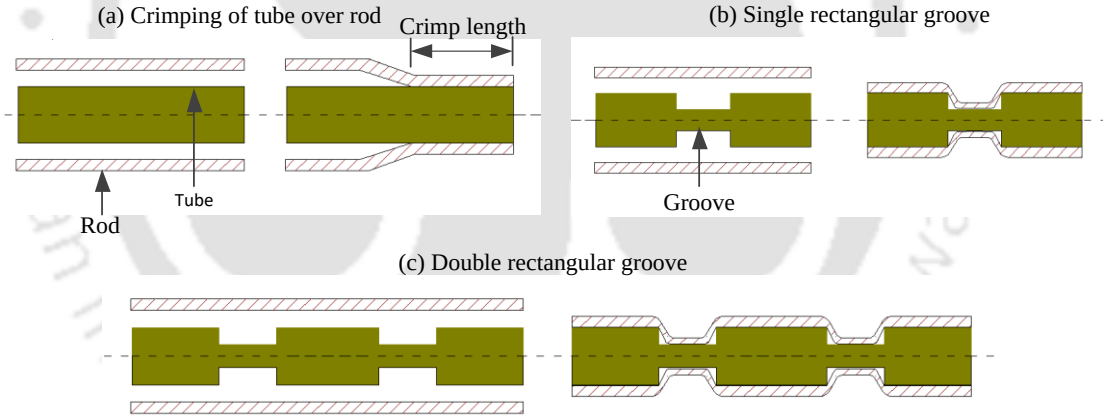


Figure 2.9 Different samples crimped out using EM crimping process

- Interference fits results by a plastic deformation of one and an elastic deformation of the other joining partner. As a result, interference stresses between both joining partners are generated.
- Form fits by forming one joining partners material into an undercut (e.g., a groove) of the other joining partner so that the joint is locked against an external load.

The major challenge in the manufacturing of any frame structure for a high strength joint especially from aluminium extruded profiles is joining of tubular hollow profiles. While joining by EM forming is a possible alternative to conventional welding and riveting processes since the achievable joint strength is within the range of the yield strength of the weakest joining partner.

Akbar et al. studied free compression of an Aluminium tube inside a solenoid coil. The most significant mechanical as well as EM time-varying or spatially distributed parameters of the process figured efficiently (Akbar et al., 2015). They concluded that only the first half of the pulse is responsible for deformation rest of the pulse does not have sufficient energy to deform the workpiece and similar conclusions were drawn by Haiping and Chunfeng (Haiping and Chunfeng, 2009). Significant deformation EM compression of steel tube was also reported by Vivek et al. They demonstrated the capability of the helical coil deformation of steel tube by using nine turn coil, demonstrating it as a versatile tool in metal forming (Vivek et al., 2011).

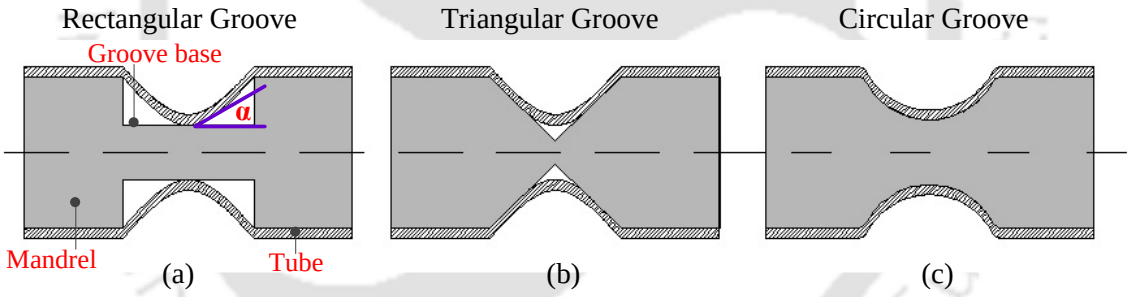


Figure 2.10 Types of groove geometry over the rod for EM crimping process

As proposed by Weddeling et al. groove characteristics have a significant influence on the possible strength of a form-fit joint. They reported the influence on the joint strength of those parameters concerning different groove geometries. Among the results gained it was possible to develop joining strategies and general design principles for the joining zone in form-fit joints. The goal of forming in groove filling was to apply the minimum amount of magnetic pressure that was required to cause contact between the tube and the bottom of the groove. The form-fit joints created by forming the tubes into grooves of three different shapes: rectangular, circular and triangular. For these shapes, the dimensions were varied to investigate their effects on the joint pull-out strength

(Weddeling et al., 2015). The triangular groove was found to be the weakest groove geometry due to the larger resulting angle, compared to the rectangular and circular grooves with equivalent dimensions as shown in Figure 2.10. Increasing charging energy for a groove of given dimensions decreased the resulting angle while creating an interference-fit between the tube and the mandrel (Faes et al., 2012).

The use of deeper or narrower grooves resulted in higher deformation of the tube and providing higher stiffness. At the same time the resulting angle, decreases and the chances for partial shearing of the tube at the groove edge increase. Rectangular grooves were found to be the providing highest strength, due to the presence of minimum tube shearing at the groove edges. This shearing locked the tubes into place, requiring a larger pull-out force to cause failure. Weddeling as reported in his thesis work that a significant joint strength increase can achieve by the application of multiple grooves to the joining zone. The disadvantage of this design is the additional mass resulting from the increased joining zone length (Weddeling, 2014). Wonterghem and Vanhulsel reported a similar observation that a significant joint strength increase could be achieved by the application of multiple grooves to the joining zone (Wonterghem and Vanhulsel, 2011).

A method for reducing wrinkles and springback produced after the EM compression of the tube by using mandrels was analyzed and introduced with the help of an impact contact algorithm by Padmanabhan. It was reported that the number of wrinkles has a linear relationship with the ratio of radii to the thickness of the tubes. It was stated that spring-back is the elastic recovery of the material after the stress is removed. Spring-back is caused by the elastic portion of the strain, and any factor that decreases the ratio of elastic to plastic reduces the spring-back. Due to higher compressive stress generated due to higher velocity deformation leads to a reduction in spring-back phenomena. For a higher effective deformation of the tube over the mandrel, a reduced spring-back is an important criterion. Besides this, it was also stated that in axisymmetric tube compression yield strength of the material, the ultimate tensile strength of the material, the thickness of tube and energy required to compress the tube are some important parameters affecting spring-back (Padmanabhan, 1997).

## 2.5 Numerical Studies

Nowadays, with the increase of calculus capacity of the computers, numerical simulation is becoming a major tool to predict the mechanical behaviour of the modelled parts. Carrying out the numerical simulation portion in EM forming is a difficult part due to the requirement of simultaneous modelling of interacting EM and mechanical part. Even though the physics about this part was well understood since 1950's but researchers were unable to carry out an accurate model due to a very complex dynamic process. The problem becomes more difficult when thermal phenomena are taken into consideration in EM forming process. Difficulty level also increases with the strong dependence of the circuit parameters on the workpiece deformation. Three approaches are developed to simulate the EM forming process. These are no coupling, loose coupling, and strong coupling. These approaches are briefly described in the below sections.

### 2.5.1 Non-Coupled Approach

A non-coupled approach is the simplest approach among the three. The circuit parameters are calculated based on the EM processing equipment. The calculation of the software is carried out using Maxwell's equation, without considering the workpiece deformation and velocity of forming. Analytically the Lorentz force is calculated and given as an input data to the mechanical problem for deformation of the workpiece.

Some initial work was carried in 1960's by Nassiri et al. on EM numerical analysis (Nassiri et al., 2015). They analytically determined the magnetic pressure distributions caused by different coils on flat conductive plates. Several simple geometries were analysed which led to the expression of the magnetic field intensity and the pressure distribution produced by a spiral coil.

### 2.5.2 Loosely Coupled Approach

In this approach, the developed Lorentz forces are calculated at each time step increment in the EM model. Then the forces as input load are transferred in the mechanical model automatically. In the mechanical analysis, the deformation undergone by the workpiece is calculated, and the geometry of the workpiece is updated as shown in Figure 2.11. The new updated geometry from the mechanical model is used to calculate the EM forces for the next time increments.

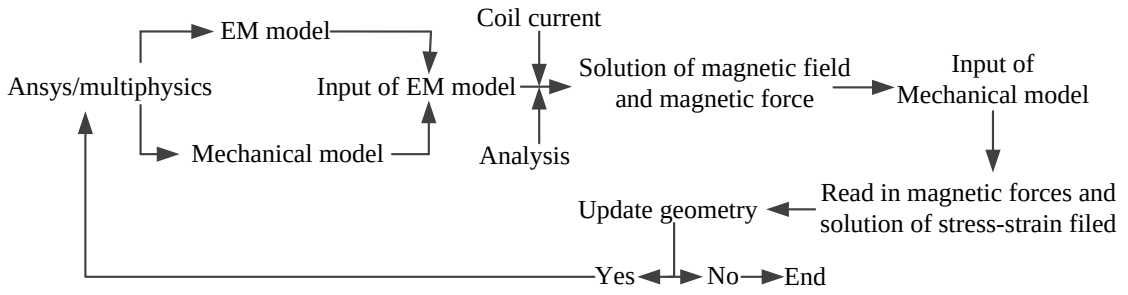


Figure 2.11 Flow chart of loosely coupled approach

This process is repeated iteratively until the end of the process time as formulated by Haiping et al. This strategy comes into use because it gives accurate results with a weak computational time. Limitation of this process is the assumption of the adiabatic condition, which is a big limitation of this process in which thermal conditions are neglected (Haiping et al., 2009).

### 2.5.3 Fully Coupled Approach

In a fully coupled procedure, the effects of the coupled EM, mechanical and thermal fields are calculated in each element of the forming system. The mathematical description of the complete EM-mechanical equations is very complicated to solve in a compact environment. The main disadvantage of this procedure is the difficulty found in obtaining a converging solution, due to the very high computational cost for solving the inter-related equations. A simple flow chart of this process can be seen in Figure 2.12. In this process, it considers the effect of EM, mechanical and thermal fields, which are numerically calculated in each element. This process involves a complicated EM-mechanical equation, to solve a problem efficiently at every time step over each element in the forming system (L 'Eplattenier et al., 2008).

Yu et al. studied the effect of coil length during tube compression. They investigated the effect of coil length on magnetic pressure and tube deformation (Yu et al., 2005). Whereas Haiping and Chunfeng examined the influence of frequency on EM tube compression using the sequential coupling numerical simulation. There is a particular range around the optimum frequency, where the higher deformation of the workpiece is achieved which corresponds to the relative skin depth is between 0.61 and 0.70 (Haiping and Chunfeng,

2009). It was stated that only the first period of the current is considered to be responsible for the tube compression or can be said that in EM forming process, the work of the first pulse of magnetic pressure to the tube contributes to the deformation and movement, including the kinetic energy and the plastic strain energy of the tube.

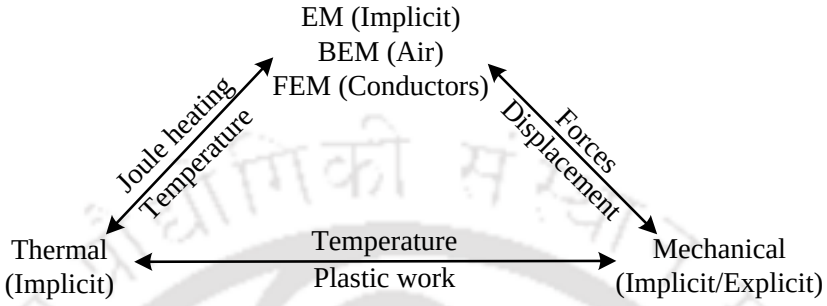


Figure 2.12 Flow chart of fully coupled approach

Haiping et al. also carried work on sequential coupling simulation for EM–mechanical tube compression by finite element analysis using FEM 2D axisymmetric model EM model. They proposed for the calculation of magnetic field and magnetic forces to calculate the dynamic plastic deformation of the tube in the mechanical model (Haiping et al., 2009). They stated that the tube compression has larger resistance to deform compared with tube expansion for its poor dimensional stability, especially when the plastic deformation is minimal, the fluctuation in velocity and displacement still exists in the calculation after plastic deformation for the elastic oscillation of tube.

Yu and Li analysed the work on the effect of the coil length on the tube compression in EM forming. They found that with the increase in the coil length, a decrease in the value of the current waveform and the current frequency was observed. While the peak value of the magnetic pressure is inversely proportional to the coil length. The distribution of the magnetic force acting over the workpiece was found to be inhomogeneous when the tube is longer than the coil. Whereas the shortened coil length increases the maximum deformation and energy efficiency (Haiping and Chunfeng, 2007).

Li et al. carried out the work on Multiphysics simulation (Loose coupling) on EM peening of predrilled holes using COMSOL Multiphysics software (Li and Cheng, 2009). They reported that by adjusting the parameters of the EM field as well as the position of the hole, compressive residual stress could be introduced along the surface of the hole to get

peening effects. In the following, this treatment is called EM peening. EM peening can be used to introduce compressive stress and work hardening around the hole surface and improve the mechanical property of the drilled hole, such as fatigue life and fracture toughness.

However, in all the finite element approaches presented in this section, the different physical phenomena are treated separately. In most of the preliminary models, the EM problem and mechanical problem are treated individually without any linkage. These models are simpler but do not provide the true description of the process. Mostly, Maxwell's equations are resolved analytically, and the EM pressure is obtained which is then introduced into the mechanical problem. The deformation of the workpiece is not taken into account for the calculation of the EM pressure.

Then, more recently the loosely-coupled techniques are presented, which are very accurate and rather uncomplicated. The EM problem calculates the basic EM parameters, which are then introduced into the mechanical problem. The coupling between the two problems is carried out; the parameters are then recalculated at each time step taking into account the new deformed geometry of the workpiece. Furthermore, the fully coupled models are moreover an extension of the loosely-coupled approach.

## 2.6 Field-Shaper

In the EM crimping process, a very important tool is the field-shaper (FS), and its purpose is to concentrate the magnetic field into the required region to achieve an efficient and higher deformation of the workpiece placed in the vicinity of the effective working length (Bahmani et al., 2009). The designing of FS is more economical and quicker than manufacturing special coils. One of the main characteristic of the FS in providing efficient magnetic field strength is its design (Cui et al., 2012).

### 2.6.1 Working Principle and Modeling

An EM wire crimping process system consists of an electrical pulsed power circuit responsible for the generation of the pulse current flowing through the work coil. Although field-shapers seem to be a mechanical part, it plays an vital role modifying the magnetic field distribution generated on the work-piece as stated by Suzuki et al. (Suzuki

et al., 1987). In this process, the electrical energy stored in the capacitor bank discharges into the coil when the trigger switch closes, which allows the pulsed current to flow through the coil as shown in Figure 2.13.

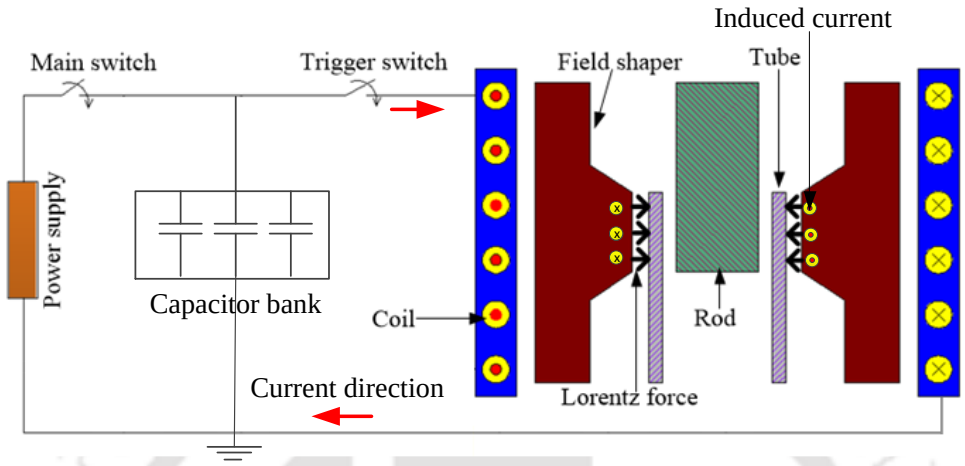


Figure 2.13 Schematic diagram of a working field-shaper

The current in the primary coil will induce a secondary current in the field-shaper. This secondary current will flow through the field-shapers outer surface to the inner surface, thus inducing another secondary current in the adjacent terminal. As a result of the interaction of the induced currents in the surface of the workpiece with the applied field, a magnetic pressure is exerted on the workpiece (tube), and it consequently helps in effective crimping operations. In actual, FS is a practical tool which helps to concentrate the magnetic flux and efficiently prolong the service life of the coil.

The principle behind the FS is similar to designing of a tool coil. In this process, the major task is to concentrate the magnetic pressure at the desired required location. The main purpose of the field-shaper is to withstands/bear high mechanical load to increase the lifetime.

Different field-shapers used for EM forming operations are shown in Figure 2.14. Most of the FS used in the research work are symmetric, so force acts uniformly when it is used for compression or expansion of tubes (Psyk et al., 2011). But especially in case of asymmetric field-shapers, where concentration area or effective working zone is not located at the center is highly affected by the repulsive pressure. So, for asymmetric FS, high strength material is chosen but without compromising the material conductivity.

More the conductivity higher the working efficiency of the process. Frequently used materials are copper and copper alloys, aluminium and aluminium alloys, brass and bronze.

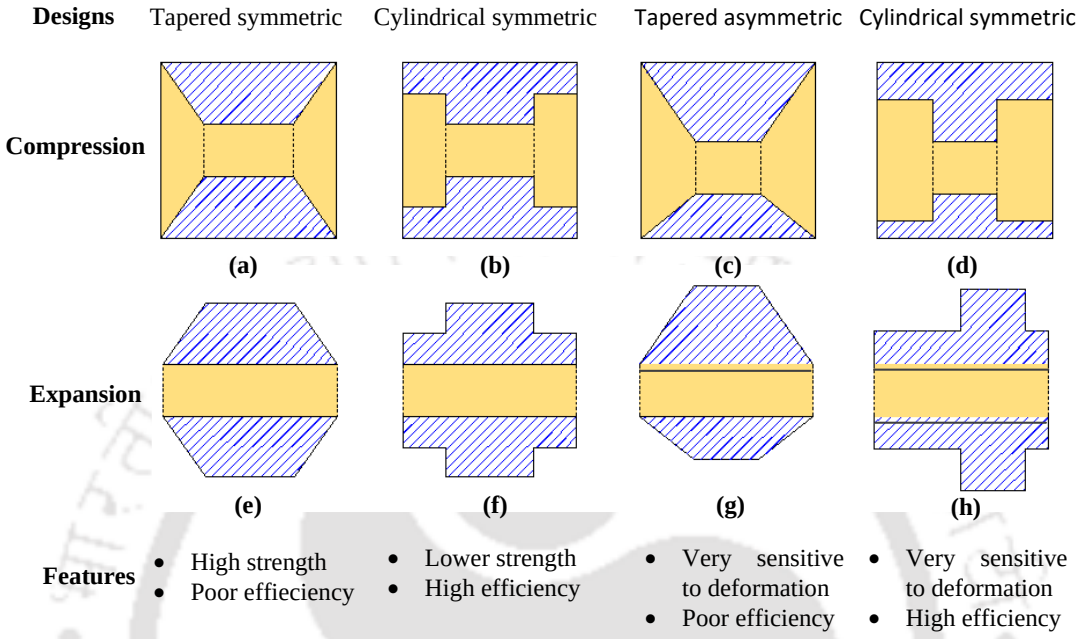


Figure 2.14 Different types of field-shaper (Psyk et al., 2011)

While designing a field-shaper, it should be considered that the coil length should be of the same length as the total length of the field-shaper. In case if the coil length is larger than the field-shaper, due to inhomogeneous loading coil lifetime decreases. While lower coil length results in a decrease in the working efficiency. It should also be noted that effective working length should not be too small, nor the magnetic field will penetrate it, and the required magnetic pressure cannot be built up. The length should not fall below a value of three times the skin depth (Cui et al., 2016).

Compared to direct acting tool coil, field-shaper concentration area leads to a more uniform distribution of magnetic pressure. It is also observed that field concentration can easily be shifted by shifting the concentration area in the desired location. Even a small modification will lead to a change in magnetic pressure so, in case of manufacturing, it's essential to make it with precision (Yu et al., 2005). Even though for tube compression and expansion work has been carried out numerically and experimentally to make field-

shaper as a more reliable tool, still designing a field-shaper in a proper manner with standard parameters are yet to be developed (Chaharmiri and Arezoodar, 2016).

Like in field-shaper slit feature plays an important role in the change in induced current direction, but this also controls the magnetic pressure and varying the Lorentz force. It's been reported by Chu and Lee, workpiece below the slit feature receives less Lorentz force than the other part around the end region of the slit Hence, an optimal slit width must be determined by considering the interaction between EM repulsion and the Lorentz force distribution. The Lorentz force will be concentrated at the end region around the slit feature. Hereafter, the slit feature design will control the distribution of the Lorentz force. The eddy current flowing on the opposite side of the slit is in a reversed direction, leading to EM repulsion between each component of the field-shaper. As a result, the wider slit feature reduces energy loss (Chu and Lee, 2013).

Even some work was carried out numerically by magnetic field distribution using field shaper, showing the distribution of magnetic flux density. Some major important conclusions were drawn are (Yu et al., 2005):

- The bigger the effective area of FS is, the longer the uniform force area of the tube is, where the radial magnetic pressure decreases.
- Effect of relative diameter of field-shaper on magnetic pressure: the ratio of outer diameter and the inner diameter is set as the relative diameter of FS. It is shown that the radial magnetic pressure decreases with the increase of relative diameter. However, in consideration of strength, the relative diameter of FS is unsuitable to be undersized.

This literature of field-shaper was based on tube compression, and important research papers and their contributions are discussed. Even though there can be different field-shaper design with even more efficiency and rigidity, which can sustain a higher repulsive load, but designing with proper parameters is still a major hurdle.

## 2.7 Analysis of EM Forming Process

Metals with high electrical conductivity and of low mechanical strength can be formed using pulsed magnetic field produced by the sudden current discharge from the capacitor

bank. In actual, this technique is more suitable for compression of tubes using compression coil. For example tubular coil surrounded by cylindrical helical coils. Practical applications are joining of the tube to tube, tube rod, etc. by deforming tube over the shaped part or insulators. To achieve a high efficiency in compression of the tube, it is essential to consider all the variables like the capacitor bank, the coil, and the workpiece. In this section important equations are written in a simplified manner for a better understanding. More importance is given to the equations involved in tube compression by EM forming process.

This section is divided into three parts,

I. Analytical calculations involved in finding the induced current in the tubular workpiece.
II. Finding out the magnetic pressure developed over the tubular workpiece and showing the significance of skin depth in EM forming process.
III. These equations help to design an EM forming coil and to understand the inner mechanism of the process. Maxwell equations which define all the laws, which are applied to EM forming process. Fully coupled EM mechanical module used in LSDYNA software, which is used for carried out simulations in this thesis is discussed in Chapter 4, Section 4.3 in detail.

**I. Analytical calculation of the current $I_1$ in the capacitor bank and of the $I_2$ in the induced workpiece**

The EM is forming machine consist of a capacitor bank $C_c$, circuit resistance $R_c$ and the inductance $Lc$. The forming coil consists of $I_1$, $L_1$, and $R_1$, surrounding the workpiece $I_2$, $L_2$, and $R_2$. The equivalent circuit diagram is shown in Figure 2.15.

The discharge current through the capacitor of an equivalent RLC circuit is given by the differential equation as shown below as given by equation (2.1) and equation (2.2) (Siddiqui, 2009)

$$(L_1 + L_c)\frac{dI_1(t)}{dt} + M\frac{dI_2(t)}{dt} + (R_1 + R_2)I_1(t) + \frac{1}{c}\int I_1(t)dt = 0 \quad (2.1)$$

$$\frac{d(L_2 I_2)}{dt} + \frac{d(MI_1)}{dt} + R_2 I_2 = 0 \quad (2.2)$$

Taking some assumptions and neglecting the variations of parameters $L_2$, $M$, $R_2$, during the forming process, the approximate solution is given as,

$$I_1(t) = \frac{U_o}{\omega L_E}\left(e^{-\delta t} sin\omega t\right) \tag{2.3}$$

$$I_2(t) = \frac{U_o M}{L_1 L_2(\omega^2 + (\alpha - \delta)^2)}\left\{\frac{\omega^2\delta(\alpha - \delta)}{\delta} e^{\delta t} sin\omega t + \omega e^{-\delta t} cos\omega t - \omega e^{-\delta t}\right\} \tag{2.4}$$

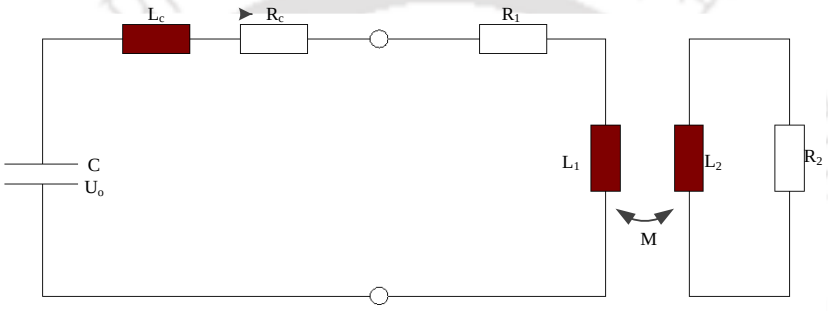


Figure 2.15 Equivalent circuit of the EM forming system

where,

$$\omega^2 = \frac{1}{L_E C_c} - \left(\frac{R_E}{2L_E}\right)^2 \tag{2.5}$$

$$\delta = \frac{R_E}{2L_E} \tag{2.6}$$

$$\alpha = \frac{R_2}{L_2} \tag{2.7}$$

$$L_E = L_c + L_1 - \frac{M^2}{L_2} \tag{2.8}$$

$$R_E = R_c + R_1 + \left(\frac{M^2 R_2}{L_2^2}\right) \tag{2.9}$$

$L_E$ is equivalent system inductance and $R_E$ is equivalent system resistance. It can be seen clearly that, primary current $I_1$, is a sinusoidal damped current pulse. The current $I_2$ in the workpiece shows a phase shift and an additional attenuation.

## II. Calculation of magnetic pressure

From the equation (2.1) and (2.3) of the discharge current and the energy balance:

$$E_o = \frac{1}{2}C_c U_o^2 = \frac{1}{2}(L_c + L_1)I_1^2 + \frac{1}{2}L_2 I_2^2 - M I_1 I_2 + \int_0^1 \left((R_c + R_1)I_1^2 + R_2 I_2^2\right)dt + \frac{1}{2}\left(\frac{I_1^2}{C_c}\right) + E_{mec} \quad (2.10)$$

Here $E_o$ is the stored energy of the charged capacitor, while $E_{mec}$ is the mechanical energy taken from the discharge circuit, which is given as,

$$E_{mec} = \int_{r_0}^{r} \left(\frac{1}{2}\frac{dL_2}{dr} I_2^2 - \frac{dM}{dr} I_1 I_2\right)dr \quad (2.11)$$

With some assumptions like during forming process, only the radius of the workpiece will change, irrespective of its length $l_o$. The geometry of the coil and tubular workpiece is shown in Figure 2.16.

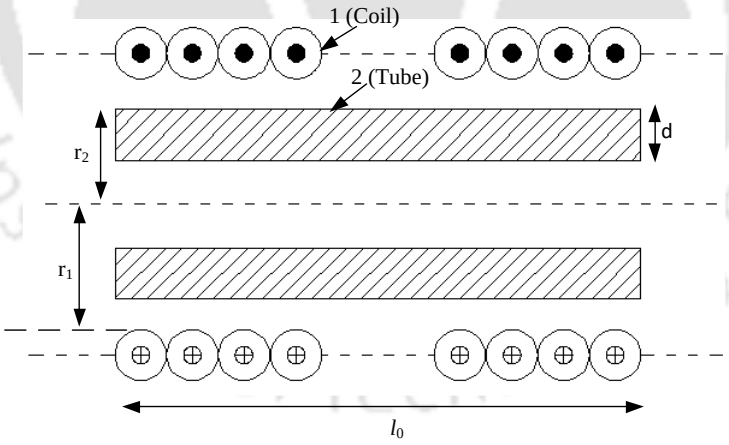


Figure 2.16 Geometry of coil (1) and the tubular workpiece (2)

With the skin depth $S$ ($S_1$ and $S_2$ for coil and workpiece) of the electric current, effective radii is defined as,

$$R = r_1 + \frac{S_1}{2} \quad (2.12)$$

$$r = r_2 - \frac{S_2}{2} \tag{2.13}$$

If $S_2 > d_0$, we replace $S_2$ by $d_0$.

So, the mechanical work done by a magnetic pressure $p$, acting on the workpiece surface can be given as,

$$E_{mec} = \int_{r_o}^{r} (2\pi l_0) p dr \tag{2.14}$$

Thus we get the magnetic pressure,

$$P = \frac{\frac{1}{2}\frac{dL_2}{dr} I_2^2 - \frac{dM}{dr} I_1 I_2}{2\pi r l_o} \tag{2.15}$$

By assuming, ideal arrangement of coil and the workpiece,

$$L_2 = \frac{\mu \pi r^2}{l_o} \tag{2.16}$$

$$M = \omega L_2 \tag{2.17}$$

So, the pressure $P$ can also be written as,

$$P(t) = \frac{\mu}{2} \frac{U_o^2 n^2}{\omega^2 L_E^2 l_o} \left\{ e^{2\delta t} \sin^2 \omega t - \left[ \frac{\alpha}{\omega \left( 1 + \left( \frac{\delta}{w} - \frac{\alpha}{\omega} \right)^2 \right)} \right]^2 \left[ \left( \frac{\alpha}{\omega} - \frac{\delta}{\omega} \right) e^{\delta t} sin\omega t - e^{-\delta t} sin\omega t - e^{-\delta t} cos\omega t + e^{\alpha t} \right]^2 \right\} \tag{2.18}$$

It can be seen that the important parameter which significantly affects the pressure is $\alpha/\omega$. So, for maximum pressure,

$$\frac{\alpha}{\omega} \ll 1 \tag{2.19}$$

To be more simplified,

$$\frac{\alpha}{\omega} = \frac{R_2}{\omega L_2} = \frac{2}{\omega \mu \sigma d_0 r_o} = S_2^2 / r_o d_o \tag{2.20}$$

$$S_2 = \sqrt{\frac{2}{\sigma\mu\omega}} \tag{2.21}$$

where $S_2$ is the skin depth. So, considering the conductivity as one of the most important parameter, copper and aluminium will be the most suited materials for EM forming. So, the important second conclusion was drawn that, for the maximum pressure $C$ need to be as large as possible. Also the number of turns per unit length $n/l_o$ need to be higher, and a low inductance and resistance of machine unit will be the important criteria.

## 2.8 Gaps in literature

Till now, none of the researchers has attempted to provide an alternative contactless terminal-wire crimping process. Even though work has been reported in EM forming, but no attempt was carried out in this field of terminal-wire crimping process. Some challenging issues are as follows:

- It is important to design a suitable EM crimping helical coil to achieve a uniform deformation of the terminal, higher pull-out strength, minimum contact resistance, higher contact length between the terminal and the wire strands to reduce voids.
- Selection of parameters like the coil length, the coil wire diameter, the coil pitch, the inner coil diameter for stand-off distance for designing of the helical coil.
- Comparison using numerical simulation and experiment on different types of the helical coil for finding the best suitable coil for crimping while keeping the parameters like coil length and coil cross-section is a complicated process. The numerical simulation takes more time as it involves a large number of contact properties and EM-structural coupled analysis.
- Comparison of different type of field-shapers using the numerical and experimental approach on geometries like the single step, double step, and tapered geometries by keeping the total length, the effective working area and the slit width is a challenging task. Due to the double mutual interaction between the primary coil-field shaper and field shaper- workpiece, numerical simulation becomes difficult.

The research plan is shown in Figure 2.17.

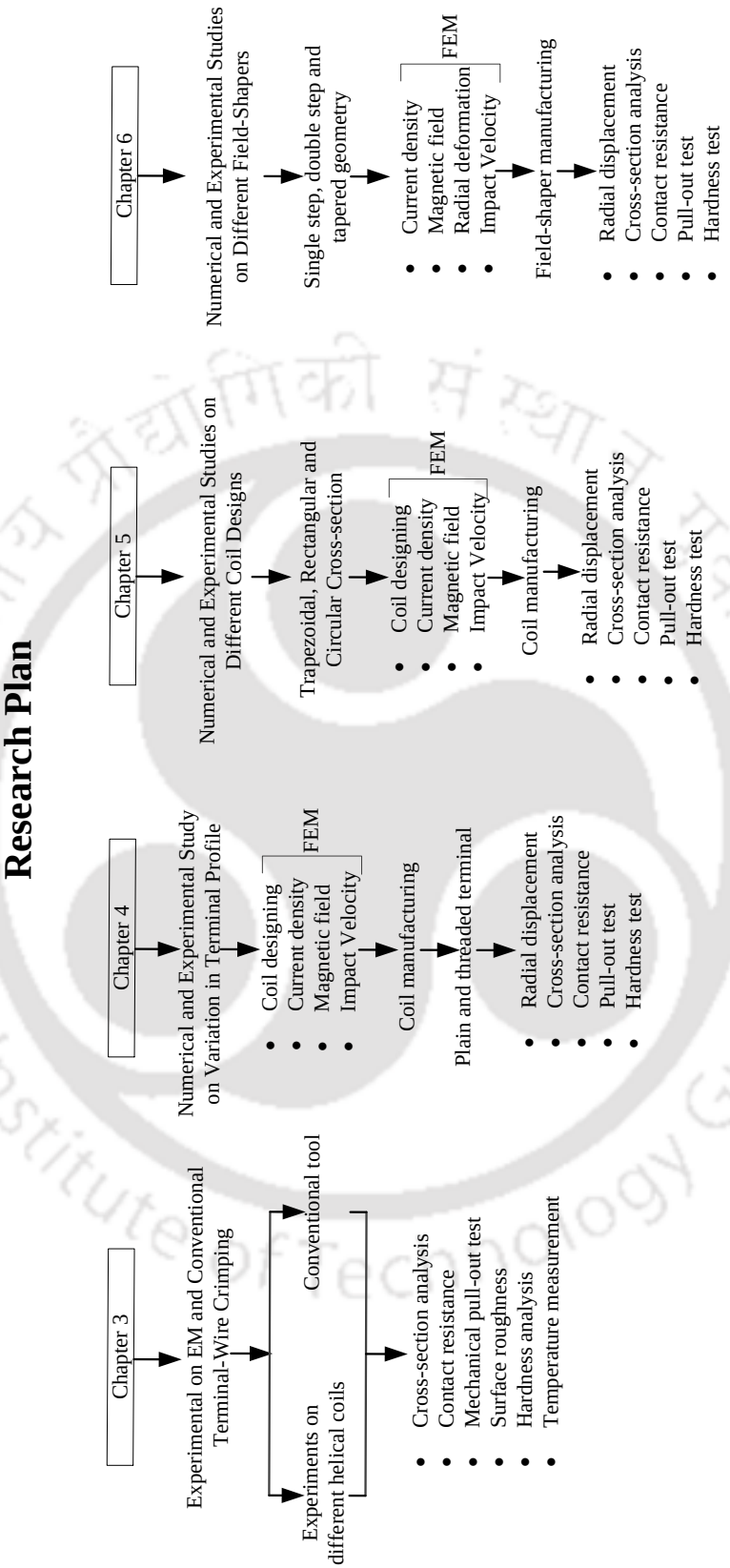


Figure 2.17 Research plan in the form of flow chart

# Chapter 3

## 3 Experiment on EM and Conventional Terminal-Wire Crimping

### 3.1 Materials and Experiment

In the previous chapter, a literature review was carried out on EM tube expansion, EM tube crimping, Field-shapers, and conventional wire crimping process. This chapter will explain experimental procedures, the equipment used for the post-processing and experiment on EM and conventional terminal-wire crimping process.

#### 3.1.1 Materials

In this section, all the material, machine and equipment directly involved throughout the research work will be addressed. The workpiece material chosen for this thesis work was aluminium alloy AA1050 of different diameter terminals while the coil material was of Copper. The composition of the material AA1050 is composed of many elements as shown in Table 3-1. Material characteristic of AA1050 and Copper is shown in Table 3-2.

Table 3-1 Material composition of AA1050 (Alves et al., 2010)

| Element | Al | Si | Fe | Cu | Mn | Mg | Zn | Ti | Others |
|---|---|---|---|---|---|---|---|---|---|
| Weight % | 99.5 | 0-0.25 | 0-0.4 | 0-0.05 | 0-0.05 | 0-0.05 | 0-0.07 | 0-0.05 | 0-0.03 |

Table 3-2 Material properties of workpiece and coil (Jeanson et al., 2016)

| Materials | Density | Thermal Expansion | Conductivity | Poisson's Ratio |
|---|---|---|---|---|
| AA1050 | 2.71 g/cm$^3$ | $23.1 \times 10^{-6}$ K$^{-1}$ | $3.68 \times 10^7$ S/m | 0.35 |
| Copper | 8.96 g/cm$^3$ | $16.7 \times 10^{-6}$ K$^{-1}$ | $5.96 \times 10^7$ S/m | 0.36 |

Before carrying out experiments, it was essential to find the composition and material properties of the terminal. For uniformity in the research work, all the terminals were purchased from the same manufacturing industry. Electron Discharge X-ray (EDX) over the terminal was carried out for the confirmation of the material property and was found to be AA1050 as shown in Figure 3.1.

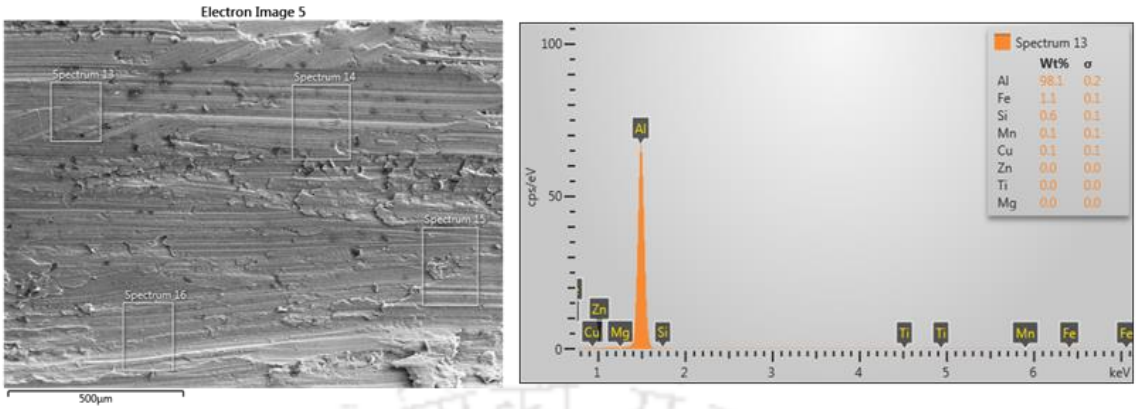


EDX over the terminal surface Chemical composition

Figure 3.1 EDX and chemical composition of the terminal

### 3.1.2 EM Machine and Equipment for Post-Processing

For carrying out EM crimping experiments EM processing machine was used. Control panel was HMI controlled, which allows the variation of the discharge voltage through the EM processing machine. The experimental setup is shown in Figure 3.2. Machine parameters are provided in Table 3-3.

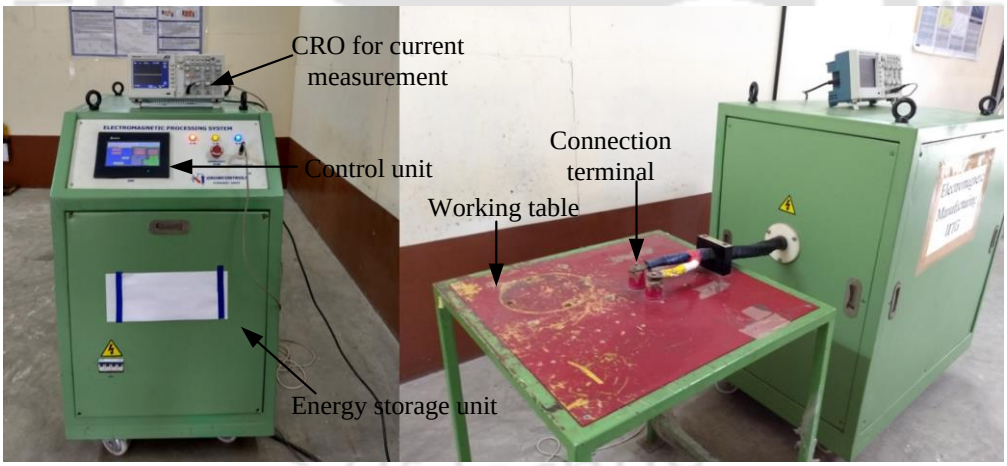


Figure 3.2 EM forming system available at IIT Guwahati

Table 3-3 EM machine parameters

| | | |
|---|---|---|
| Circuit | Capacitor bank | 90 µF |
| | Maximum energy | 10 kJ |
| | Maximum voltage | 15 kV |
| | Circuit inductance | 0.7 µH |
| | Circuit resistance | 12.5 mΩ |

For measurement and carrying out post-processing of the samples, different types of equipment are used as shown in Figure 3.3, which were calibrated before taking the readings to avoid any error.

(a) Oscilloscope for current measurement

(b) RLC measuring equipment

(c) Optical microscope

(d) Digital microscope


(e) Universal testing machine


(f) Vicker hardness testing machine

Figure 3.3 Testing equipments used for post-processing

## 3.2 Experimental Procedure

In this chapter, EM terminal-wire crimping is carried out with different parameters and analyzed with conventional crimping process. A new method of crimping is developed for terminal-wire crimping that can be an alternative option for existing traditional crimping of wire. The experiment aims to give advantages in uniform terminal deformation, minimum electrical contact resistance, high pull-out strength, excellent surface finish, increased hardness number and improved thermal property.

### 3.2.1 EM Terminal-Wire Crimping Coil

The EM wire crimping process utilizes a helical coil of copper material to concentrate the magnetic field. For carrying out the experiments, dimensions of the workpiece are included in Table 3-4, and machine specification as listed in Table 3-3. A standoff distance (SOD) was varied for the deformation process. A SOD is a distance kept between the coil and workpiece, where mutual interaction develops the magnetic pressure.

Table 3-4 Workpiece dimensions

| | | |
|---|---|---|
| Workpiece | Outer diameter of terminal connector | 12 mm |
| | Inner diameter of terminal connector | 10 mm |
| | Length of terminal connector | 27 mm |

Table 3-5 Variation done in coil geometry for finding the suitable coil for crimping

| | Coil Crossection Diameter (mm) | No. of turns | Gap (mm) | SOD (mm) | Total length (mm) | Inner diameter of coil (mm) | Terminal deformation (mm) | Remarks |
|---|---|---|---|---|---|---|---|---|
| Coil 1 | 4 | 4 | 1 | 0.5 | 20 | 13 | 3.0 | Non uniform |
| Coil 2 | 4 | 5 | 0.8 | 0.6 | 24 | 13 | 3.1 | Non uniform |
| Coil 3 | 5 | 4 | 1 | 0.6 | 25 | 13 | 2.9 | Less deformation and non uniform |
| Coil 4 | 5 | 5 | 0.8 | 0.5 | 29 | 13 | 3.2 | Uniform and maximum deformation |

It was important to predict the suitable parameters of the helical crimping coil. Parameters like pitch, coil length, number of turns and diameter of the cross-section of copper wire

used are included in Table 3-5. Different coils used for the EM wire crimping process are shown in Figure 3.4. Experiments were conducted using four different coil geometries as shown in Figure 3.5. It was found that the coil 4 produced the maximum deformation with uniformity along the axis. Hence, coil four which provided the best results was used to carry out further experiments and compared to conventional crimped samples.

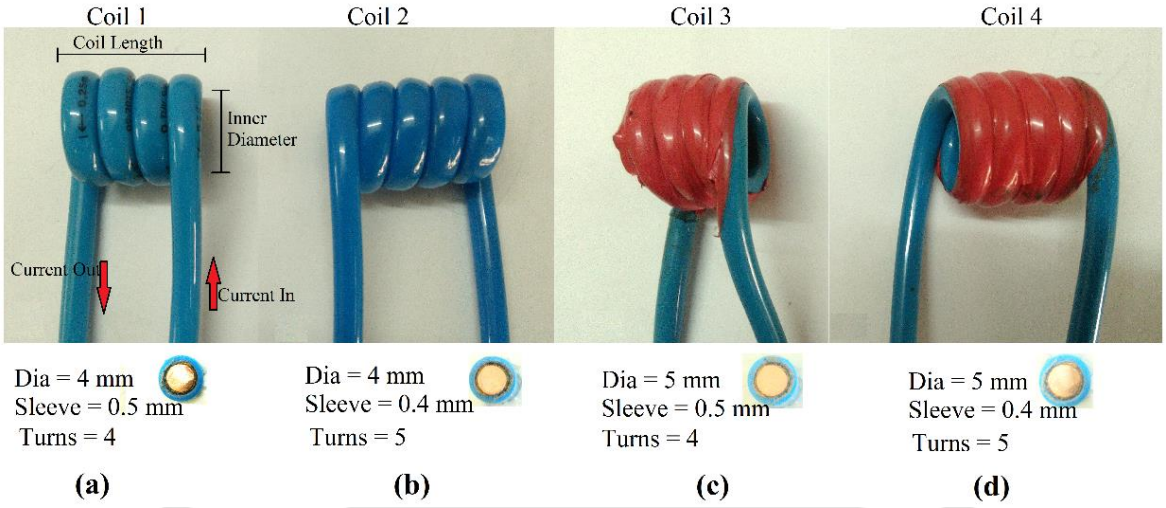


Figure 3.4 Different types of experimental coil used for the crimping process

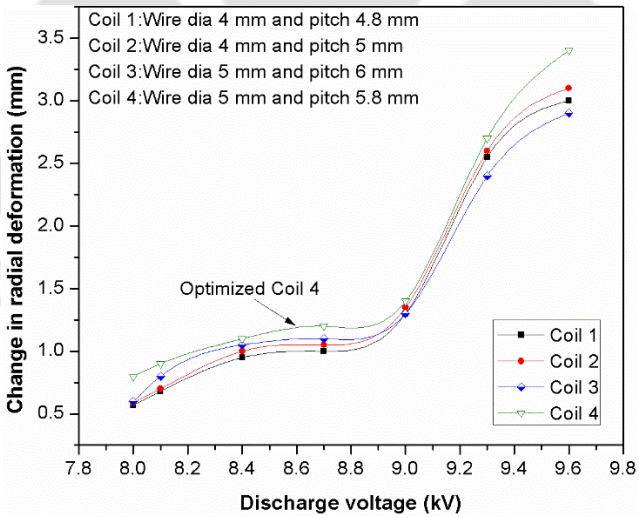


Figure 3.5 Change in radial deformation for different types of the helical coil

After obtaining the most suitable coil, experiments were carried out at various discharge energy to study the influence of EM high strain rate deformation process on terminal-wire crimping applications on multiple parameters which are discussed in subsequent section.

## 3.3 Experimental Work Carried out on the Optimized Coil

A five-turn solenoidal copper coil four was used to carry out the experiments. The isometric view of coil cross-section with an aluminium terminal and copper wire strands can be seen in Figure 3.6. Experiments were carried out at different voltages from 8.1 kV to 9.6 kV for crimping the samples. The standoff distance of 0.5 mm between the coil and the terminal connectors was kept constant for different iterations of the experiment.

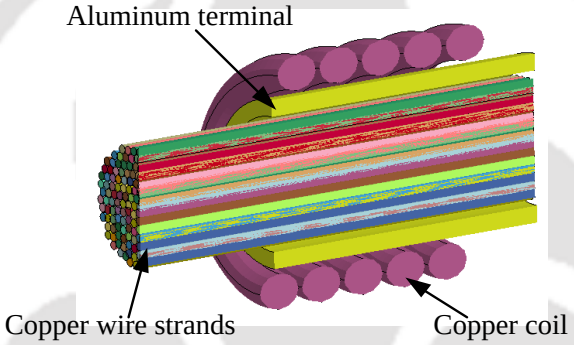


Figure 3.6 Modelled cross-sectional view of the assembly

Discharge energy for various discharge voltages is calculated and shown in Figure 3.7, and crimped samples are shown in Figure 3.8.

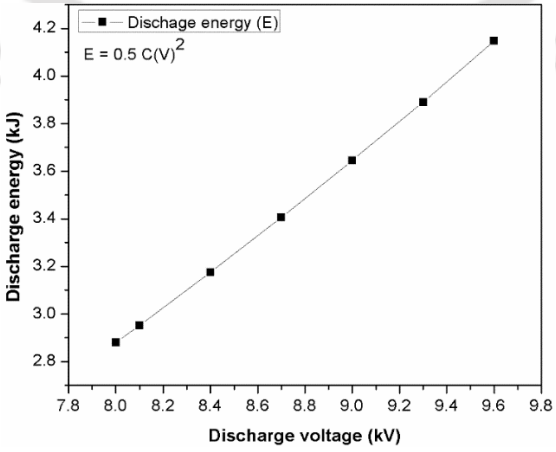


Figure 3.7 Variation in discharge energy for different discharge voltage


Figure 3.8 EM crimped samples at various discharge energy

With the increase in discharge voltage deformation of terminal kept increasing due to increase in magnetic pressure. At discharge energy of 4.1 kJ maximum radial deformation of 3.4 mm was obtained and as per the standard of crimping of 35 $mm^2$ a deformation of 3.34 mm is required to avoid damage inside the terminal ("Connectivity TE," n.d.). Variation of current with time was obtained from a Rogowski coil as shown in Figure 3.9. The current waveform measures different parameters such as amplitude, frequency, rise time and time interval. Frequency was calculated to be 20 kHz which remained constant throughout the experiments and value of current was found to be 127 kA for discharge energy of 2.8 kJ.

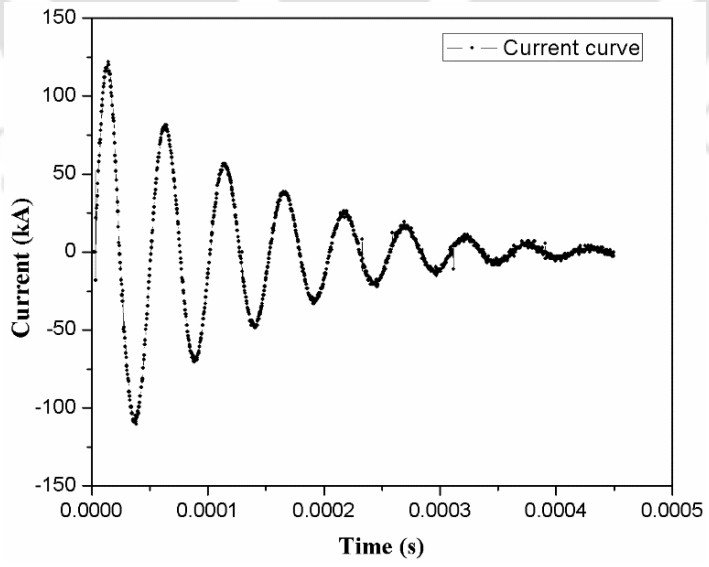


Figure 3.9 Damped current graph obtained in experiments for 2.8 kJ energy

## 3.4 Conventional Crimping

The commonly used crimp shape for cable terminal connector is the hexagonally shaped crimp as this crimp profile is best suitable for copper and aluminium conductors. The advantage of a hexagonally shaped crimp is the uniformity of radial forces which are applied consistently from all directions and over a whole area during the crimping operation. Due to the uniform compression, the hexagonal shaped crimp is used for medium and high voltage applications ("Klauke," n.d.).


(a) Conventional crimping tool (b) Conventional crimped samples

Figure 3.10 Samples crimped using conventional crimping tool

Hence, EM terminal-wire crimping process is compared with the standard hexagonal shaped crimping conventional tool. Crimped samples for both methods were of same materials. Crimping tool and samples crimped using traditional crimping tool are shown in Figure 3.10

## 3.5 Result and Discussion

### 3.5.1 Cross-Section Analysis

Comparison of the cross-section of EM and traditional terminal-wire crimping process was carried out using upright optical microscope at 20X. Images of the cross-section are shown Figure 3.11, Where (a) compressed wire strands of conventional crimped sample (b) conventional sample (c) gap between wire strands and a compressed terminal of the conventional sample (d) compressed wire strands of EM crimped sample (e) EM sample (f) gap between wire strands and a compressed terminal of EM sample.

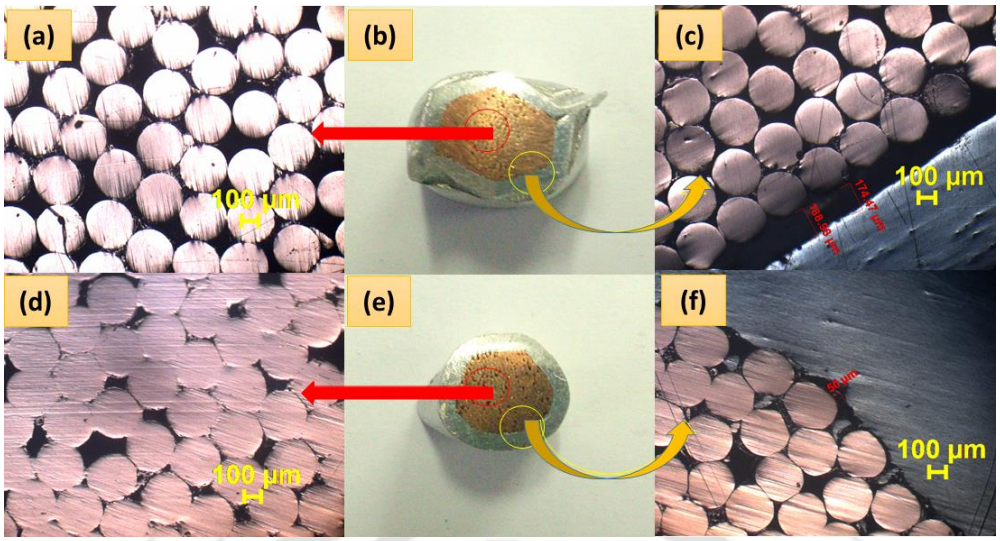


Figure 3.11 Cross-section of crimped samples under an optical microscope

It was found that compression done using EM process was more effective than conventional crimping process as compression of wire strands was higher, giving denser compaction of wire strands where the minimum gap was observed. A gap of 50 µm between the copper wire strand and the aluminium terminal exists for EM crimping process, while in traditional crimping, a gap of 174 µm was observed. It was also found that due to uniform pressure generated by a helical coil in EM process a consistent, uniform deformation of the aluminium terminal was obtained compared to a conventional method.

### 3.5.2 Electrical Characterization

In terminal-wire crimping process, it is essential to know the value of contact resistance. The electrical resistance of the samples was measured using Hewlett Packard 4263B LCR meter as illustrated in Figure 3.12. The probe used was initially calibrated to avoid any error. While measuring all the crimped sample length of 50 mm was cut for comparison. Insulation over the wire strands was carefully removed for connecting probe. As shown in Figure 3.13, it was found that EM crimped samples gave lower resistance value by 4.4 µΩ compared to conventional crimped samples. With the increase in the discharge energy, resistance value kept decreasing and became constant after 4.0 kJ due to the maximum compaction of copper wire strands.

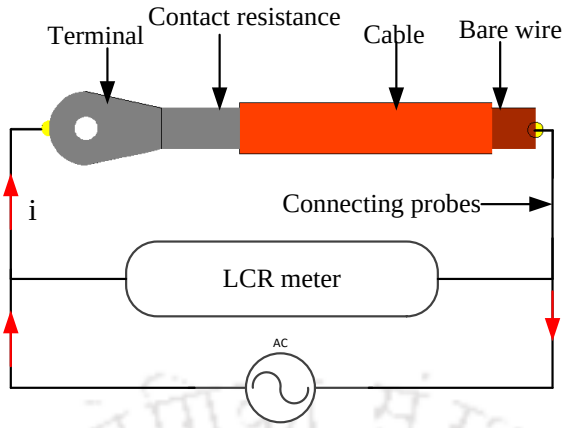


Figure 3.12 Contact resistance measuring setup

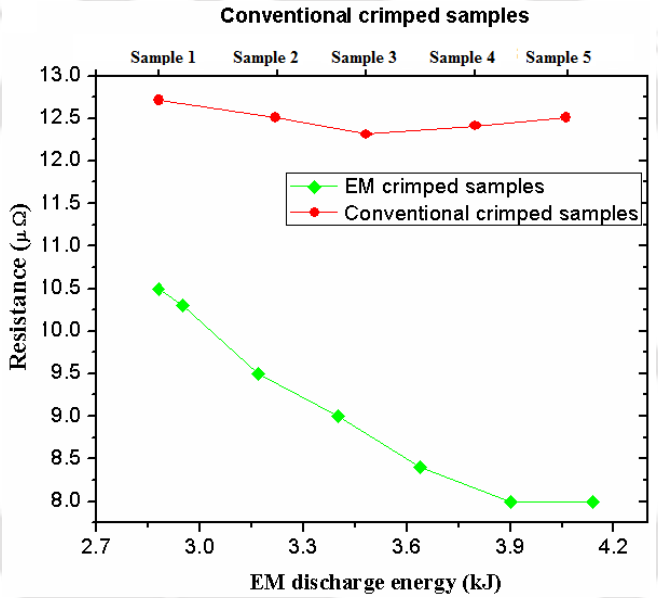


Figure 3.13 Comparison of resistance value for EM and conventionally crimped samples

The effect of high impact velocity may result in the cleaning of the oxide layer and moisture content between the contact surfaces. While in conventional crimped samples a higher value of resistance was found. Which also shows that a complete compression of wire strands using a hexagonal crimp or standard crimping die is not possible which is a highly used tool for compression of the aluminium terminal over the copper wire strands in industry. As the moisture and oxides always remain between the terminal and wire due to quasi-static die compression process in conventional crimping process, this results in increase in the contact resistance.

### 3.5.3 Mechanical Pull-Out Testing

Comparison of pull out load value between EM and conventional crimping was carried out. The arrangement of the pull-out process of a wire crimped sample is shown in Figure 3.14.

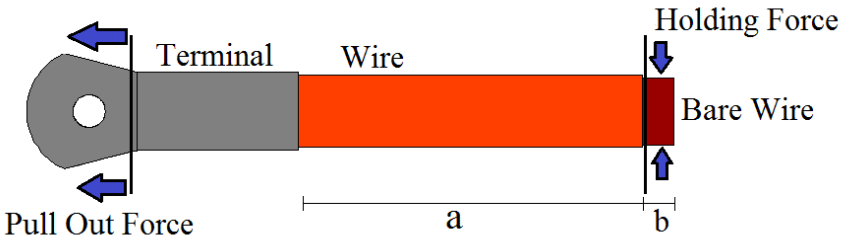


Figure 3.14 Configuration of pull-out test for terminal crimped over cables

Standard procedure for cable pull-out test was carried out where a transverse speed of 50 mm/min was maintained (Use, 2003). For holding wire at one end, insulation over the wire was stripped for effective gripping to prevent any slip (where a: 165 mm, b: 15 mm).

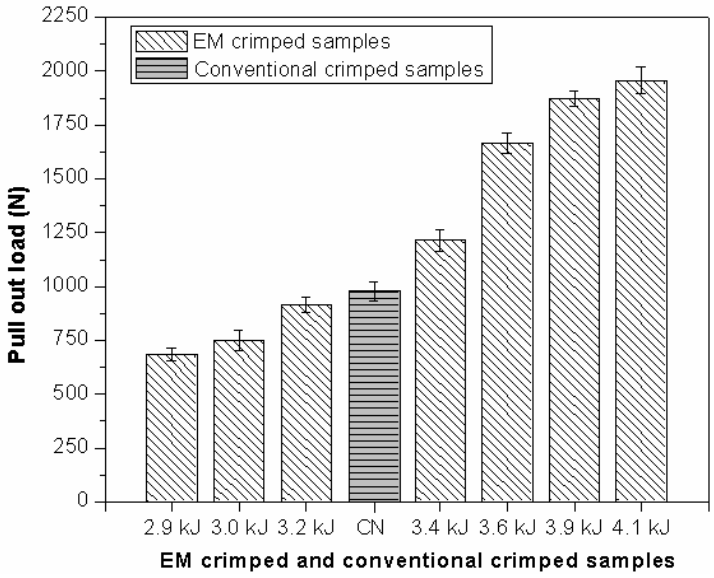


Figure 3.15 Comparison of pull out value between EM and conventionally crimped sample

Pull-out load for EM crimped, and conventional crimped samples are shown in Figure 3.15. Pull out load of 685 N, 750 N and 913 N was observed for samples crimped at 2.9 kJ, 3.0 kJ and 3.2 kJ. These values are below the load value of 980 N, which was obtained

by conventional crimping process. As per the standard minimum, pull-out value for 35 $mm^2$ crimped sample is 801 N ("Quality C Rimping," n.d.). As the discharge energy was increased above 3.4 kJ to 4.1 kJ, the value of pull-out exceed the conventional crimped sample for the terminal deformation value of 3.34 mm.

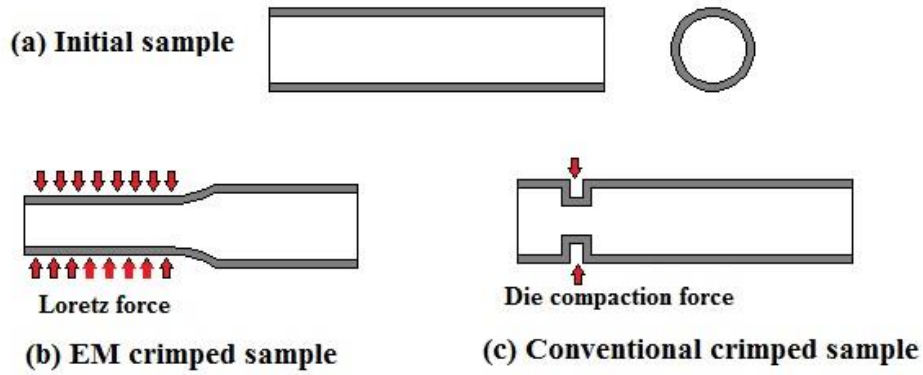


**Figure 3.16** Comparison of deformation of a terminal in EM and conventional crimped

The maximum value obtained for 4.1 kJ was found to be 1958 N which is 978 N more than the conventional crimped sample, which is due to the increase in deformation with the rise in discharge energy and uniform radial compaction as illustrated in Figure 3.16. While in conventional crimping process only terminal coming in contact with die to get crimp resulting in lesser pull-out strength.

### 3.5.4 Surface Roughness

The surface roughness was measured on the outer surface of the terminals which was deformed on the application of magnetic pressure and conventional tool die pressure in crimping process. It was measured using a surface profilo meter as illustrated in Figure 3.17. As shown Figure 3.18, an average roughness value of 0.8 µm on EM crimped samples while the value of 2.4 µm on the conventional sample was found. It was found that traditional process of crimping leads to increases in surface roughness due to contact between crimping tool and the terminal connector. EM crimping process being contactless crimping process uses generated Lorentz force resulting to a smoother surface with a lower value of the average surface number of 0.8 µm.

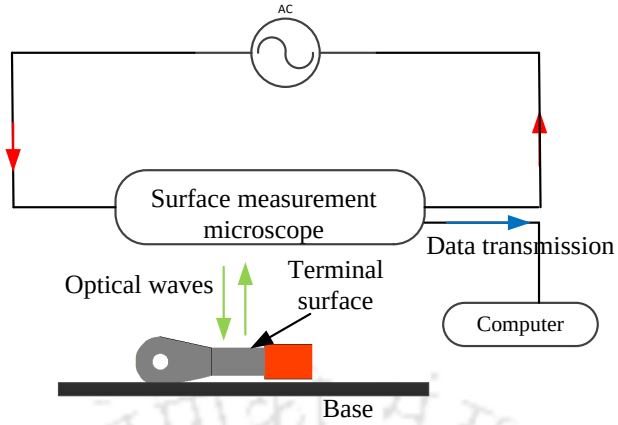


Figure 3.17 Surface roughness measurement over the crimped samples

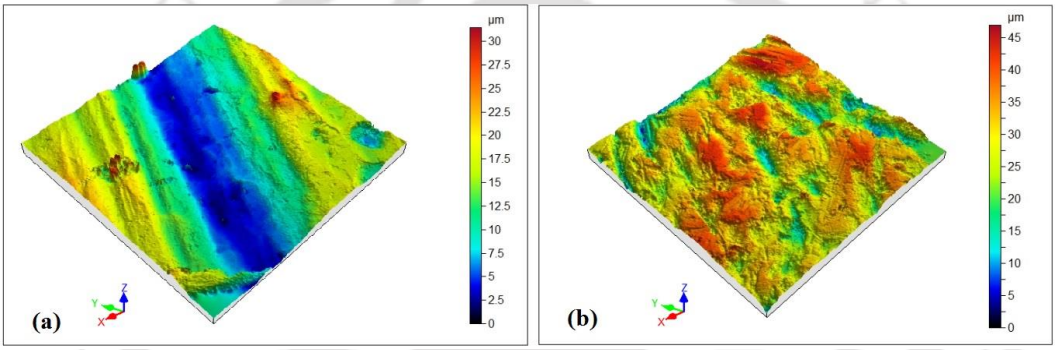


Figure 3.18 Surface roughness of the area exposed to crimping (a) EM crimped, and (b) Conventional crimped

### 3.5.5 Hardness Analysis

By adjusting the parameters of the EM field, compressive residual stress can be introduced along the surface to get peening effects (Golowin et al., 2007). This compressive residual stresses due to EM peening keeps varying with the thickness of the workpiece. The Vickers hardness test was carried across the cross-sectioned sample of EM and conventional crimped sample on different locations as shown in Figure 3.19. For testing, the 100 gram force was chosen. It can be seen from Figure 3.20, in EM crimped sample the hardness of connector terminal increases with the increase of the discharge energy. The hardness has a drastic rise moving away from the contact surface. The most substantial value of 47 was obtained for 4.14 kJ of discharge energy.

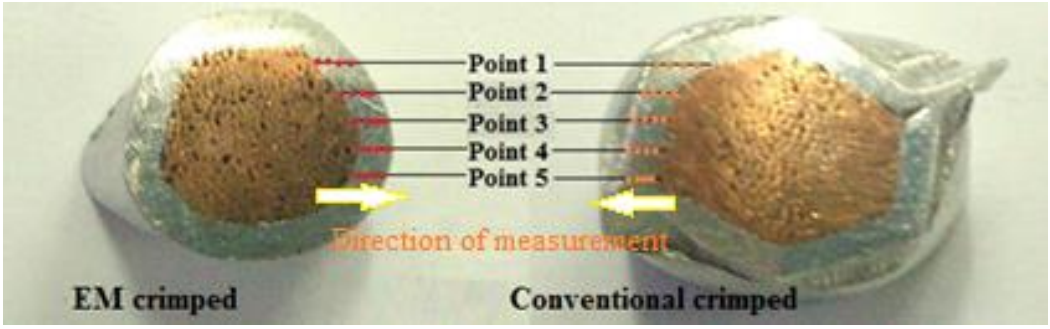


Figure 3.19 Cross-section area for measuring Vickers hardness test

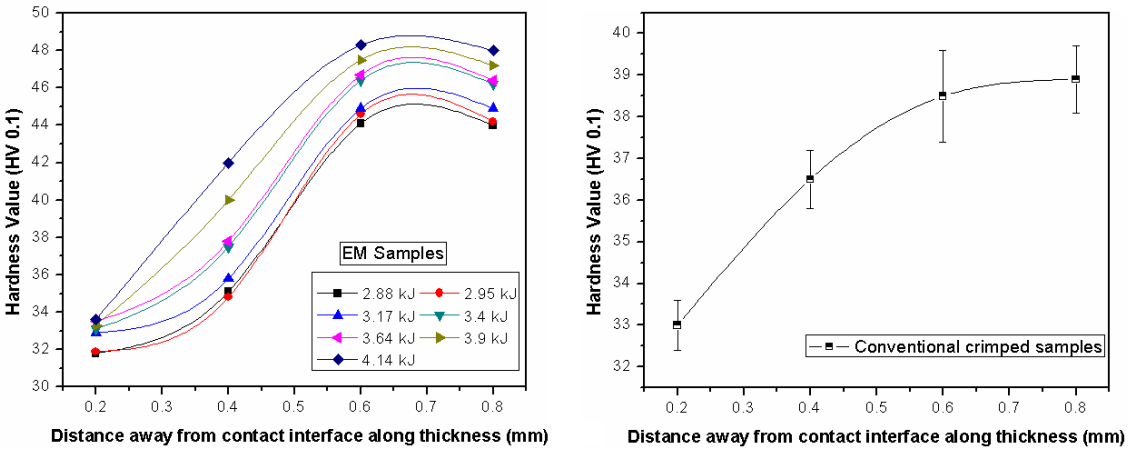


Figure 3.20 Vickers hardness value carried over the crimped samples

While in conventional crimping process a maximum value of 39.6 was obtained. Increase in hardness along the thickness is due to more compressive residual stresses developed by EM process compared to conventional crimping process. To find the compressive residual stresses X-ray diffraction (XRD) technique was used. Residual stress analysis is determined where only the peak shift occurs. As shown in Figure 3.21 any change in the lattice spacing, results in a corresponding change in the diffraction angle 2θ. Measuring the difference in the angular position of the diffraction peak provides the data for calculation of residual stress of the sample lying in the plane of diffraction, which contains the incident and diffracted X-ray beams.

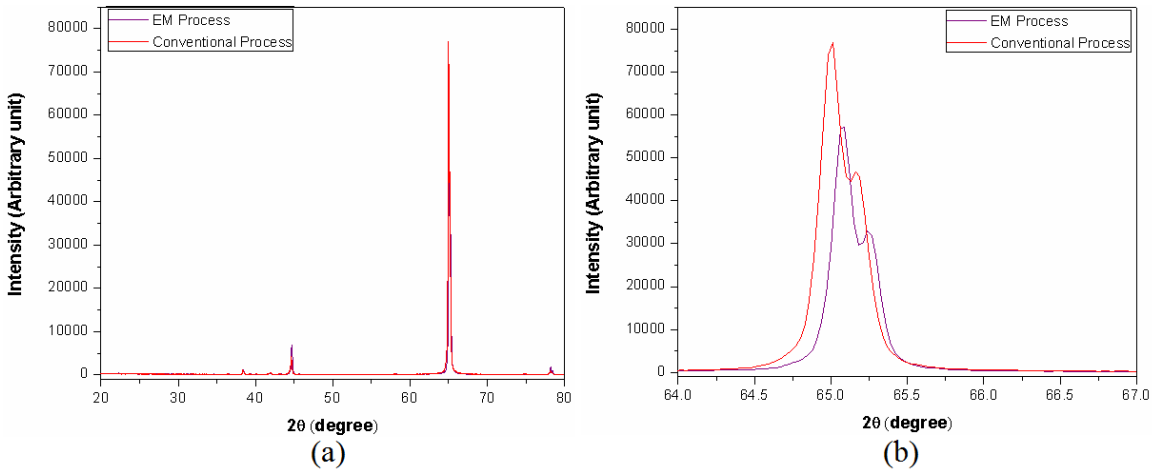


Figure 3.21 XRD analysis of EM and conventional crimped sample

Williamson Hall method was used to calculate the induced strain utilizing the equation (3.1):

$$\beta cos\theta = \left(\frac{k\lambda}{d}\right) + (4\eta sin\theta) \qquad (3.1)$$

where $d$ is the lattice spacing, $\lambda$ is the wavelength of radiation, $\kappa$ is constant with a value of 0.94, $\beta$ is the peak width, $\eta$ is strain induced due to crystal distortion, and $\theta$ is peak position. Here residual strain was given by Y-intercept, and the value of EM crimped sample and the conventional crimped sample was found to be 0.00184 and 0.00162.

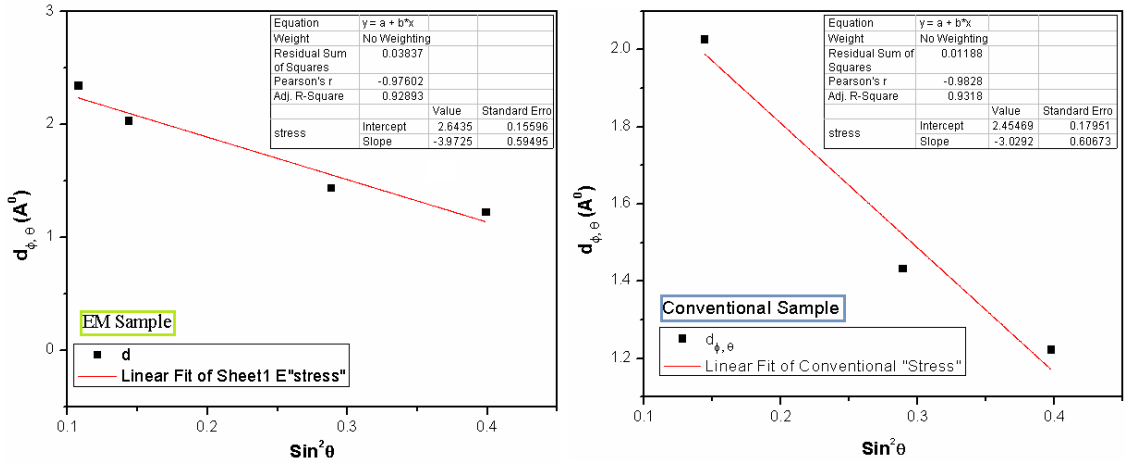


Figure 3.22 Stress calculation from the slope obtained from the peak points from XRD data for (a) EM crimped sample and (b) Conventionally crimped sample

Applying Hooke's law approximations residual stress was calculated using the equation (3.2):

$$\beta cos\theta = \left(\frac{k\lambda}{d}\right) + \left(\frac{4\sigma sin\theta}{Y}\right) \quad (3.2)$$

Where $\sigma$ is the stress of the crystal and $Y$ is the modulus of elasticity. This equation slope represents residual stress as shown in Figure 3.22. Value of residual stresses for EM crimped sample and the conventional crimped sample was calculated to be 3.972 MPa and 3.029 MPa. This increases in compressive residual stresses Due to the higher compressive residual stress along the thickness in EM crimping process resulted in the improvement of the mechanical property compared to conventional crimped samples.

### 3.5.6 Temperature Measurement

In a circuit, the too high electrical current passage can cause overheated. This additional heat is detrimental to the integrity of the termination means, conductor insulation and even the overcurrent protective device which transfers into the devices through the terminals.

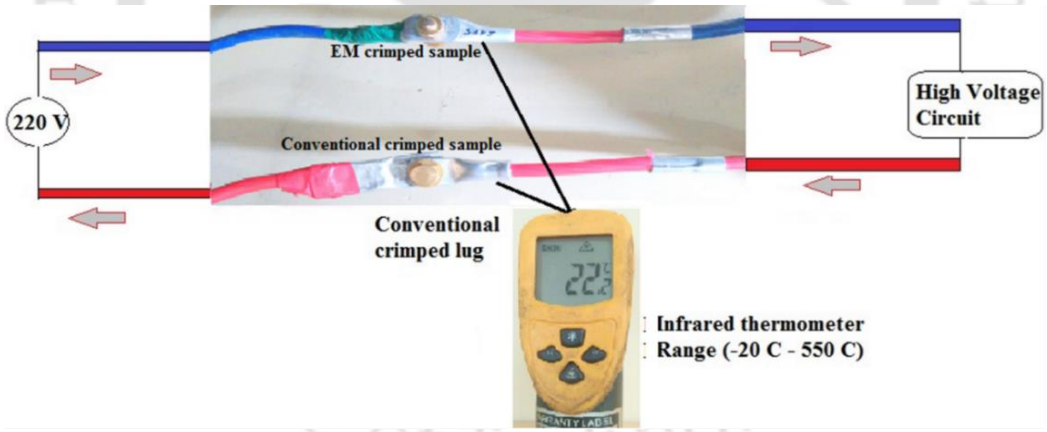


Figure 3.23 EM crimped and a conventional crimped terminal connected to a high power consumption unit

Excess heat could cause integrity issues. If there were loose terminal connections, then:

a) The terminal might overheat, and the insulation might break down, which could lead to a fault, typically line to ground. Conductors of different potential were

touching, the insulation of both may deteriorate, and a phase-to-neutral or phase-to-phase fault might occur.

b) Arcing could occur between the terminal and wire strands.

The test was carried on EM crimped terminal and conventional crimped terminal, where both the terminals were connected to a high power consumption device as shown in Figure 3.23. The test was carried out for 12 hours where the temperature of the terminals was measured periodically after 30 minutes using an infrared thermometer with a precision of 0.5 ℃.

The experiment was carried at controlled room temperature of 25 ℃. It was observed that temperature rise in both the terminal took place as shown in Figure 3.24. Near room temperature the electrical resistance of the material increased linearly with rising temperature and the resistance equation (3.3) is given by,

$$R = R_0\,(1+\propto(\Delta T)) \qquad (3.3)$$

Where $R_o$ is the initial resistance of the metal, $\propto$ is temperature coefficient of resistance (for Aluminium it is $3.9\times10^{-3}$ /℃), and $\Delta T$ is the temperature change.

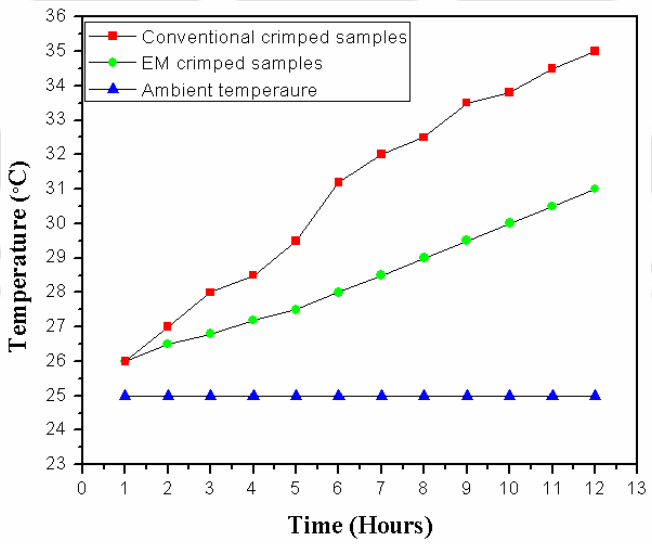


Figure 3.24 Temperature reading of EM and conventional crimped terminal

It was found that after 12 hours, the conventionally crimped terminal connector surface temperature of 35 ºC was observed and for EM crimped sample it was observed to be 31 ℃. As the resistance value was higher for the conventionally crimped sample, it resulted

in higher heat ($H_r$) dissipation compared to EM crimped sample with lower resistance value using. The heat produces in the circuit is given by equation (3.4).

$$H_r = I^2Rt \tag{3.4}$$

where *I* is the current passing through wire and *R* is the resistance. The rise in temperature even by 0.1 ℃ is vital in electronics, power consumption circuit as it may lead to fatal. Temperature over the EM crimped sample was found to be lower than the conventionally crimped sample due to the minimum change in resistance in the contact area and lower heat dissipation making it more attractive option to conventional crimping process.

## 3.6 Summary

In present chapter comparison of EM crimping and conventional crimping of the aluminium terminal to the copper wire was carried out. The main summarized points are:

- Deformation of aluminium terminal increased with the increase in discharge voltage but after 9.6 kV it remained constant as copper strands restricted further radial deformation of the terminal.
- With this method of EM terminal-wire crimping average gap was reduced by 70 % compared to conventional crimping process.
- The resistance of EM crimped samples decreased with the rise in discharge energy, and after 4.0 kJ, it remained constant as 8.1 μΩ, which was lower by 34 % compared to conventional process.
- The pull-out strength value increased with discharge energy. A maximum of 1.604 kN was observed for 4.14 kJ discharge energy while conventionally crimped sample maximum value was found to be 0.995 kN.
- The mean surface roughness value of 0.8 μm was obtained in EM crimped sample while in conventional process the value was more than 2.4 μm.
- The hardness increased up to 47 $HV_{0.5}$ for EM process while the conventional method it was 39 $HV_{0.5}$. In traditional die crimping process, the area in die contact was hardened, whereas in EM crimping complete terminal exposed to EM pressure waves was hardened.

- Temperature over the EM crimped sample showed 30.5 ℃, which was lower than the conventionally crimped sample by 4 ℃ due to the minimum change in contact resistance.

Overall, in this chapter, a comparison was carried out by comparing EM and conventional terminal-wire crimping process. Which shows that EM crimping process can be an alternative and advantageous to the existing traditional crimping process. As there is no mechanical contact between the tool coil and workpiece exists, subsequently no imprints occur on the workpiece surface which results in no cracks in the terminal as occurs in conventional crimping tool on excessive pressure. Since in EM crimping process, deformation of the terminal is easily controllable by simple adjustment of the discharge voltage. So, chances of under deformation and over deformation can easily be avoided in this process.

# Chapter 4

## 4 Numerical and Experimental Study on Variation in Terminal Profile

### 4.1 Introduction

Power cables either overhead or underground are the most essential and critical part of electricity transmission system. Transmission through overhead wire sometimes causes wildfires causing a problem in the distribution in the power lines, which results in thermal expansion of connector terminal leading to loosening the strength constraining the wire strands and eventually failure (Soulinaris et al., 2014; Tohidi et al., 2017).

In the previous chapter 3, work was carried out on the comparison of EM terminal- wire crimping process and compared it to conventional wire crimping process, showing the advantage of EM crimping method. But no numerical simulations have been carried out yet for EM terminal-wire crimping process to understand the physics occurring during the process which takes microseconds for the completion of this process.

This chapter shows the simulation carried out in the EM module of LS-DYNA module software. Simulations were carried out to find suitable coil dimensions which act as a crimping tool in EM crimping process and to find the required discharge voltage for the uniform deformation of the aluminium terminal over the copper wire strands. Results of the simulations were used for the fabrication of the coil. Experiments were carried out on the plain and threaded terminal for comparison. Results like terminal deformation, contact resistance, cross-section analysis, hardness along terminal thickness and pull-out test were carried out and discussed in subsequent sections.

### 4.2 Methodology

The schematic flowchart of the implemented method to achieve quality crimp joint is shown in Figure 4.1. The numerical simulations were carried out to find a suitable coil and to study parameters like current density, magnetic field, radial displacement and impact velocity which can provide required uniform deformation of the terminals. Coil

was fabricated using numerical simulations data to carry out the experiments on plain and threaded terminals.

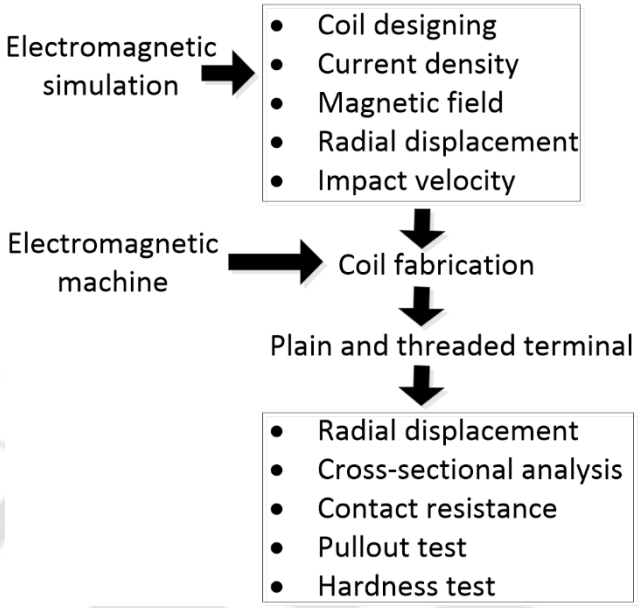


Figure 4.1 Flow chart of the implemented procedure

## 4.3 Finite Element Analysis of Electromagnetic Crimping

### 4.3.1 Fully coupled EM module in LSDYNA

In this chapter, EM module under the LSDYNA is used to perform coupled EM – mechanical simulations. Flow chart of EM-mechanical structural coupling process is shown in Figure 4.2. The EM module allows to introduce electrical current inside the solid conductor, and to compute the associated magnetic field, electric field and induced current by using the governing Maxwell equations which is solved by FEM method.

#### I. Circuit parameters

Before running numerical simulations, the first step of the modeling is the determination of the electric current running through the coil. The system of EM crimping can be represented as a transformer since it is characterized by an electric energy transfer by electromagnetic induction between the pulse generator-coil unit (primary circuit) and the workpiece (secondary circuit).

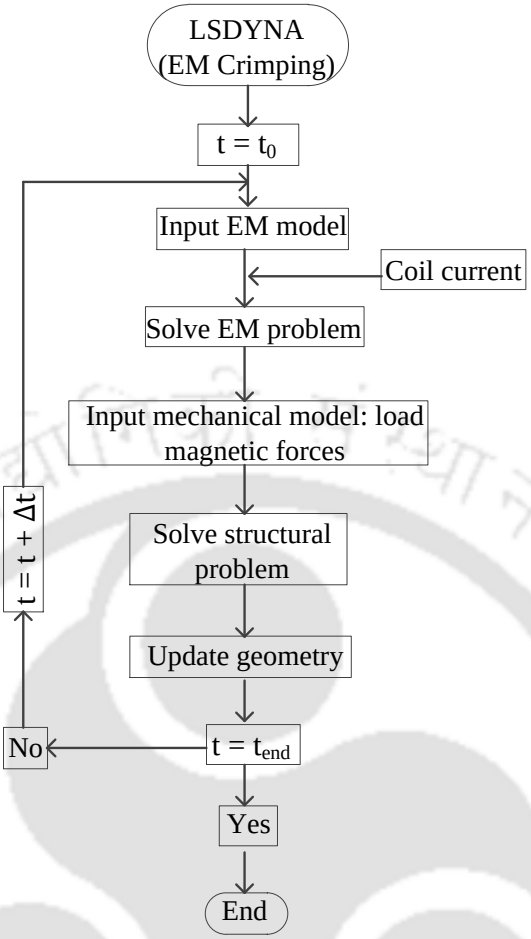


Figure 4.2 Flowchart of the EM-mechanical structural coupling process

These two circuits are coupled through a mutual inductance and are traveled by the discharge current and the induced current, respectively. Analytical portion is already discussed in Section 2.7. A damped pulsed current is the load during the EM forming process. Only initial part of the current is responsible for the plastic deformation. The current is given by equation (4.1):

$$I = U_o \sqrt{\frac{C}{L}}\, e^{-\delta t} \sin \omega t \qquad (4.1)$$

where, *Uo* is the discharge voltage, *C* is the capacitance, *L* is the inductance, $\delta$ is the damping exponent, and $\omega$ is the angular frequency. The capacity and the charging voltage are the best known and controllable parameters.

**II. EM Governing equations**

The EM model is governed by Maxwell's equations (L Eplattenier et al., 2008):

$$\vec{\nabla} \times \vec{E} = \frac{-\partial \overrightarrow{B_m}}{\partial t} \tag{4.2}$$

$$\vec{\nabla} \times \left(\frac{\overrightarrow{B_m}}{\mu}\right) = \vec{J} \tag{4.3}$$

$$\nabla . \overrightarrow{B_m} = 0 \tag{4.4}$$

$$\nabla . \varepsilon \vec{E} = 0 \tag{4.5}$$

$$\nabla . \vec{J} = 0 \tag{4.6}$$

$$\vec{J} = \sigma \vec{E} + \overrightarrow{J_s} \tag{4.7}$$

$$\vec{\nabla} \times \vec{H} = \vec{J} + \varepsilon \frac{\partial \vec{E}}{\partial t} \tag{4.8}$$

$$\vec{B}_m = \mu \vec{H} \tag{4.9}$$

where, $\sigma$ = electrical conductivity, $\mu$ = magnetic permeability, $\mathcal{E}$ = electrical permittivity, $E$ = electric field, $B_m$ = magnetic flux density, $H$ = magnetic field intensity, $\rho$ = total charge density, $J$ = total current density, $J_s$ = source current density. The divergence condition in equation (4.4) allows writing the magnetic flux density as:

$$\vec{B}_m = \overrightarrow{\nabla} \times \vec{A} \tag{4.10}$$

where, $A$ is the vector potential. Using equation (2.23) electric field is given by

$$\vec{E} = -\vec{\nabla}\emptyset - \frac{\partial \vec{A}}{\partial t} \tag{4.11}$$

where, $\emptyset$ is the electric scalar potential. By using the gauge condition it allows the separation of the vector potential from the scalar potential.

$$\nabla \cdot \sigma \vec{A} = 0 \tag{4.12}$$

Using equation (4.6, 4.7, 4.11, and 4.12) we get,

$$\nabla \cdot \sigma \vec{\nabla} \emptyset = 0 \tag{4.13}$$

Using (4.3, 4.7, 4.10, and 4.11) the induced total current density $\vec{J}$ over the workpiece can be expressed as get Maxwell equation in terms of potential as,

$$\vec{J} = \vec{\nabla} \times \frac{1}{\mu}\left(\vec{\nabla} \times \vec{A}\right) + \sigma \frac{\partial A}{\partial t} + \sigma \vec{\nabla} \emptyset \tag{4.14}$$

## III. Boundary conditions

The boundary condition is given by,

$$\vec{n} \cdot \vec{\nabla} \emptyset = 0 \; on \; \Gamma \tag{4.15}$$

$$\emptyset = \emptyset_c \; on \; \Gamma_c \tag{4.16}$$

$$\vec{n} \times \vec{\nabla} \times \vec{A} = \overrightarrow{A_c} \; on \; \Gamma \tag{4.17}$$

$$\vec{n} \times \vec{A} = A_c \; on \; \Gamma_c \tag{4.18}$$

where, $\Gamma$ represents the surface of the coil and tube, $\Gamma_c$ represents the region where the coil is connected to the external current supply. Equation (4.15) states that the gradient of the electric potential is orthogonal to the surface normal $\vec{n}$, while equation (4.16) shows that the potential at the coil current input surface is equal to the source potential i.e. connection of the conductor to a voltage source and equation (4.18) to the current source

Meshing of the air which is a very complicated part in other software. In LSDYNA it is done by using Boundary Element Method (BEM) method. The BEM method need no meshing of air surrounding the conductor. It thus significantly avoids meshing problem when complicated conductor geometries are used. Another advantage of this process is that, it removes the introduction of artificial infinite boundary conditions.

## IV. Mechanical Solver

Once the EM field has been computed, Lorentz force $\vec{f}$ is evaluated at the nodes and added to the mechanical solver. According to Maxwell's equation, the Lorentz force $\vec{f}$ is expressed by

$$\vec{f} = \vec{J} \times \overrightarrow{B_m} = \left(\vec{\nabla} \times \frac{\overrightarrow{B_m}}{\mu}\right) \times \overrightarrow{B_m} \tag{4.19}$$

Both the electromagnetic and mechanical solver each have their own time step for computing. In LSDYNA, computing the mechanical structural portion time step, it is ten

times smaller time compared to EM part. The explicit mechanical solver computes the deformation of the conductor and so the new geometry is used to compute the EM field in a Lagrangian way. In LSDYNA meshing is carried out using hexahedral element only for EM module.

The Lorentz force calculated is then substituted to the transient dynamic equilibrium equation (4.20). Knowing that the workpiece in the forming process is plastically deformed, dynamic equilibrium equation is used to evaluate the exact deformation of the workpiece at each time increment.

$$M\ddot{u} + C\dot{u} + Ku = \vec{F} \tag{4.20}$$

Where *M* represents the structural mass matrix, *C* is the structural damping matrix, *u* is the nodal displacement vector, *K* is the structural stiffness matrix, and *F* is the load vector.

If the magnetic field is completely shielded, then the charging energy of the capacitors is transferred most efficiently into a desired course and distribution of the magnetic field in the gap. Then the magnetic field inside a solenoid is given as

$$\mathrm{B_m(t)} = \frac{n}{l_o}\mathrm{I_1(t)} \tag{4.21}$$

The magnetic field *B(t)* depends on the coil current $I_1(t)$ and the number of turns per unit length $n/l_o$. If the skin depth is small in comparison to the thickness of the workpiece, the penetrated magnetic field is frequently neglected, and then the magnetic pressure is given by simple equation,

$$P = \frac{1}{2}\mu\,\vec{H}^2 \tag{4.22}$$

The highest velocity vector was observed at the collision point and the magnitude of the velocity vector reduced as the distance from the collision point increased. High velocities creates high plastic deformation and shear stress at the interface. Impact velocity $V_i$ is given by (Psyk et al., 2011),

$$V_i = \frac{B_m^2}{2\mu_o \rho s}\, t \tag{4.23}$$

where, $\rho, s$ and $t$ are the workpiece density, thickness and time in seconds.

## 4.4 Designing of EM Crimping Process

EM crimping due to high strain rate forming process takes microseconds for completion of the process. EM crimping process requires coupling between mechanical and EM field for the numerical simulations to be carried out (Chaudhary and Kore, 2016). In the current work, EM wire crimping model was designed in the EM module of LS- DYNA software which involves good coupling between mechanical and EM process.

### 4.4.1 Numerical Model

One important objective of the numerical simulations was to find suitable dimensions of the coil which is a crucial component, which creates a transient magnetic field to produce magnetic force to deform the workpiece uniformly. The manufacturing of different coil with a different pitch, wire diameter and length is a time-consuming process and an entirely expensive process. Hence, the numerical simulations were carried out, to predict the suitable coil dimensions and optimum discharge voltage required for terminal deformation.

### 4.4.2 Coil Modeling and Material Properties

For crimping of the aluminium terminal over the copper wire strands, the helical solenoidal coil was modeled and designed considering workpiece geometrical dimensions as shown in Figure 4.3. The number of turns in the coil was decided based on the copper wire cross-section that makes the solenoid coil. The dimensions used for modeling are summarized in Table 4-1. Following boundary conditions were assumed while carrying out the simulations:

- The copper helical coil is assumed to be rigid
- The interaction coefficient of friction is assumed to be negligible between the wire strands
- Electrical losses through Joule heating effect is not accounted in this study
- Terminal material property is isotropic

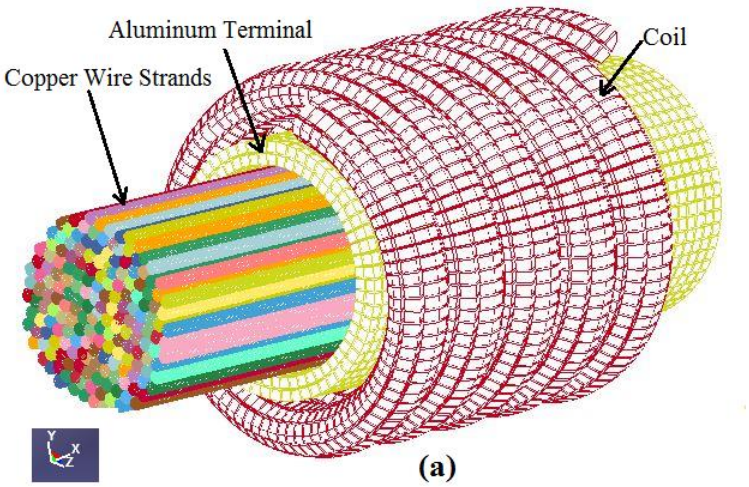


Figure 4.3 Numerical simulation model developed in LS-DYNA

Table 4-1 Dimensions of the coil and workpiece used in simulations

| | |
|---|---|
| Coil | Material: Copper<br>No. of turns: 05<br>Cross-sectional area: 19.6 sq mm<br>Inner diameter: 10.5 mm<br>Outer diameter:15.5 mm<br>Diameter of wire used: 5 mm<br>Coil length: 27 mm |
| Workpiece | Terminal material: Aluminium<br>Outer diameter: 9 mm<br>Inner diameter: 7 mm<br>Crimping length: 25 mm<br>Wire strands material: Copper<br>Diameter of wire strands: 5.7 mm<br>No. of wire strands: 192 |

In the numerical simulation for high strain rate deformation process, the Johnson-Cook (J-C) constitutive was used, to model the behaviour of deforming terminal (Sobolev and Radchenko, 2016). The J-C equation which is a combination of plastic strain and plastic strain rate can be described in Equation (4.24):

$$\sigma = (A + B\,\varepsilon^{n})\left[1 + C\,ln\left(\frac{\dot{\varepsilon}}{\dot{\varepsilon}}\right)\right]\left[1 - \left(\frac{T - T_{room}}{T_m - T_{room}}\right)^{m}\right] \qquad (4.24)$$

This model considers the separated effects of strain hardening, strain rate and thermal softening. Where σ is the equivalent plastic stress (MPa), $\varepsilon$ is the equivalent plastic strain,

$\dot{\varepsilon}$ is the equi valent plastic strain rate ($s^{-1}$), $\dot{\varepsilon}$ is the reference equivalent plastic strain rate ($s^{-1}$), $T$ is the temperature ($^oC$), $T_m$ is the melting temperature, and $T_{room}$ is the room temperature ($^oC$). $A$, $B$, $C$, $m$, and $n$ are material constants obtained using mechanical tests. The J-C material properties for AA 1050 and copper are shown in Table 4-2.

Table 4-2 Johnson-Cook material constant parameter (Hustad and Lindland, 2014)

| Materials | $A$ (MPa) | $B$ (MPa) | $n$ | $C$ | $T_m$ (K) | $m$ |
|---|---|---|---|---|---|---|
| 1050AA | 110 | 150 | 0.36 | 0.014 | 918 | 1 |
| Copper | 90 | 292 | 0.31 | 0.025 | 1331 | 1.09 |

Mechanical properties of AA 1050 and copper were listed in Table 3.2. In EM crimping process, the input current is an important factor which was taken from the experimental EM setup for various discharge voltage as shown in Figure 4.4. The EM parameters of the machine are listed in Table 3.3.

The input current obtained from the EM machine setup was transferred as a current time graph in the EM module of the software to analyze the dynamic plastic deformation of the terminal. In EM crimping process as the first period of the current is responsible for considerable deformation (Haiping and Chunfeng, 2009). Hence, results are discussed for 16 µs and 39 µs of the current curve. FEM input conditions used for running simulations is listed in Table 4-3. CPU running time is the time taken for the server to run the simulation for single discharge voltage. Since, quadrilateral elements can be used for EM module of the software, so meshing of complicated geometries were carried out in Hypermesh software and imported in LSDYNA software for computing.

Table 4-3 FEM input conditions for EM terminal wire crimping model

| Model elements | No. of element | EM time | Mechanical time | Time step | Iteration | CPU running time |
|---|---|---|---|---|---|---|
| Quadrilateral | 455160 | 39 µs | 39 µs | 1 µs | 10000 | 198 hrs. |

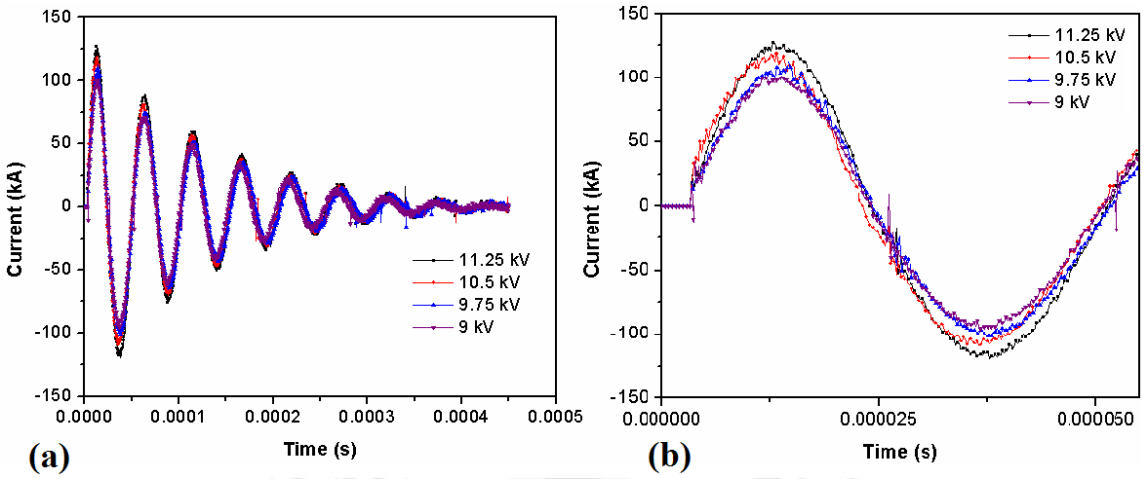


Figure 4.4 (a) Curve of the current waveform in the coil (b) First pulse of the current waveform

## 4.5 Numerical Simulations Results

Figure 4.5 shows the deformation of the aluminium terminal over the copper wire strands for 11.25 kV discharge voltage, where deformation of the terminal with a change in time could be seen.

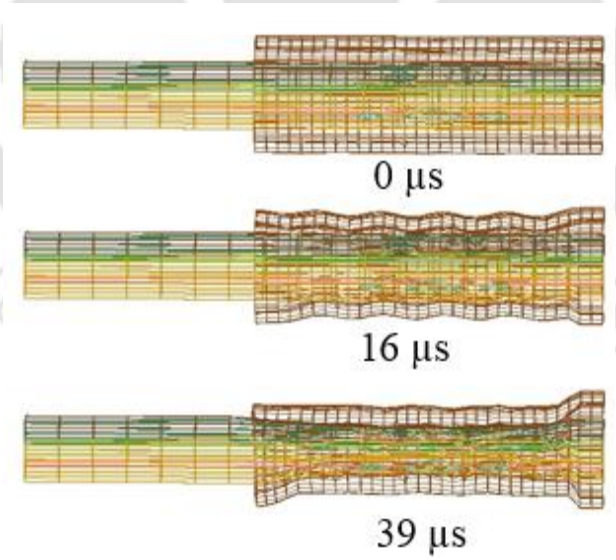


Figure 4.5 Sequential deformation of the aluminium terminal at 16 µs and 39 µs for 11.25 kV discharge voltage

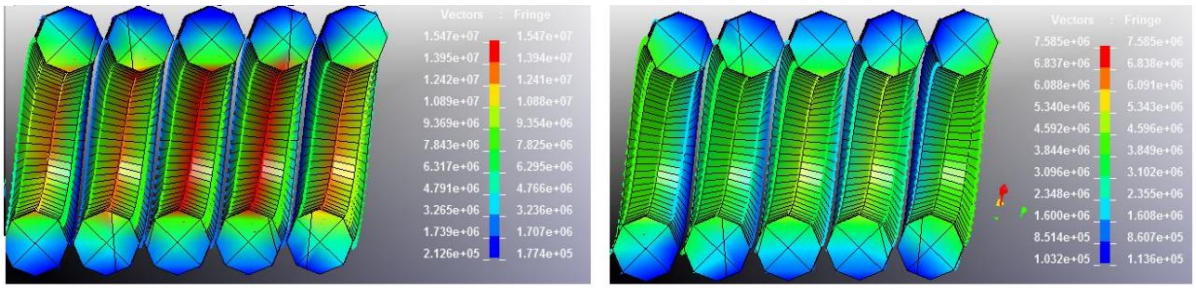


(a) 16 $\mu$s (b) 39 $\mu$s

Figure 4.6 Current density vectors of the coil at 16 µs and 39 µs

Figure 4.6, shows the cross-section side view of the current density vectors of the helical coil, during the EM crimping process. The current density in the center of the helical coil is stronger than in the other areas and decreases the flow of current with the time due to damped current. The maximum value of current density was found to be 15.47 kA/mm$^2$ at 16 µs for 11.25 kV of discharge energy. The value of the current density reduced, as time passed. While at 39 µs the value was found to be 7.58 kA/mm$^2$ and direction of current density also changed during the process, because the direction of input current changed as time passes. The vectors of the magnetic field in the coil are shown in Figure 4.7 Magnetic field density vectors of the coil at 16 µs and 39 µs. The maximum value of the magnetic field was 5.506 T (Wb/m$^2$) at 16 µs, and its direction was inside the coil from the center. The value of the magnetic field was reduced to 4.565 T (Wb/m$^2$) at 39 µs, and its direction was also changed. The same as for the current density case the vector direction of magnetic field changed with the anti-clockwise and clockwise direction of the current.

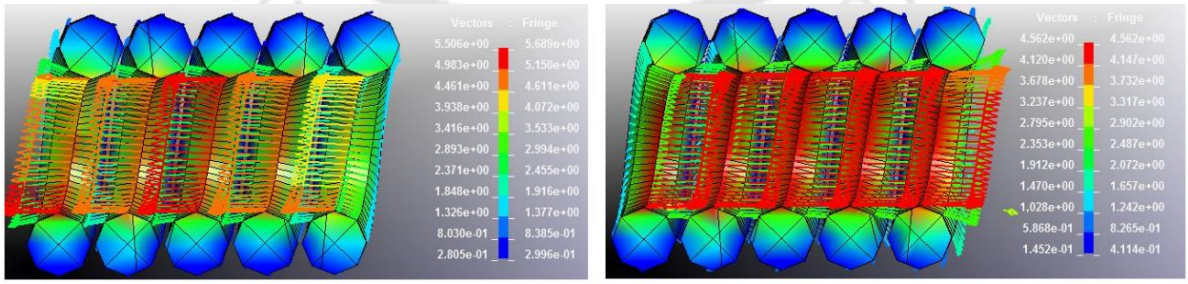


(a) 16 $\mu$s (b) 39 $\mu$s

Figure 4.7 Magnetic field density vectors of the coil at 16 µs and 39 µs

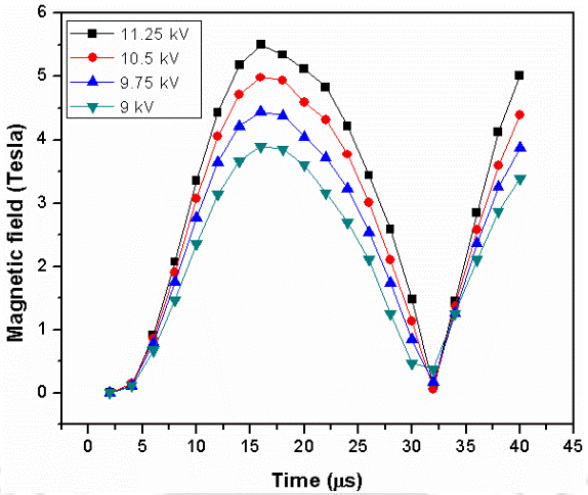


Figure 4.8 Variation of the magnetic field with time for various discharge voltages

Variation of the resultant magnetic field for different discharge voltages is shown in Figure 4.8. The magnetic field values of 5.5 T, 4.98 T, 4.44 T and 3.89 T for 11.25 kV, 10.5 kV, 9.75 kV and 9 kV of discharge voltages were obtained in numerical simulations. The increase in a magnetic field is due to increase in current flowing through the coil which increases the discharge voltage. So, the value of the magnetic field was found to be increased with the increase of the discharge voltage.

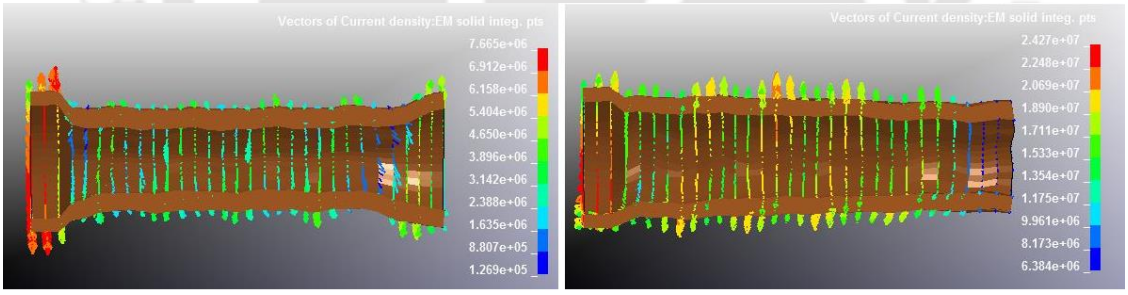


(a) 16 $\mu$s (b) 39 $\mu$s

Figure 4.9 Current density of vectors on the workpiece for 16 µs and 39 µs

Figure 4.9, shows the direction of the current density on the terminal is in the opposite direction, compared with the direction of the coil due to Faraday's Law. As the magnetic field vectors are perpendicular to the current density vectors, thus Lorentz forces occurred to deform the connector terminal. As shown in Figure 4.10, the magnetic field acting over the workpiece with the increase in discharge voltage which leads to increase in Lorentz force and radial deformation.

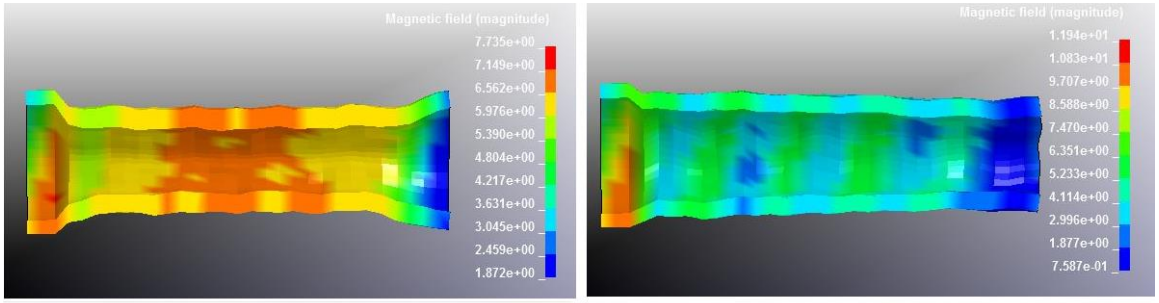


(a) 16 $\mu$s (b) 39 $\mu$s

Figure 4.10 Magnetic field density ( in Tesla) on the workpiece for 16 µs and 39 µs

The value of magnetic pressure acting over the terminal is proportional to the magnetic field, where the value of skin depth was calculated to be 0.597 mm using equation (2.21). With the increase in discharge voltage, magnetic pressure tends to increase, and resulted in increased radial deformation as shown in Figure 4.11. Maximum radial deformation was found to be 2.2 mm for 11.25 kV discharge voltage. It was also found that the plastic deformation was initiated in the surface of terminal placed in the mid of the coil where maximum current density was observed. Figure 4.12, shows the impact velocity of terminal deformation. It was observed that impact velocity increased with the increase in the discharge voltage and peak velocity were found to be 209.1 m/s for 11.25 kV discharge voltage at 16 µs, due to rise in magnetic pressure.

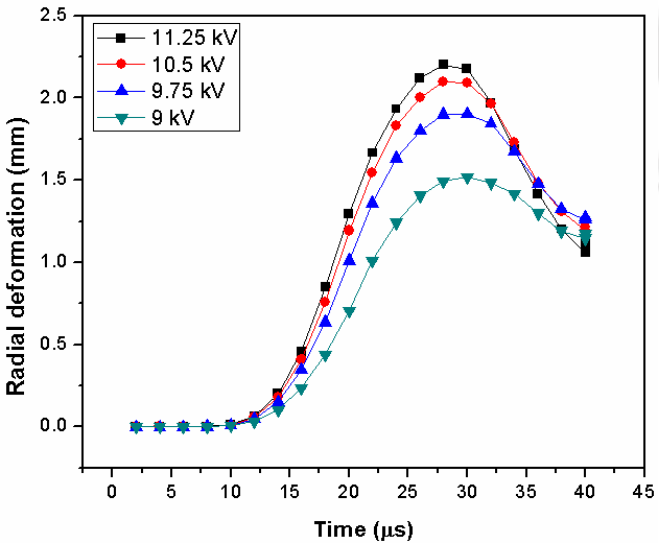


Figure 4.11 Change in resultant radial displacement of the terminal

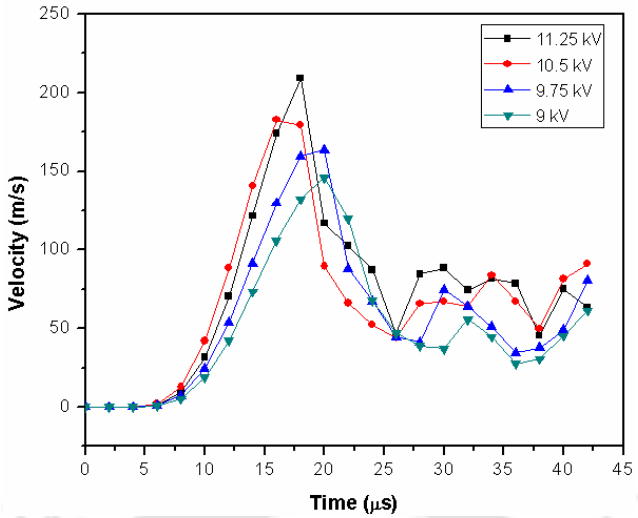


Figure 4.12 Variation in impact velocity of the terminal

Using the simulation, the solenoid coil was designed and fabricated to carry out experiments. From the simulation, the required machine discharge voltage was found to be between 9 kV to 11.25 kV. So, the experiments were carried out in these discharge voltages to avoid trial and error.

## 4.6 Experimental Work

A five-turn solenoidal copper coil dimensions were obtained using the simulation results to carry out the experiments as shown in Figure 4.13. The workpiece dimensions are given in Table 4-4.

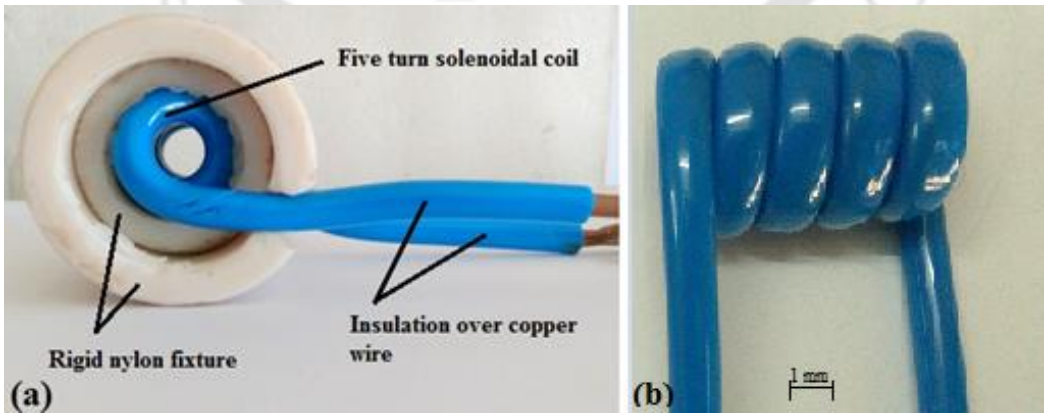


Figure 4.13 Five turns solenoidal coil used for carrying out experiments

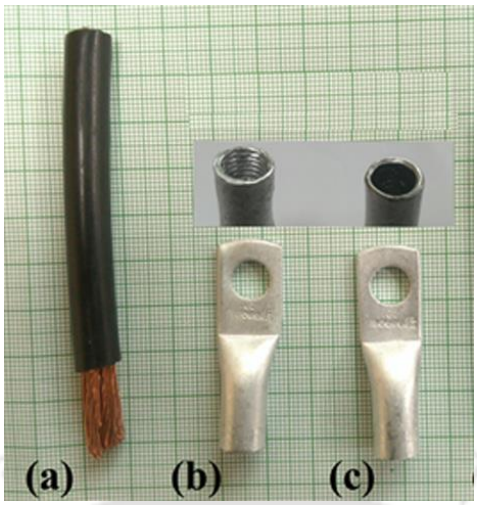


Figure 4.14 (a) 25 $mm^2$ copper wire, (b) Internal threaded terminal, and (c) Plain terminal

Internal threading inside the plain connector terminal was carried out using the tapping tool M8 to make thread pitch of 1.25 mm and thread height of 0.76 mm. Samples used for carrying out experiments are shown in Figure 4.14.

Table 4-4 Geometry of workpiece

| | | |
|---|---|---|
| Work | Material | Aluminium |
| | Outer diameter of plain terminal | 9 mm |
| | Outer diameter of thread terminal | 9 mm |
| | Thickness of plain terminal | 1 mm |
| | Thread pitch (coarse) | M8, 1.25 mm |
| | Thread height | 0.76 mm |
| | Diameter of wire strands | 5.69 mm |

### 4.6.1 Results and Discussion

Experiments were carried out at different voltages from 9 kV to 11.25 kV for crimping of samples. The standoff distance between the coil and the terminal was kept constant (0.75 mm) for different iterations of the experiment. Crimped samples are shown in Figure 4.15. Repetition of experiments on the same discharge voltages were carried to minimize the error.

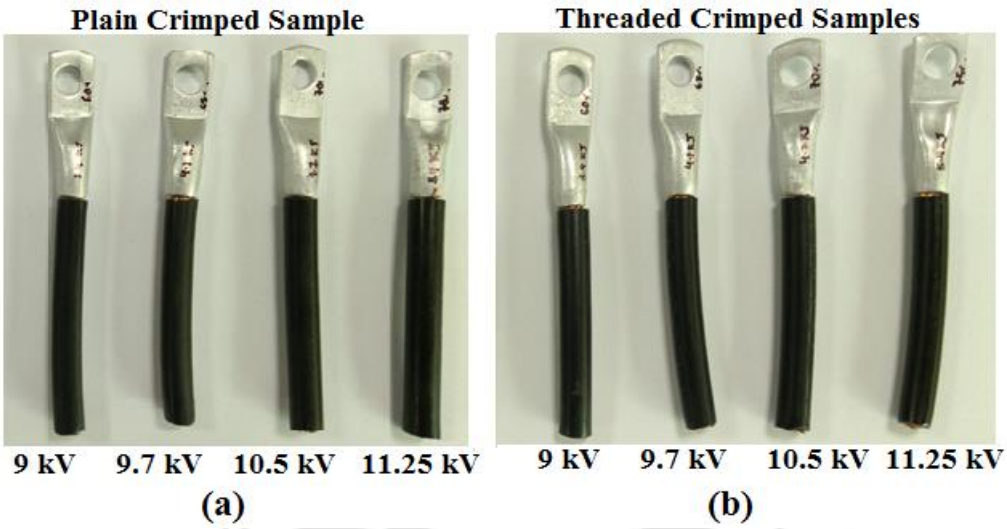


Figure 4.15 EM crimped samples at various discharge energy (a) Plain crimped terminal (b) Threaded crimped terminal

### 4.6.2 Terminal Radial Deformation

The deformation of terminal increased, which kept increasing with the increase in the discharge voltage. Because the value of Lorentz force increased with increase in the discharge voltage (Equations (4.19, 4.21)). So, for discharge voltage of 11.25 kV maximum radial deformation for the threaded terminal was found to be 2.2 mm and for the plain terminal, it was 2.1 mm terminal as shown in Figure 4.16.

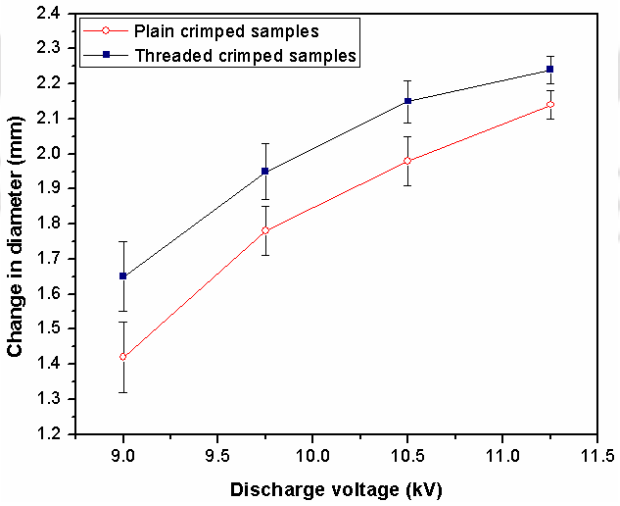


Figure 4.16 The effect of processed voltage on change in diameter for threaded and plain EM crimped terminal

At discharge voltage of 11.25 kV, maximum radial compression of the terminal was obtained. Further increase in energy will increase the deformation. But to avoid damage to the wire strands as per standard maximum deformation should not exceed 2.2 mm for 25 $mm^2$ wire strands ("TE Connectivity," n.d.).The deformation of the threaded terminal was found to be more compared to the plain terminal. The internal threading was done using tapping tool, causing the removal of material inside the terminal to create threads. The magnetic pressure developed on the plain terminal and threaded terminal is same for a different thickness. Lesser the thickness more the deformation was found in the threaded terminal.

### 4.6.3 Cross-Section Analysis

Comparison of the cross-section of EM crimped samples was carried out using upright optical microscope at 5X magnification. Images of the cross-section are shown Figure 4.17. It was found that compression done for threaded terminals crimped showed more uniform and minimum voids between the wire strands and the terminal compared to the plain terminal. As terminal deformation was more for the threaded crimped sample, it gave better compaction of wire strands where minimum voids were found comparatively. In plain terminal due to lesser compaction, a gap of 0.3 mm, 0.1 mm, and 0.4 mm was measured at the interface. While in the threaded sample that gap was covered up by the threads, and no such interface gap was observed.

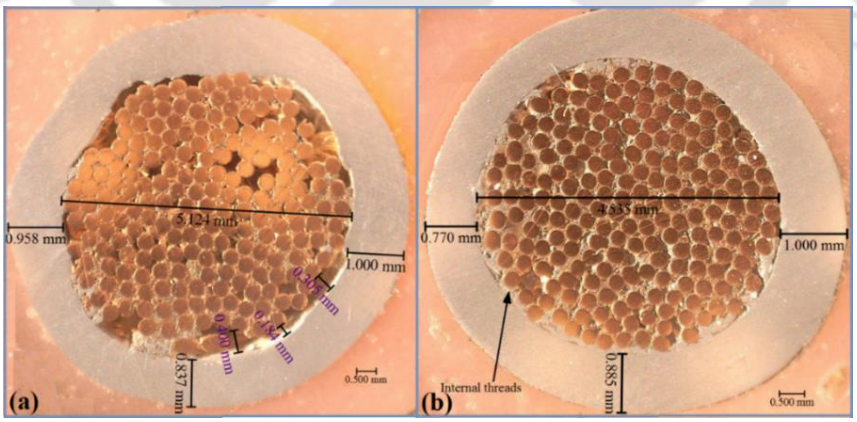


Figure 4.17 Cross-section images are taken under a digital microscope

### 4.6.4 Electrical Characterization

One important criterion of a contact terminal crimping process is electrical resistance. The crimped contact resistance was measured using LCR meter. Lesser the contact area

resistance, less is the heat generated across the terminal and minimum is a loss of energy. An adequately crimped terminal should provide minimum contact resistance for a maximum flow of current through it. As shown in Figure 4.18, it was found that the threaded samples showed contact resistance of 23.5 mΩ while the plain crimped terminal it was 25.08 mΩ for 11.25 kV discharge voltage.

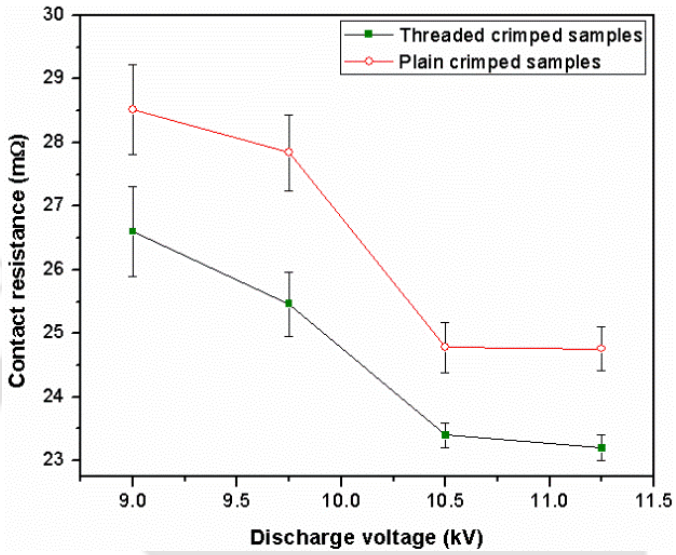


Figure 4.18 Comparison of resistance value for crimped samples of plain and threaded terminal

With the increase in the discharge energy, resistance value kept decreasing and became constant after 10.5 kV due to maximum compaction of copper wire. The threaded terminal provides more compaction and minimum contact gap at the interface, due to which resistance value of threaded crimped terminal was found to be lower compared to the plain samples by 1.58 μΩ. Further, it was observed that contact resistance value of both types of terminal becomes constant after 10.5 kV as further compaction of the terminal is restricted by the copper strands. So, a further increase in energy may not necessarily provide a lowering of contact resistance value.

### 4.6.5 Mechanical Pull-Out Testing

Comparison of pull out load value of EM crimped samples were carried out as shown in Figure 4.19 for various discharge voltages from 9 kV to 11.25 kV.

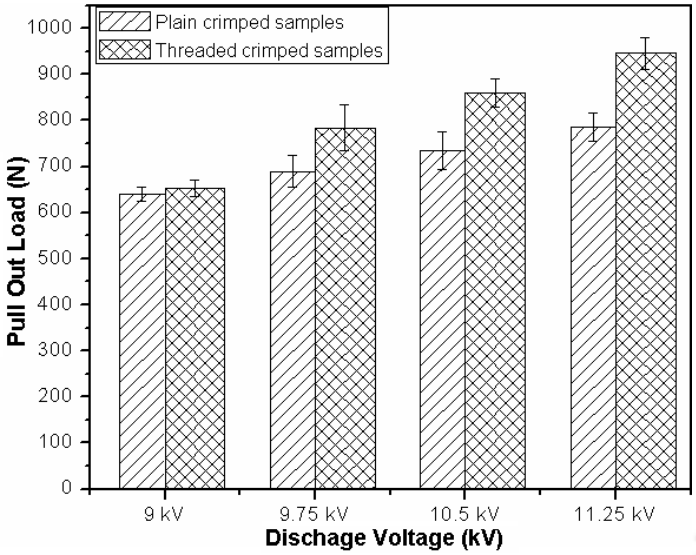


Figure 4.19 Pull-out strength of plain and threaded crimped samples

Due to increase in the radial deformation, with the rise in the discharge voltage, pull-out strength was found to be increased for both the type of samples. The threaded samples, for 11.25 kV discharge voltage gave the maximum pull out value of 946 N compared to 776 N for the plain terminal. Due to internal threads, threaded sample provided more gripping area and thus providing more barrier for the removal of wire strands compared to the plain crimped terminal. The pull out the strength of threaded terminals was found to be 170 N more than crimped plain terminals for 11.25 kV discharge voltage. This shows the advantage of making thread inside the terminal which increases mechanical strength.

### 4.6.6 Hardness Analysis

By adjusting the parameters of the EM field, compressive residual stress can be introduced along the surface to get peening effects (Gary and Cheng, 2009). This compressive residual stresses due to EM peening keep varying the thickness of the workpiece. The Vickers hardness test was carried across the cross-sectioned sample of plain and threaded terminals. For testing, 100 gram force is chosen. As shown in Figure 4.20, in the EM crimped sample the hardness of terminal increases with the increase of the discharge voltage.

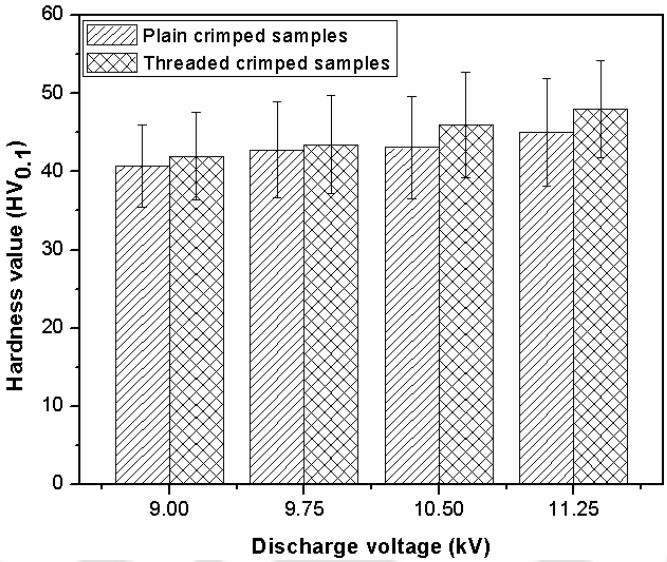


Figure 4.20 Vickers hardness over the cross-section of plain and threaded crimped sample

The increase in hardness is due to strain hardening and compressive residual stresses developed because of high-velocity impact which usually occurs in high strain rate forming operations. The maximum value of 52.4 $HV_{0.1}$ was obtained for a threaded crimped sample at 11.25 kV of discharge voltage. While for the plain crimped sample maximum value of 49.6 $HV_{0.1}$ was obtained. As the thickness of threaded terminal was lesser due to material removal in thread formation compared to the plain terminal, EM peening effect was found to be more in the threaded terminal.

## 4.7 Summary

In the present chapter, numerical simulations were carried out to find out a suitable coil for EM terminal-wire crimping process. Experiments were carried out to compare plain and threaded crimped terminals at various discharge voltages. The observations from this chapter could be summarized as follows:

- Numerical simulations were carried out to find the suitable dimension of the coil and range of discharge voltage for uniform crimping of the aluminium terminal over the copper wire strands.
- The magnitude of current density and magnetic field of the coil for maximum discharge voltage of 11.25 kV was found to be 15.47 kA/mm$^2$ and 5.5 T.

- Maximum impact velocity of the aluminium terminal over the copper wire strands was found to be 209.1 m/s for 11.25 kV, where the maximum radial displacement of 2.2 mm was observed.
- Deformation of the threaded crimped aluminium terminal was found to be more compared to the plain crimped aluminium terminal by 0.5 mm for maximum discharge voltage of 11.25 kV.
- Voids between the wire strands in the threaded terminal were found to be minimal due to the presence of thread compared to the plain terminal.
- Resistance value was observed to be 20 % lesser in threaded terminal compared to the plain terminal.
- Pull out test value shows that value was increased by 17.89 % in 11.25 kV for threaded terminal compared to the plain terminal.
- Hardness value reveals that by EM crimping process there is an increase in the hardness along the thickness due to peening effect. The value of hardness was found to be 8 % more in threaded profile.

It was concluded that formation of thread inside the terminal could enhance the electrical and mechanical properties by using EM crimping process

# Chapter 5

## 5 Numerical and Experimental Studies on Different Coil Designs

### 5.1 Introduction

Compression using conventional crimping tool deteriorates the material due to relaxation or partial release which results in increasing resistivity and huge losses in the wiring system and battery power system. In previous two chapters, work was carried out on a comparison of EM wire crimping process to conventional crimping process and numerical simulation for understanding the inside physics of the EM terminal-wire crimping process. But, due to 198 contact properties and total mesh numbers exceeding more than 2.5 lakhs and increasing FEM and BEM timing, it was found difficult to run simulations with various parameters.

So, in this chapter, numerical simulations were carried out on three different types of helical coils with different cross-section (CS) geometry keeping the CS area constant. For comparison number of turns and the total length of coil remains same so that the total inductance of the coil remains same of all the three cases. The material of the terminal remains the same as in the previous chapter to maintain the uniformity of the work. For the validation, aluminium seven wire strands are taken under the examination for a proper understanding on the deformation of wire strands on various coil geometry and EM parameters. Results of the simulations were used to fabricate the coil for carrying out the experiments. This chapter aims to develop a new, different coil design for terminal- wire crimping that can be an alternative to existing coils in EM crimping process with many advantages.

### 5.2 Numerical Analysis

Coils with different CS geometry were modeled and simulated in LS-DYNA. In the numerical simulation, the EM and mechanical models were established respectively. A link between EM field and mechanical was used by the LS-DYNA EM module software

for finite element modeling of EM terminal-wire crimping process (Patel et al., 2017). During the solution, the first analysis solves for the EM loading on the conductor using EM field analysis. Then second analysis uses mechanical solver to solve the dynamic response of the terminal using the result from the first analysis. This coupling between the EM and mechanical solver was used in carrying out simulations. FEA involved in the software is already explained in previous Chapter 4, Section 4.3.

### 5.2.1 Modelling Process

The explicit general contact algorithm was used for this analysis. In the general contact, the software automatically defines all the surfaces used and is the simplest way to define contact in the model. A total of 8 contacting parts in the model, needs 18 contact pairs for all possible two surface combination. A seven wire strands with each having 1.5 mm diameter was used in the model.

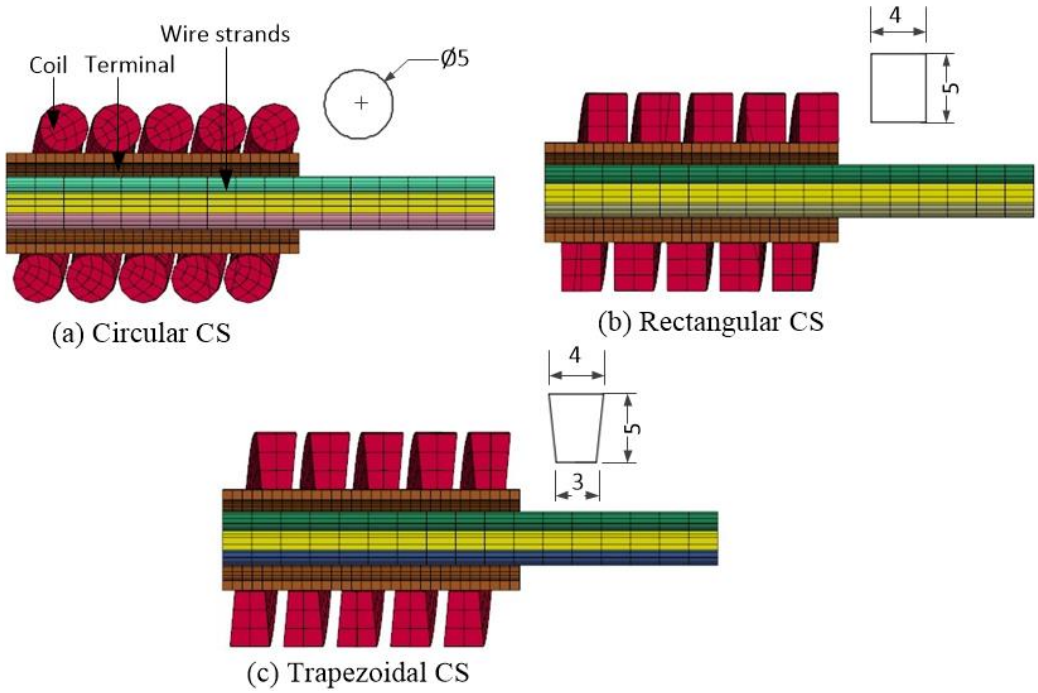


Figure 5.1 Sectional CS view of the assembly with different cross-section (a) Circular (b) Rectangle and (c) Trapezoidal

The deformable wires and the terminals were modelled with C3D8R, eight-node elements. The coil as the part was modeled using R3D4 elements. Modelled CS assembly for all the three types of variation in coil geometry is shown in Figure 5.1. For comparison

CS area, numbers of turn and length of all the coils were kept constant as summarized in Table 5-1 and geometry of the workpiece dimensions are shown in Table 5-2. In the finite element simulation, the Johnson-Cook (J-C) constitutive equation was used to model the behavior of deforming aluminium terminal. The J-C equation (as written in equation (4.1), Chapter 4) which is a combination of plastic strain and plastic strain rate material properties are listed in Table 4-2. The wire strands and terminals are made of AA 1050, where Johnson-Cook (J-C) material property was used, while coil material is assigned to be copper. To be more precise in comparison, a total number of 3583 elements remains the same for all three types of models. FEM input conditions used for running simulations is listed in Table 5-3.

Table 5-1 Designing of coil types

| Factors | Coil 1 | Coil 2 | Coil 3 |
|---|---|---|---|
| Geometry type | Trapezoidal | Rectangular | Circular |
| CS area ($mm^2$) | 20 | 20 | 20 |
| Inner diameter of coil (mm) | 10.5 | 10.5 | 10.5 |
| Length (mm) | 27 | 27 | 27 |
| Dimensions of CS (mm) | Top : 4<br>Base : 3<br>Height : 5.7 | Length : 4<br>Width : 5 | Dia : 5 |

Table 5-2 Workpiece dimensions

| | | |
|---|---|---|
| Workpiece | Material | Aluminium |
| | Outer diameter of terminal | 9.0 mm |
| | Thickness of terminal | 1.0 mm |
| | Wire strands diameter | 5.8 mm |

Table 5-3 FEM input conditions for EM terminal wire crimping model

| Model elements | No. of element | EM time | Mechanical time | Time step | Iteration | CPU running time |
|---|---|---|---|---|---|---|
| Quadrilateral | 4492 | 50 µs | 50 µs | 1 µs | 10000 | 94 hrs. |

### 5.2.2 Analysis and Discussion

In EM crimping process input current is an important factor which was taken from the experimental EMF setup for various discharge voltages as shown in Figure 5.2. This input

current was used as input current time graph in the software to analyze the dynamic plastic deformation of the terminal. As in EM process first period of the current is responsible for considerable deformation (Haiping and Chunfeng, 2009), so results are discussed for the first period of the current curve.

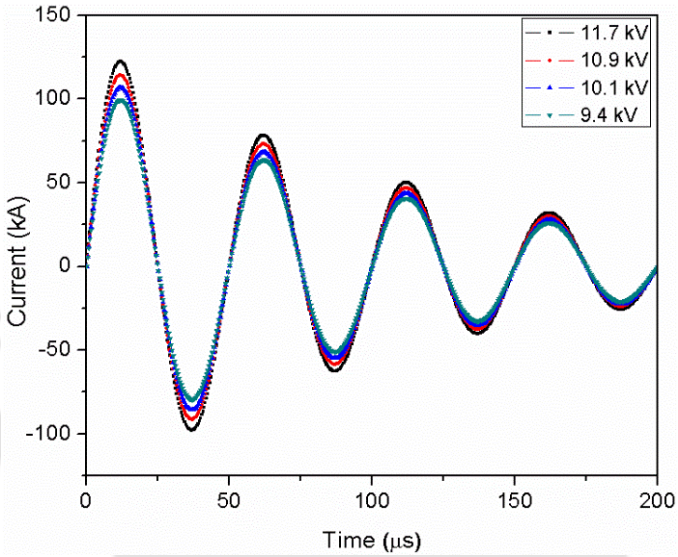


Figure 5.2 Typical waveform of current for various discharge voltages

5.2.2.1 Current Density

Figure 5.3 shows the value of peak current density on the terminal for different CS coils. The current density J is given by equation (5.1) as;

$$J = n\frac{I}{A} \tag{5.1}$$

where *n* is the number of turns, and *A* is the CS area of the wire.

It was observed that for trapezoidal, rectangular and circular CS coil, a current density magnitude of 25.31 kA $mm^{-2}$, 23.28 kA $mm^{-2}$, and 22.61 kA $mm^{-2}$ was found for the 11.7 kV discharge voltage. The trapezoidal CS coil geometry showed the maximum current density among the three different types of the coil. Because of generation of strong current peaks due to the more accumulation of current over the tapered zone. When compared to circular CS coil, rectangular CS coil showed more current density by 0.67 kA $mm^{-2,}$ due to the uniform gap which is maintained throughout its geometry while, in a circular, a gap is maintained just over the diameter section of the coil as explained in Figure 5.4.

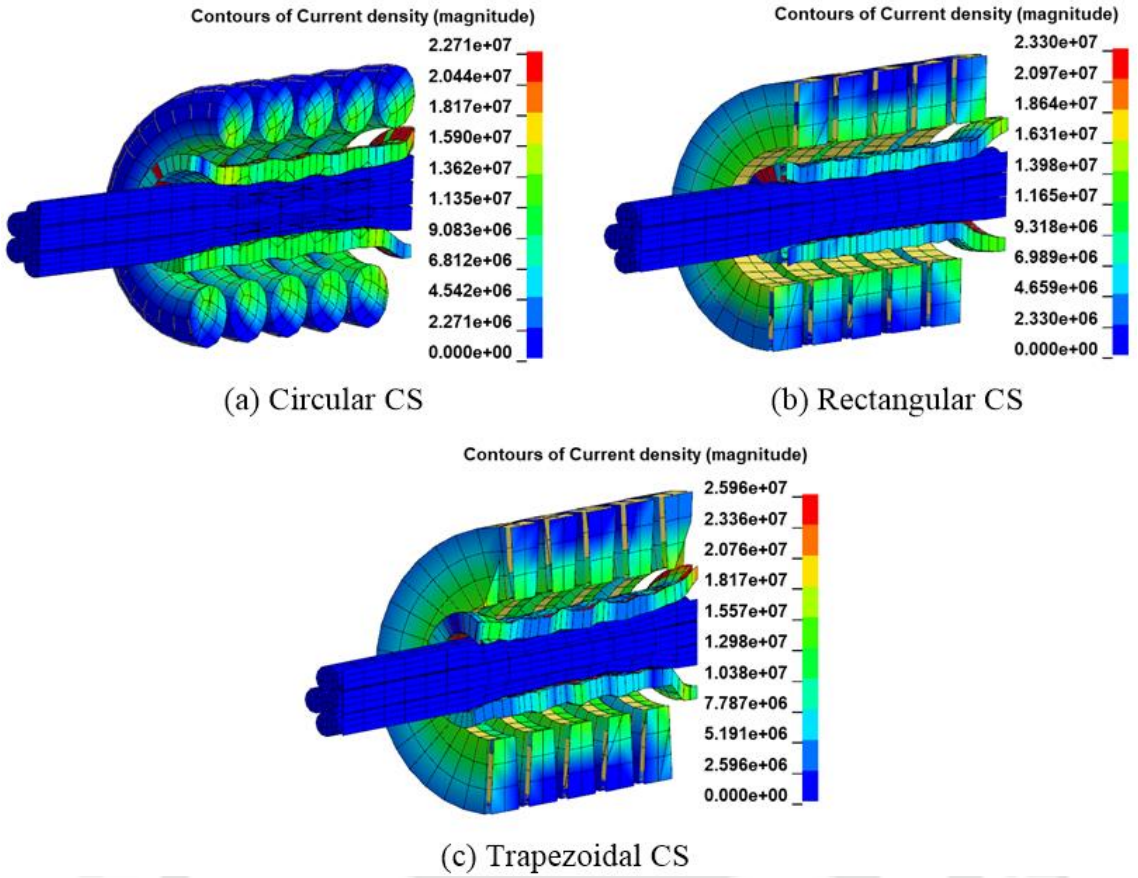


Figure 5.3 Current density for different CS (a) Circular (b) Rectangular and (c) Trapezoidal

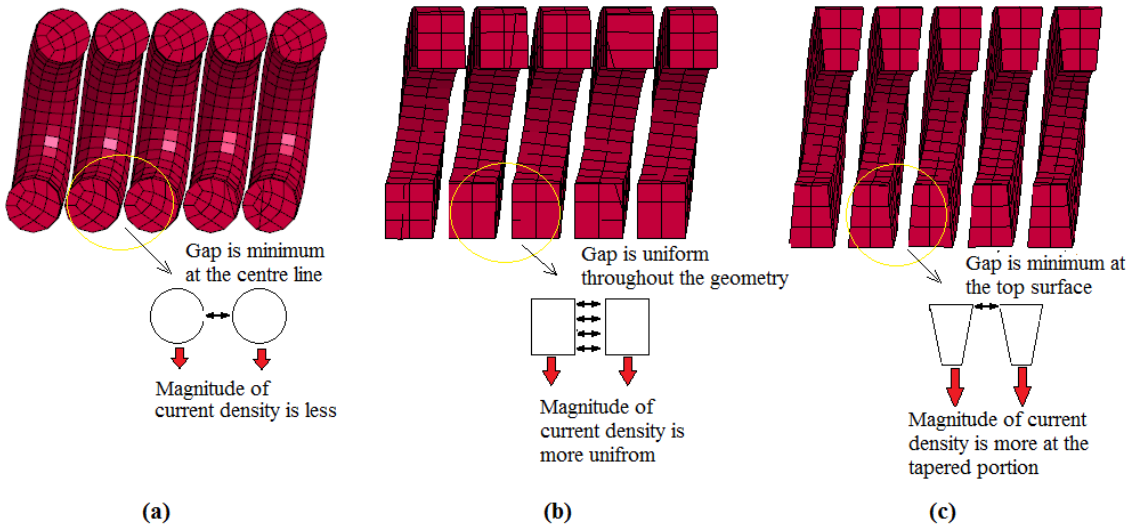


Figure 5.4 Influence of coil CS geometry on current density (a) Circular (b) Rectangular and (c) trapezoidal CS

5.2.2.2 Magnetic Field

As shown in Figure 5.5, tapered CS coil generates the maximum value of a magnetic field of 8 T followed by a rectangle CS and circular CS coil with the value of 7.1 T and 6 T. In tapered CS coil magnetic flux due to tapered geometry, it generates a high current density peak around the narrowed portion increasing the magnitude of magnetic field. Followed by rectangular CS and circular CS coil, due to variation in the gap between the turns.

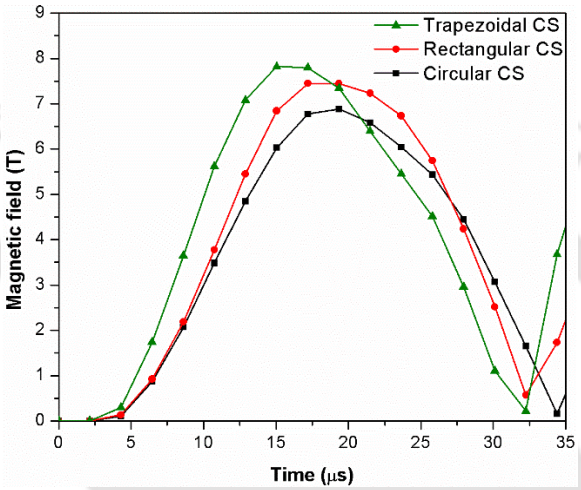


Figure 5.5 Variation in a magnetic field for same discharge energy for different coil CS

5.2.2.3 Radial Deformation

It was found that change in diameter of the aluminium terminal increases which is in relation to the peak value of magnetic pressure (Equations 4.22).

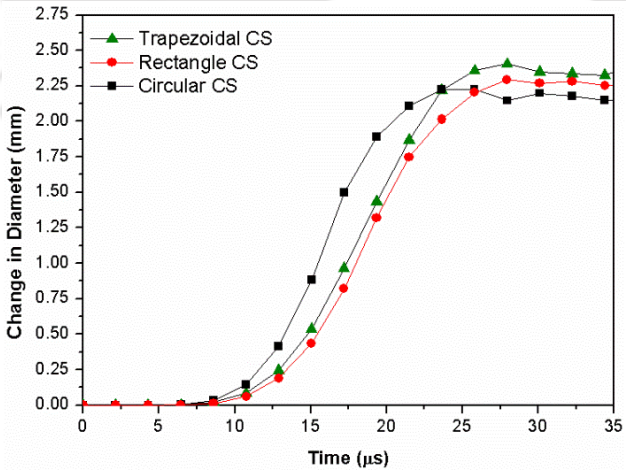


Figure 5.6 Effect of discharge energy of 11.7 kV on radial displacement for different coil CS

Figure 5.6, shows the variation of terminal deformation as the function of time for different coil CS geometry. The trapezoidal CS helical coil gives the maximum change in diameter, with a value of 2.4 mm, while the rectangular and the circular CS helical coil change in deformation were found to be 2.3 mm and 2.25 mm, for 11.7 kV discharge voltage.

Even though the CS area and length of all the coil was same, it was observed that with a change in geometry like trapezoidal, square and circular, it significantly affects the radial displacement. As current density and magnetic field are higher for trapezoidal CS coil, so resultant radial displacement was found higher compared to other two coils.

#### 5.2.2.4 Impact Velocity

The highest velocity vector was observed at the collision point and the magnitude of the velocity vector reduced as the distance from the collision point increased (Equation 4.23).

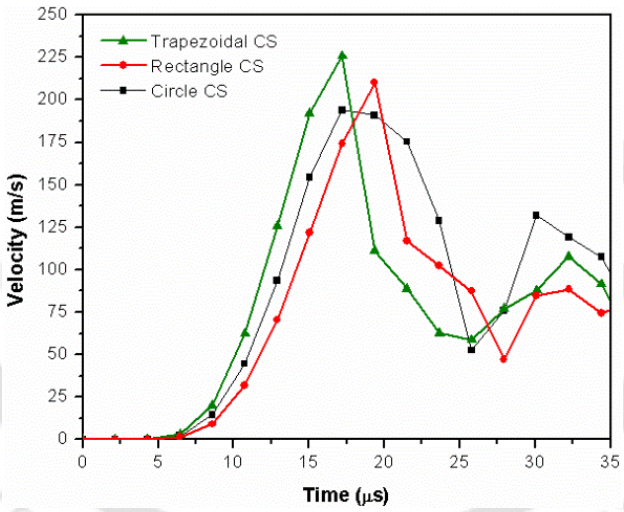


Figure 5.7 Variation in impact velocity for different coil CS

High velocities create high plastic deformation. As shown in Figure 5.7, resultant impact velocity of the terminal over the wire strands was found to be maximum for trapezoidal CS coil with a magnitude of 225 m/s, while for rectangular CS and circular CS coil the velocity was 207 m/s and 194 m/s. It can be seen clearly that maximum velocity was achieved in 17.19 μs which is in good agreement with the peak magnetic field and peak current density.

## 5.3 Experimental Work

Five turn solenoidal copper coils were fabricated as per the dimensions used in the simulations to carry out the experiments as shown in Figure 5.8. Experiments were carried out at optimized discharge voltages varying from 9.4 kV to 11.7 kV, obtained from the simulation results to find the most suitable coil for a proper effective crimping to occur. Test like radial deformation, CS analysis, contact resistance, hardness and pull-out tests were carried over the crimped samples obtained from different coils. The standoff distance between the coil and the connector terminal was kept constant (0.5 mm) for different iterations of the experiment. Crimped samples are shown in Figure 5.9. Repetitive experiments were carried to avoid errors in post-processing.

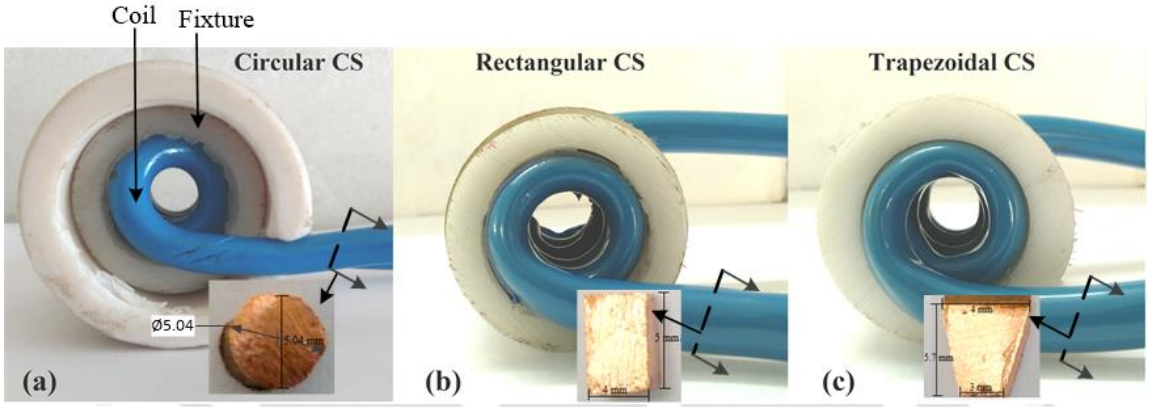


Figure 5.8 Different CS coil (a) Circular (b) Rectangular and (c) Trapezoidal CS

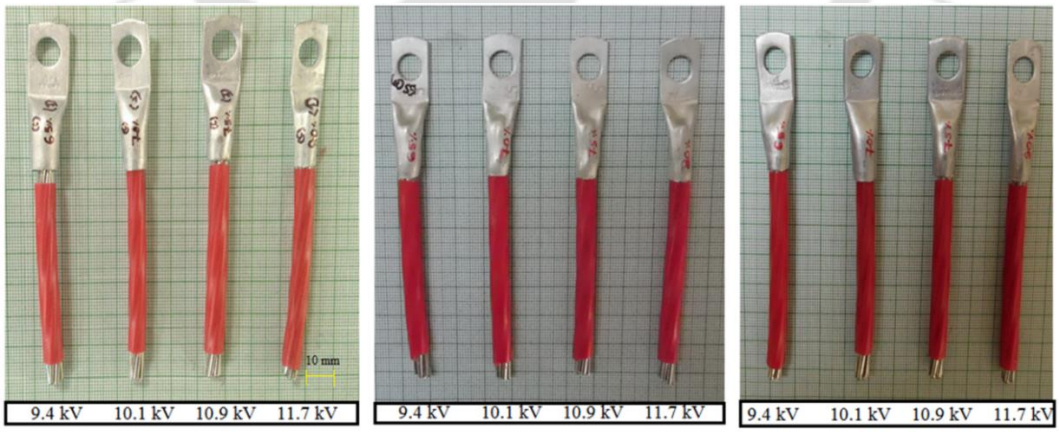


(a) Crimped samples using trapezoidal CS coil

(b) Crimped samples using rectangular CS coil

(c) Crimped samples using circular CS coil

Figure 5.9 Crimped samples for various discharge energy for different type of coil CS

### 5.3.1 Deformation Measurement in the Samples

The deformation in crimped samples was measured. Radial deformation of all the coils was found to be increasing with the increase in discharge voltage, due to increase in the magnetic field inside the coil (Equation 4.19, 4.20, 4.21, and 4.22). As shown in Figure 5.10, it was found that out of three coils, the trapezoidal CS coil gave the maximum deformation of 2.2 mm for 11.7 kV compared to 2.1 mm and 2.0 mm for the rectangular and the circular CS helical coil. Repetitive experimental data is listed in Table 5-4.

Deformation at various discharge voltages for simulation and experiment is listed in Table 6. Maximum deformation that can take place for this size of the terminal is 2.2 mm as per the conventional crimping standard [12]. The error in the results may be due to the losses in current at the contact terminal of the coil (inductor) which was connected to the EM machine or in the form of heat, which was not accounted in the simulation process. The trapezoidal CS coil has been optimized in such a way that the trapezoidal CS concentrates the magnetic field on the workpiece more than the rectangular and the circular CS helical coil.

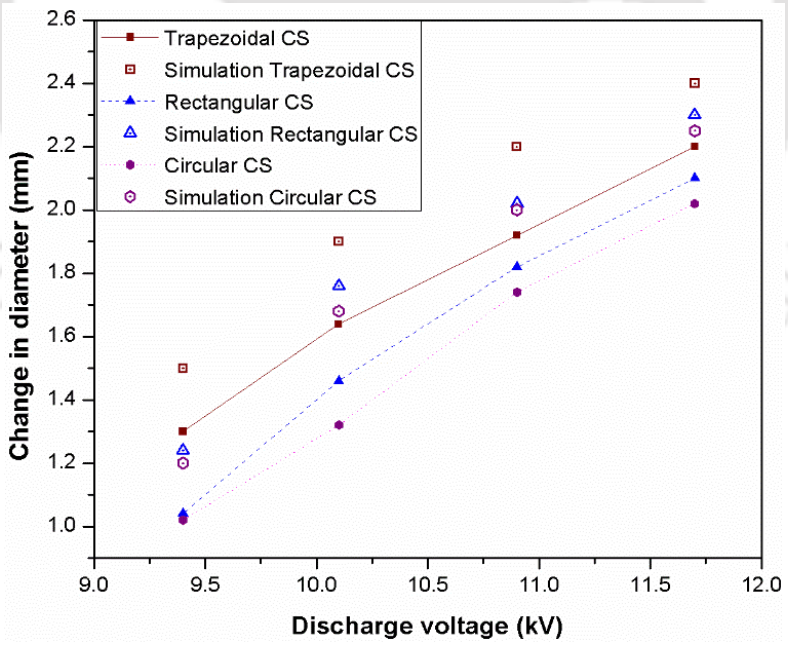


Figure 5.10 Change in diameter for samples crimped using different coils, experimental and simulations results

Table 5-4 Repetitive experimental values for diameter deformation and contact length

| | | Diameter deformation (mm) | | | | Contact length (mm) | | | |
|---|---|---|---|---|---|---|---|---|---|
| (kV) | CS | Expt. 1 | Expt. 2 | Expt. 3 | Average | Expt. 1 | Expt. 2 | Expt. 3 | Average |
| 9.4 | Trapezoidal | 1.36 | 1.30 | 1.24 | 1.3 | 7.3 | 7.1 | 6.9 | 7.1 |
| | Rectangular | 1.02 | 1.04 | 1.06 | 1.04 | 6.78 | 6.8 | 6.82 | 6.8 |
| | Circular | 1 | 1.02 | 1.04 | 1.02 | 6.36 | 6.4 | 6.44 | 6.4 |
| 10.1 | Trapezoidal | 1.60 | 1.64 | 1.70 | 1.64 | 7.54 | 7.6 | 7.66 | 7.6 |
| | Rectangular | 1.52 | 1.46 | 1.4 | 1.46 | 7.93 | 7.9 | 7.87 | 7.9 |
| | Circular | 1.30 | 1.32 | 1.34 | 1.32 | 7.59 | 7.6 | 7.61 | 7.6 |
| 10.9 | Trapezoidal | 1.98 | 1.92 | 1.86 | 1.92 | 8.68 | 8.65 | 8.62 | 8.65 |
| | Rectangular | 1.82 | 1.82 | 1.81 | 1.82 | 7.90 | 7.9 | 7.89 | 7.9 |
| | Circular | 1.71 | 1.74 | 1.77 | 1.74 | 7.51 | 7.6 | 7.69 | 7.6 |
| 11.7 | Trapezoidal | 2.16 | 2.2 | 2.2 | 2.2 | 9.79 | 9.8 | 9.81 | 9.8 |
| | Rectangular | 2.0 | 2.1 | 2.1 | 2.1 | 9.39 | 9.4 | 9.4 | 9.4 |
| | Circular | 1.98 | 2.02 | 2.06 | 2.06 | 9.15 | 9.2 | 9.25 | 9.2 |

Table 5-5 Variation of simulation and experimental values

| | | Diameter deformation (mm) | | | Contact length (mm) | | |
|---|---|---|---|---|---|---|---|
| (kV) | CS | Simulation | Experiment | Error % | Simulation | Experiment | Error % |
| 9.4 | Trapezoidal | 1.5 | 1.3 | 13.3 | 8.1 | 7.1 | 12.3 |
| | Rectangular | 1.24 | 1.04 | 16.1 | 7.4 | 6.8 | 8.1 |
| | Circular | 1.2 | 1.02 | 15 | 7.28 | 6.4 | 11.6 |
| 10.1 | Trapezoidal | 1.9 | 1.64 | 13.6 | 8.9 | 7.6 | 14.6 |
| | Rectangular | 1.76 | 1.46 | 17 | 8.6 | 7.9 | 8.1 |
| | Circular | 1.68 | 1.32 | 21.4 | 8.5 | 7.6 | 10.5 |
| 10.9 | Trapezoidal | 2.2 | 1.92 | 12.7 | 9.4 | 8.65 | 7.9 |
| | Rectangular | 2.02 | 1.82 | 9.9 | 8.6 | 7.9 | 8.1 |
| | Circular | 2 | 1.74 | 13 | 8.5 | 7.6 | 10.5 |
| 11.7 | Trapezoidal | 2.4 | 2.2 | 8.3 | 10.6 | 9.8 | 7.5 |
| | Rectangular | 2.3 | 2.1 | 8.6 | 10.2 | 9.4 | 7.8 |
| | Circular | 2.25 | 2.02 | 10.2 | 10.1 | 9.2 | 8.9 |

### 5.3.2 Contact Length Measurement and CS Analysis

In wire crimping process, the gap between the terminal and the wire strands is a crucial factor, because it determines the quality of the crimp joint and contact resistance. With the increase in discharge voltage, terminal deformation increases resulting in a decrease in gap and increase in contact length. It was found that for all the three CS coils, the gap was reduced with the increase in the deformation of the terminal as shown in Figure 5.11, as it was difficult to measure the gap between the wire strands and terminal. So, contact length between the wire strands and the terminal was measured using an optical microscope. The maximum contact length of 9.8 mm was found for trapezoidal CS coil compared to 9 mm and 8.7 mm for rectangular CS and circular CS coil, respectively.

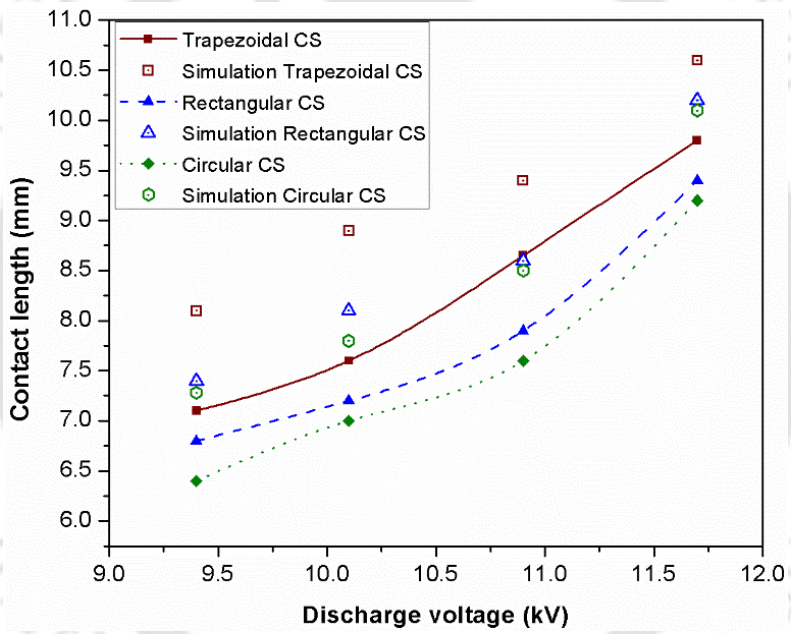


Figure 5.11 Variation in contact length for different coil CS geometry, experimental and simulation results

Maximum contact length was found to be for trapezoidal CS, followed by rectangular CS and circular CS. Simulation results also show the same pattern which is in 93 % agreement with the experimental results. Variation in the simulation and experimental results is shown in Table 5-5. In CS analysis similar deformation and contact, the pattern was observed in numerical simulation results as shown in Figure 5.12.

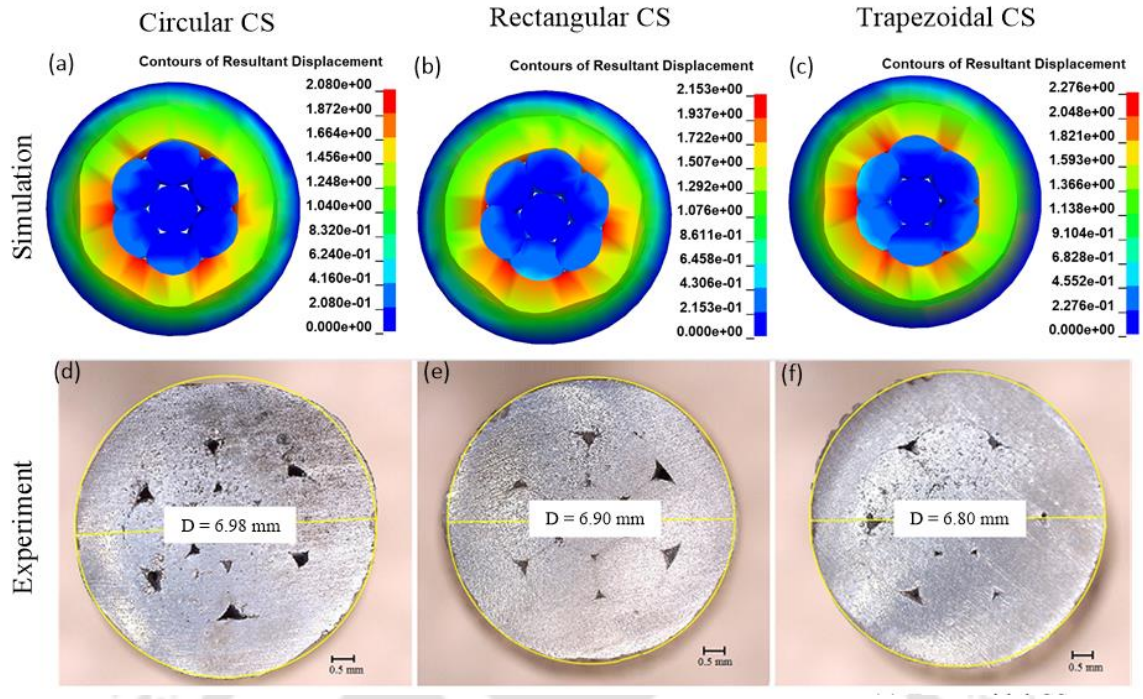


Figure 5.12 Experimental CS analysis for samples crimped at 11.14 kV

The contact length was higher for trapezoidal CS coil compared to other two coils. The main advantage of this process is no spring back of terminal due to the advantage of high strain rate deformation process, which is a major issue in conventional crimping process.

### 5.3.3 Contact Resistance of the Crimped Junction

The contact resistance of the crimped region was measured using an LCR meter. The contact resistance for samples crimped using different CS coils is shown in Figure 5.13. Contact resistance is an important parameter for any wire crimped samples.

It was found that samples crimped using trapezoidal CS coil shows a minimum resistance value of 14.5 mΩ contact resistance, while rectangular CS and circular CS coil shows 16 mΩ and 18.94 mΩ contact resistance, respectively for maximum discharge voltage of 11.41 kV. It was found that resistance kept on decreasing with the increase in discharge voltage, due to increase in deformation and contact length. Due to maximum contact length between the wire strands and terminal, a minimum contact resistance was observed for trapezoidal CS coil. It is because the tapered CS concentrates the magnetic field on the workpiece the most among all the three coils.

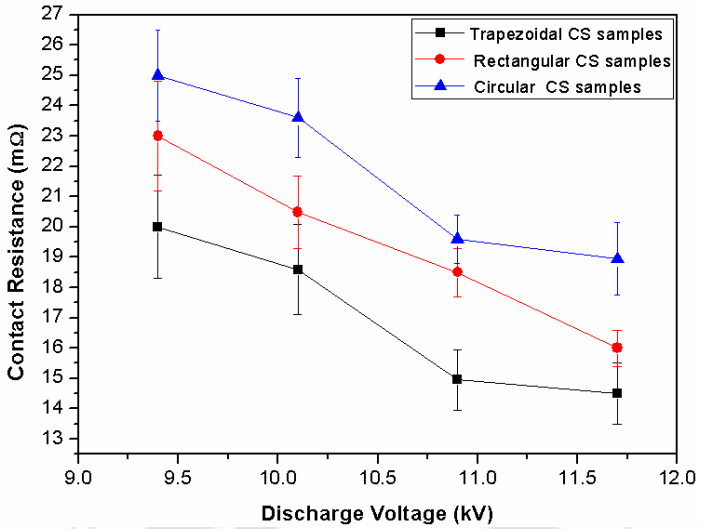


Figure 5.13 Variation of contact resistance for different helical coil geometry

### 5.3.4 Hardness Analysis

By adjusting the parameters of the EM field, compressive residual stress can be introduced along the surface to get peening effects (Li and Cheng, 2009) (Golowin et al., 2007). This compressive residual stresses due to EM peening (EMP) keeps varying with the thickness of the workpiece.

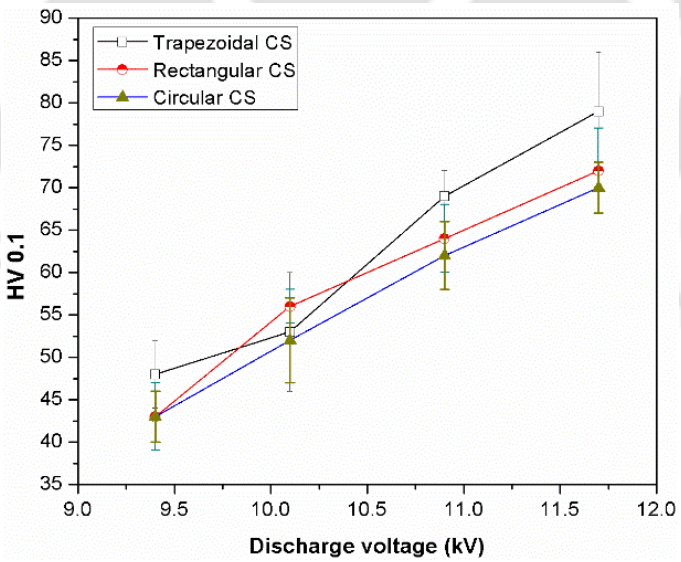


Figure 5.14 Variation of hardness with the discharge voltage

The Vickers hardness test was carried across the cross-sectioned sample of the terminals, over the thickness. Hardness test was carried out at 100-gram load. As shown in Figure 5.14, the value of hardness increased with the increase in the discharge voltage. The

maximum hardness value of 57 $HV_{0.1}$ was observed for trapezoidal CS coil, compared to 50 $HV_{0.1}$ and 47 $HV_{0.1}$ for rectangular CS and circular CS coil, respectively. There was an increase of 38 % in the hardness value compared to parent hardness value of 34 $HV_{0.1}$. The reason for this increase in hardness is due to residual strain induced by the high-speed forming process. This adds advantage when compared to conventional crimping process.

### 5.3.5 Pull-Out Test

Comparison of the pull-out test was carried out using standard procedure (Use, 2003). Transverse speed was maintained at 50 mm/min. It was found that with an increase in discharge voltage pull-out value increases. The maximum pull-out value was found to be 2237 N for trapezoidal CS coil as shown in Figure 5.15. For rectangular and circular CS coil value was found to be 1733 N and 1326 N. This is because the pull-out strength depends on the contact length of the plasticized crimped interface between the wire strands and terminal. The contact length increases with deformation which increases with the discharge voltage. Hence the pull-out strength increases with discharge voltage. For the same discharge voltage, the pull out strength was found to be maximum for tapered CS and least for circular CS coil. Due to maximum contact length in the crimped region for tapered CS coil, a higher pull out strength was observed compared to other two coils.

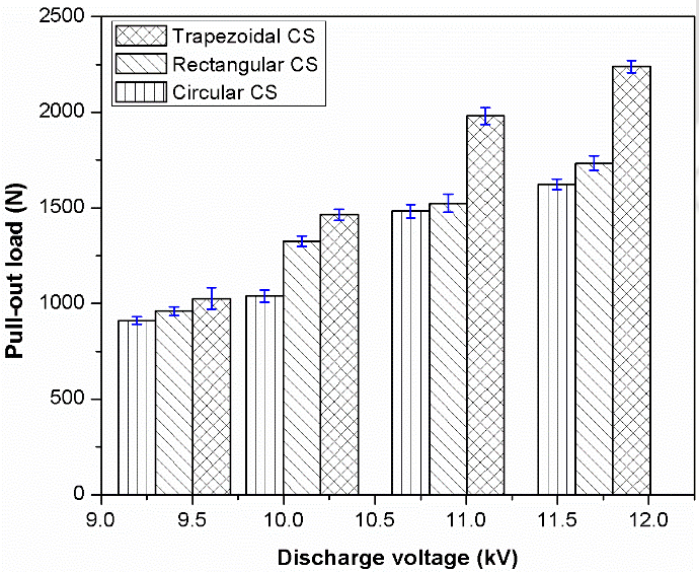


Figure 5.15 Pull-out value for samples crimped with different CS coil for various discharge energy

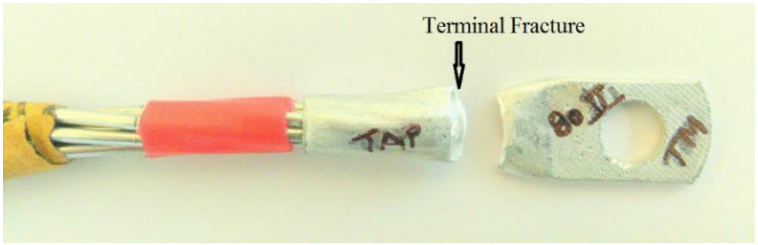


Figure 5.16 Terminal fracture at 11.7 kV discharge voltage for trapezoidal CS coil

As shown in Figure 5.16, at 11.14 kV for trapezoidal CS coil, fracture of the crimped terminal was observed. This shows that the strength of the crimped sample was found to be more than the terminal fracture strength. It is also a good indication of highest strength which can be achieved by simply modifying the CS of the helical coil.

## 5.4 Summary

In present chapter, numerical simulations and experiments were carried out on modified cross-sections of the helical coil. Different types of the helical coil were used and compared to find the most suitable helical coil. Important conclusions of numerical simulations and experimental work are summarized below.

- The current density was found to be 25.31 kA/mm$^2$ for trapezoidal CS coil compared to 23.28 kA/mm$^2$ and 22.61 kA/mm$^2$ for rectangular CS and circular CS coil, respectively.
- The magnetic field was found to be 8 Tesla for trapezoidal CS coil compared to 7.1 Tesla and 6 Tesla for rectangular CS and circular CS coil, respectively.
- The impact velocity was found to be 225 m/s for trapezoidal CS which is higher by 10 % and 15 % compared to rectangular CS and circular CS coil, respectively.
- Radial deformation of terminal carried out by trapezoidal CS coil was found to be higher compared to rectangular CS and circular CS profile helical coil. Simulation deformation results are in 90 % agreement with the experimental results.
- Contact length was found to be more in trapezoidal CS coil due to maximum terminal deformation. Simulations results are in 95 % in agreement with the experimental contact length.

- Contact resistance value of crimped samples were observed to be 24.13 % lesser for trapezoidal CS coil compared to circular CS coil and 10.3 % lesser compared to rectangular CS coil due to more area in contact.
- Hardness value reveals that by EM crimping process there was an increase in the hardness over the thickness due to peening effect. Value of hardness was found to be 57 $HV_{0.1}$ for samples carried out by trapezoidal CS coil, resulting in an increase in 38 % hardness value compared to parent value.
- Pull out test value show increase in strength by 22.5 % for 11.25 kV discharge voltage for trapezoidal helical coil compared to rectangular CS coil and 40.7 % compared to circular CS coil. Fracture over the samples crimped using trapezoidal CS coil was observed, which shows the maximum strength that can be achieved in EM crimping process.

The important prospect of this chapter was to find the most optimized coil to get a uniform radial crimping at minimum energy. From the simulation carried out in LS-DYNA and experimental work, trapezoidal CS coil was found to be the most suitable coil among rectangular CS and circular CS coil.

# Chapter 6

## 6 Numerical and Experimental Studies on Different Field-Shapers

### 6.1 Introduction

The rise in temperature causes the thermal expansion of terminal connectors loosening the connection resulting in sparks and creating safety issues (Jiang et al., 2014). Metallic electrical terminals which are good conductors can easily be deformed through pressure generated by the intense transient magnetic field in EM crimping process (Correia et al., 2008). Since the process takes place without any physical contact, it can produce highly durable connection terminal (Shim et al., 2016). There can be a significant improvement in the surface property of the material exposed to EM process due to peening effect (Li and Cheng, 2009), which can improve the fatigue life of the connection terminals which are exposed to wear and tear during connections.

In the EM crimping process, a very important tool is a field-shaper (FS) and its purpose is to concentrate the magnetic field onto the required region to achieve an efficient and higher deformation of the workpiece placed in the vicinity of the effective working length (Bahmani et al., 2009). The advantage of using FS is to increase the life of the coil by increasing the efficiency for the same amount of current passed through the coil thus improving the flexibility of the process. The designing of FS is more economical and quicker than manufacturing special coils (Psyk et al., 2011). Working of FS is explained in Section 2.6.

But, FS also comes with some disadvantages like, as it is not directly connected to the coil, there occur energy losses resulting in inefficient energy transfer. Moreover, the material of the field-shaper must be chosen such that it can bear high mechanical loads. One of the main characteristic of the field-shaper in providing efficient magnetic field strength is its design (Chaharmiri and Arezoodar, 2016).

In this chapter, the effects of three FS geometry, single-step, double-step and tapered geometry on EM terminal-wire crimping process is studied. As, no numerical and

experimental comparison of three types of FS with geometries like single-step, double-step, and tapered FS has been reported yet. The comparison was carried out by keeping the total FS total length and effective working area constant. As the slit in the FS plays an important role because it affects the performance, so slit width was also kept constant.

The simulation on EM terminal-wire crimping process was carried out on LS-DYNA EM module software, and the experimental work was carried out by comparing the results obtained from the simulations. The general objective was to find the most suitable FS among single-step, double-step and tapered, for effective crimping of the terminal over the wire strands Validation of the simulation was done using terminal radial deformation and wire strands contact length. The results will be helpful in determining the geometry of the field-shapers for similar applications. Post-processing results like contact resistance, surface hardness, hardness along cross-section and pull-out tests were carried out and compared simultaneously. Finite Element Analysis involved in the LSDYNA is already explained in detail in Chapter 4, Section 4.3.

## 6.2 Numerical Analysis

The coupled EM and structural, mechanical numerical analysis for the wire crimping with different field-shaper geometry were carried out in LS-DYNA EM module. The solver computes the EM fields by solving Maxwell's equations in the conductor, calculating the eddy current and Lorentz force using finite element method coupled with the boundary element method for the surrounding air (L Eplattenier, Cook, and Ashcraft, 2008). The simulation computes the EM field under each step of the time increment. A total of 8 contacting parts in the model, needs 18 contact pairs for all possible two surface combination. A seven wire strands were used in the model. The deformable wire strands and the terminals were modeled with C3D8R, eight-node elements. The field-shaper and the primary coil were modeled using R3D4 elements. For comparison, total FS length, the slit width and the effective working length were kept constant as shown in Figure 6.1. The wire strands and connection terminal were made of AA 1050, where Johnson-Cook (J-C) material property was used while working coil and field-shaper material is assigned to be copper. J-C material properties are listed in Table 4-2. The mechanical and electrical properties of the materials used in the simulation are listed in Table 6-1.

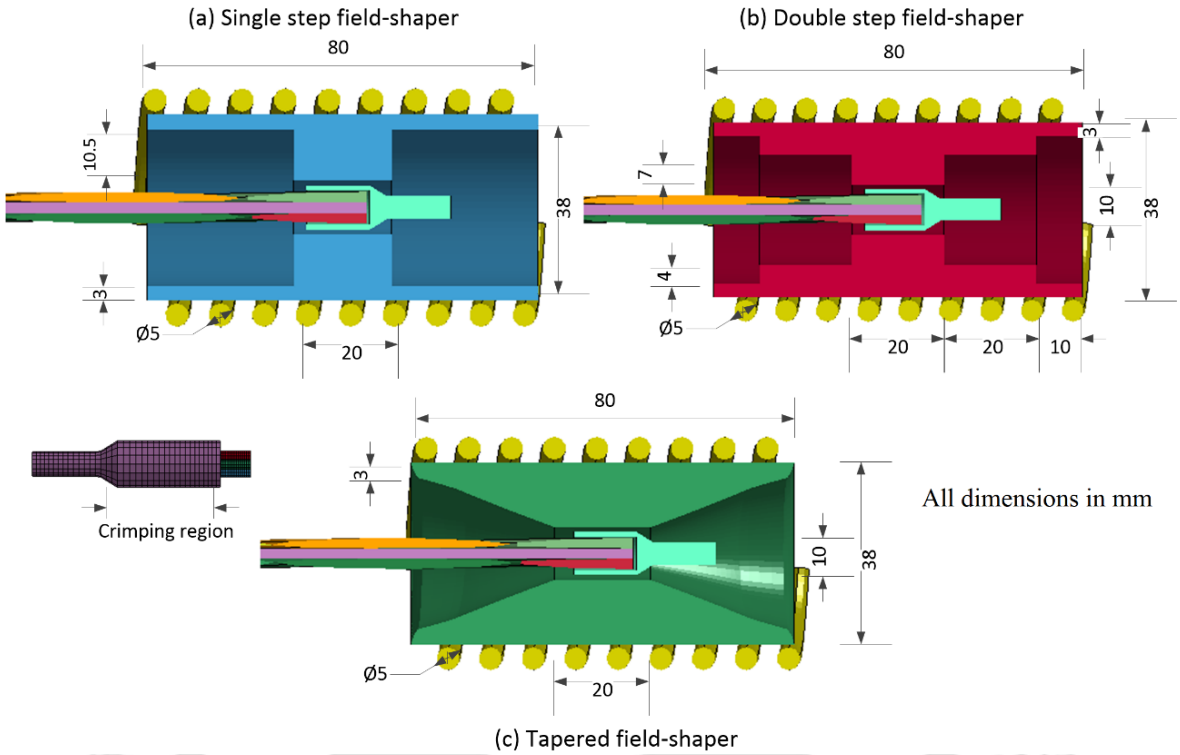


Figure 6.1 Cross-sectional view showing dimensions of (a) Single-step FS (b) Double-step FS (c) Tapered FS

Table 6-1 Material properties of the coil/FS and workpiece (Correia et al., 2008)

| Parameters | Coil/FS | Workpiece |
|---|---|---|
| Material | Copper | AA 1050 |
| Conductivity (S/m) | $5.96 \times 10^7$ | $3.68 \times 10^7$ |
| Density ($Kg/m^3$) | 8960 | 2700 |
| Poisson's ratio | 0.36 | 0.35 |

The input circuit condition was obtained from the experimental setup, and the dimension of the workpiece is shown in Table 6-2. In EM crimping process, the input current is an important factor which was taken from the experimental EM forming setup for various discharge voltages as shown in Figure 6.2. This input current was used as loading curve in the software to analyze the dynamic plastic deformation of the terminal. As in EM process, the first period of the current is responsible for considerable deformation as stated by Haiping and Chunfeng. So, to reduce total FEM and BEM calculation time, the

simulation was carried out for the first pulse only. FEM input conditions used for running simulations is listed in Table 6-3.

Table 6-2 Workpiece dimensions

| | | |
|---|---|---|
| Workpiece | Material | Aluminium |
| | Outer diameter of terminal | 9.0 mm |
| | Thickness of terminal | 1.0 mm |
| | Length | 20 mm |
| | Wire strands diameter | 5.8 mm |

Table 6-3 FEM input conditions for field shaper models

| Model | No. of element | EM time | Mechanical time | Time step | Iteration | CPU running time |
|---|---|---|---|---|---|---|
| Single step FS | 9588 | 37 µs | 37 µs | 1 µs | 10000 | 84 hrs. |
| Double Step FS | 9772 | | | | | 91 hrs. |
| Tapered FS | 9841 | | | | | 96 hrs. |

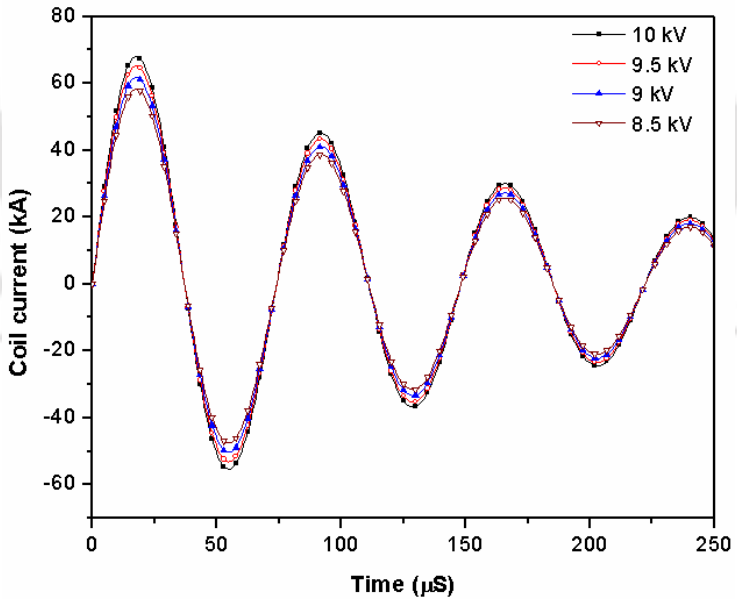


Figure 6.2 Typical waveform showing the current values for various discharge voltages

### 6.2.1 Current Density

As the voltage increases, the current amplitude increases and thus the induced current density on the conductor increases (Equation 4.1). From Figure 6.3, the current density obtained at 10 kV at the effective working zone of the field-shaper for single-step is 14.32 kA/m$^2$, whereas, for double-step, it is 13.45 kA/mm$^2$ and for tapered it is 9.88 kA/mm$^2$, respectively.

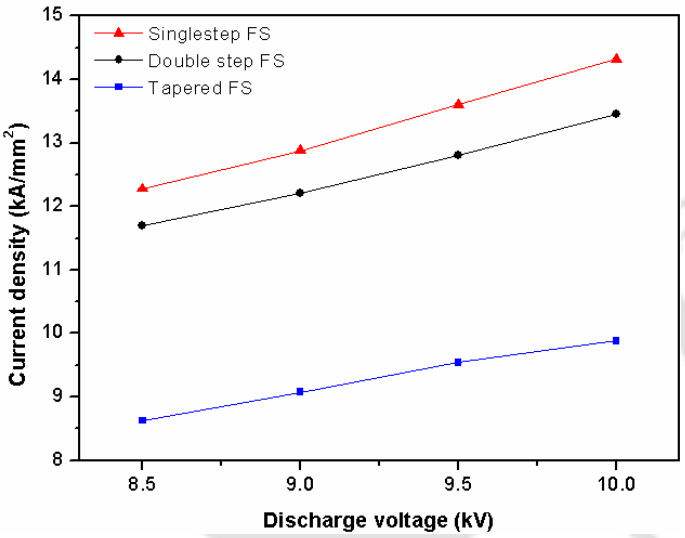


Figure 6.3 Current density vs. Discharge voltage graph for different FS geometry

It was found that, though the same amount of current is passed through the working coil around the different field-shapers, the current density induced in single step field-shaper was more compared to double step and tapered field-shaper. The fringe pattern for all the three field-shapers for 10 kV of discharge voltage is shown in Figure 6.4

### 6.2.2 Magnetic Field

It was found that magnetic field increases with the increase in current amplitude passed through the coil (Equation 4.21). As shown in Figure 6.5, it was found that the magnetic field induced over the terminal surface in case of single-step field-shaper was more than that of tapered and double-step field-shaper. The peak value of magnetic field obtained at 10 kV discharge voltage is found to be 10.84 T in the case of single step field-shaper, whereas it was 10.76 T and 9.64 T for double step and tapered FS, respectively.

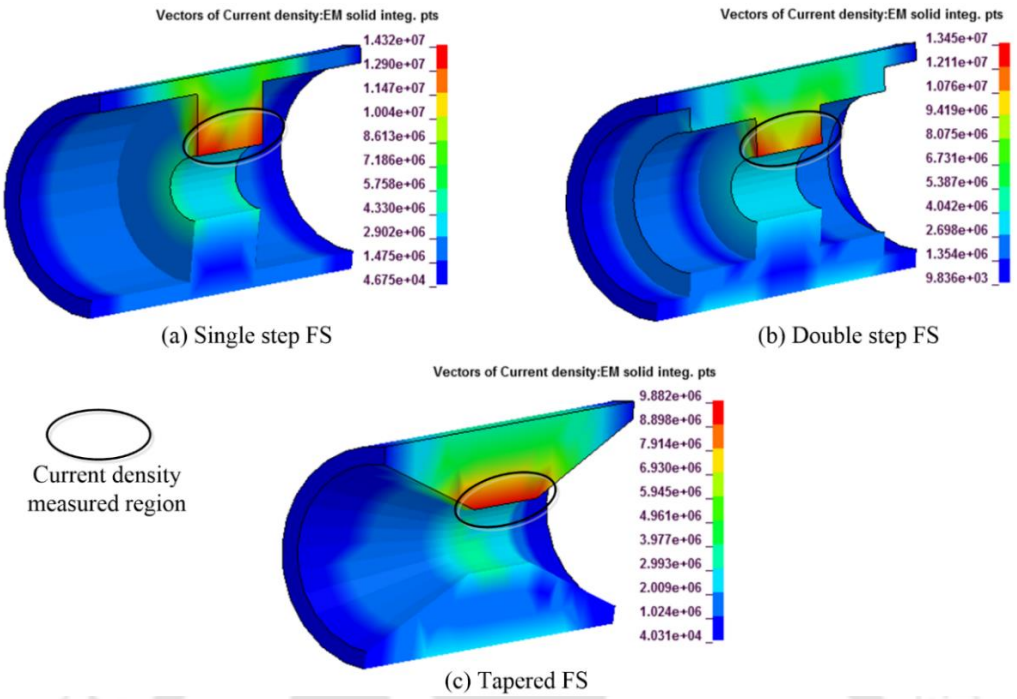


Figure 6.4 Fringe pattern of peak current density obtained for different FS (a) Single-step (b) Double-step (c) Tapered

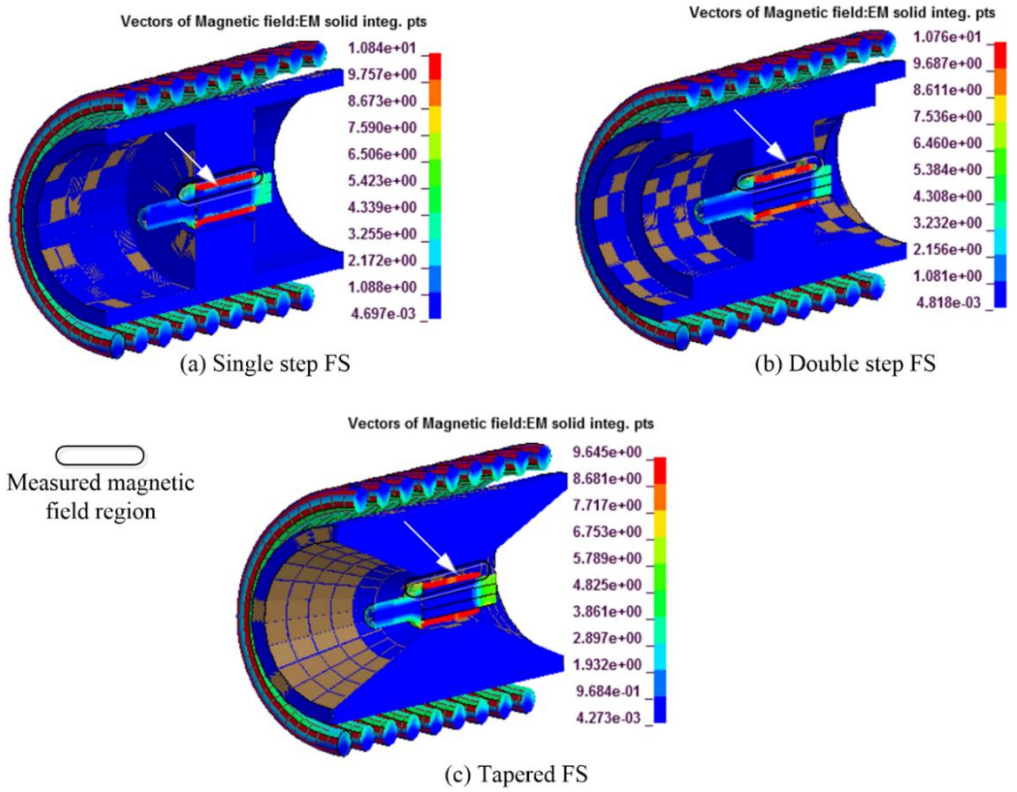


Figure 6.5 Fringe pattern of peak magnetic field obtained for different FS

It is to be noted that, even though the field-shaper length and effective working length remains the same for all the three FS, the magnetic field was found to be maximum for single step FS compared to other two FS. The high value of magnetic field over the terminal surface in case of a single step is due to the more spatial distribution of magnetic field and flux. According to Maxwell equation, field gradient can be expressed in terms of current density. So, high value of current density in single step FS resulted in an increase in the magnetic field compared to double step and tapered FS.

### 6.2.3 Lorentz Force

Lorentz force, $F$ is the result of combination of forces due to the electric and magnetic force, expressed as,

$$F = qE + (qv \times B) \tag{6.1}$$

where $q$ is the charged particle, $v$ is the velocity of the charged particle, $E$ is the electric field and $B$ is the magnetic field. The first term of the above equation is the force generated by the electric field and the second term is the force generated by the magnetic field. So, it can be seen that the Lorentz force is directly proportional to the electric field and the magnetic field.

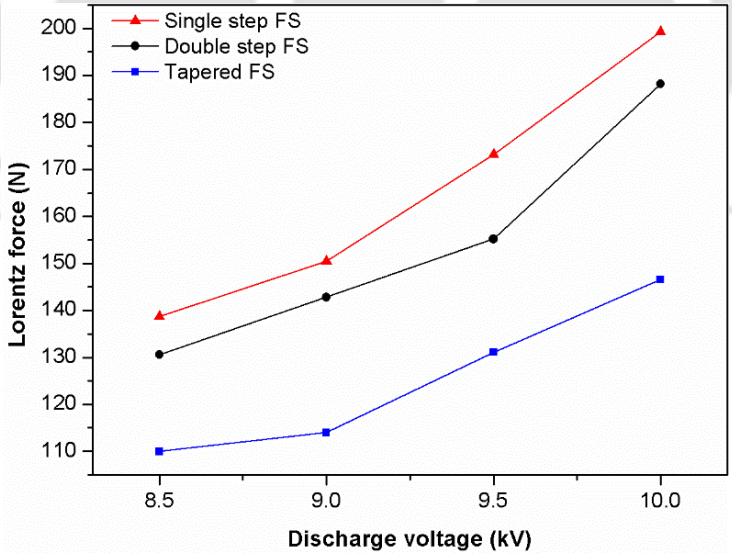


Figure 6.6 Lorentz force for different FS geometry

As shown in Figure 6.6, the value of Lorentz force was found to increase with the increase in discharge voltage. It was found that for 10 kV of the discharge voltage maximum

Lorentz force of 199.3 N was obtained for single step FS, whereas the value of 188.2 N and 146.6 N was obtained for double step and tapered FS, respectively. Since the magnetic field and the current induced was more in the case of single step field-shaper than tapered and double step field-shaper, so the Lorentz force produced was more in the case of single step field-shaper than the other two field-shaper profiles from the above equation (6.1).

### 6.2.4 Impact Velocity

The peak amplitude of the impact velocity of the terminal over the wire strands was obtained. From the results, obtained, the value of impact velocity obtained using the single-step field-shaper was higher than the other two field-shaper geometry. In EM forming, the forming velocity is directly proportional to the square of magnetic flux density.

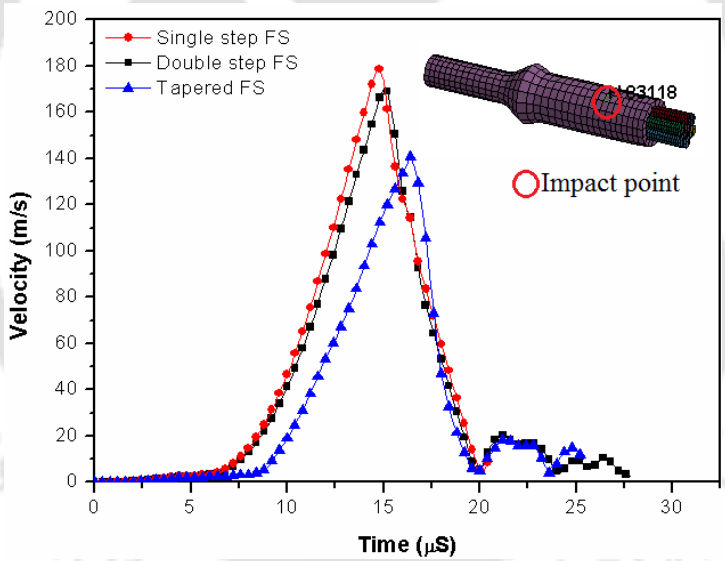


Figure 6.7 Impact velocity of the terminal over the wire strands at 10 kV

As shown in Figure 6.7, impact velocity of the terminal over the wire stands was found to increase with the increase in discharge voltage (Equation 4.23). It was found that for 10 kV of discharge voltage, 179 m/s velocity was obtained for single step FS, whereas the value of 170 m/s and 141 m/s was obtained for double step and tapered FS, respectively. From the results of the magnetic field obtained above, it is clear that the magnetic field produced in case of single-step FS is higher than that produced in case of tapered and double step FS.

### 6.2.5 Effective Plastic Strain

For crimping of the terminal to take place, the minimum value of effective plastic strain must be achieved. As the impact velocity of the terminal over the wire strands increases with increase in the current amplitude. As a result, higher plastic deformation takes place. The plastic strain, being directly proportional to the impact velocity, increases with increase in the impact velocity due to increase in current amplitude.

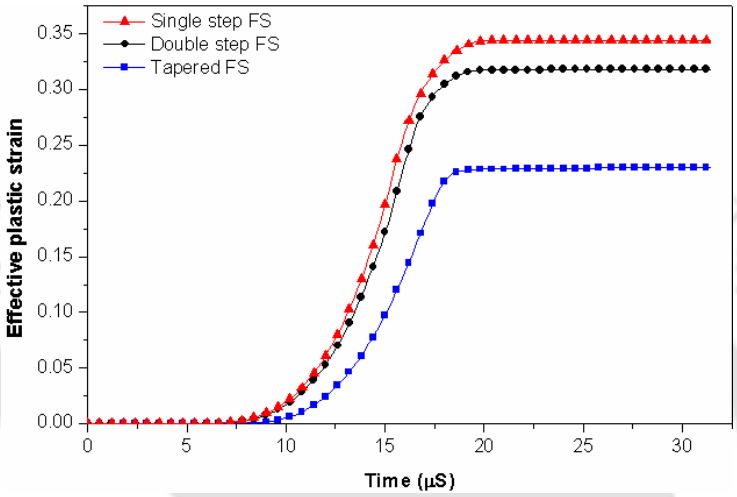


Figure 6.8 Effective plastic strain over the terminal for different FS at 10 kV

As shown in Figure 6.8, the maximum plastic strain of 0.344 was observed for single step FS, whereas 0.318 and 0.230 were observed for double step FS and tapered FS, respectively.

## 6.3 Comparison between Experiment and Simulation

Assembly consisting of the fixture, primary coil and field-shapers are shown in Figure 6.9. All the three different types of field-shaper were manufactured as per the dimensions used in the simulation as shown in Figure 6.10. In all the FS, length of 80 mm, effective working length of 20 mm and slit width of 1 mm was made constant. Crimped samples carried out using different field-shaper are shown in Figure 6.11.

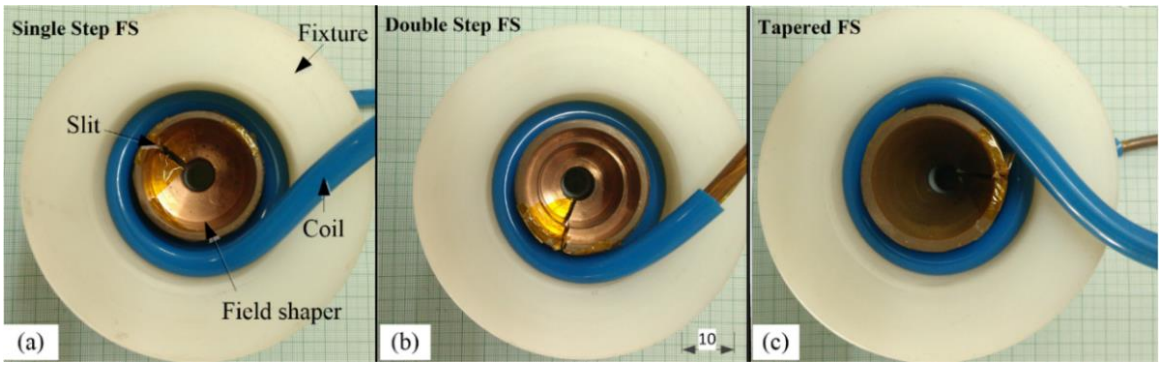


Figure 6.9 Assembly of different types of FS (a) Single-step , (b) Double step and (c) Tapered FS

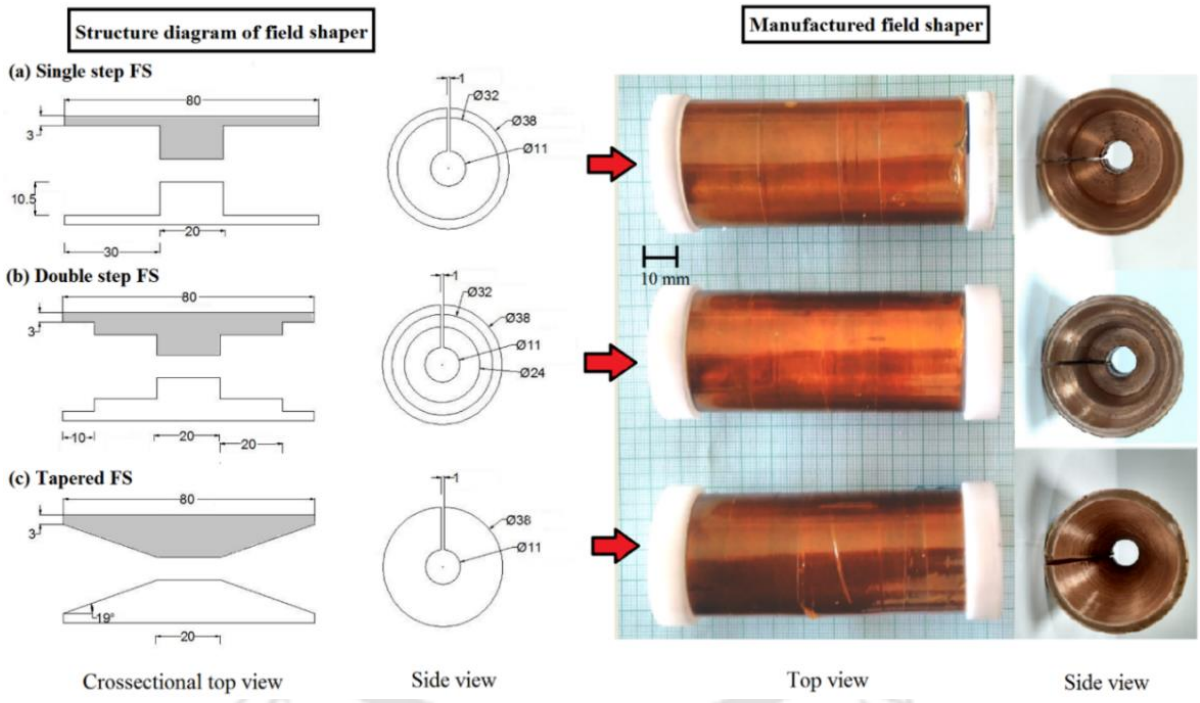


Figure 6.10 Schematic diagram and fabricated different FS

### 6.3.1 Radial Deformation

It was found that radial deformation increases with increase in magnetic flux density due to increase in discharge voltage. As shown in Figure 6.12, the change in radial deformation was found to increase with the increase in discharge voltage for all the three field-shapers because of increase in Lorentz force and the magnetic pressure on the workpiece.

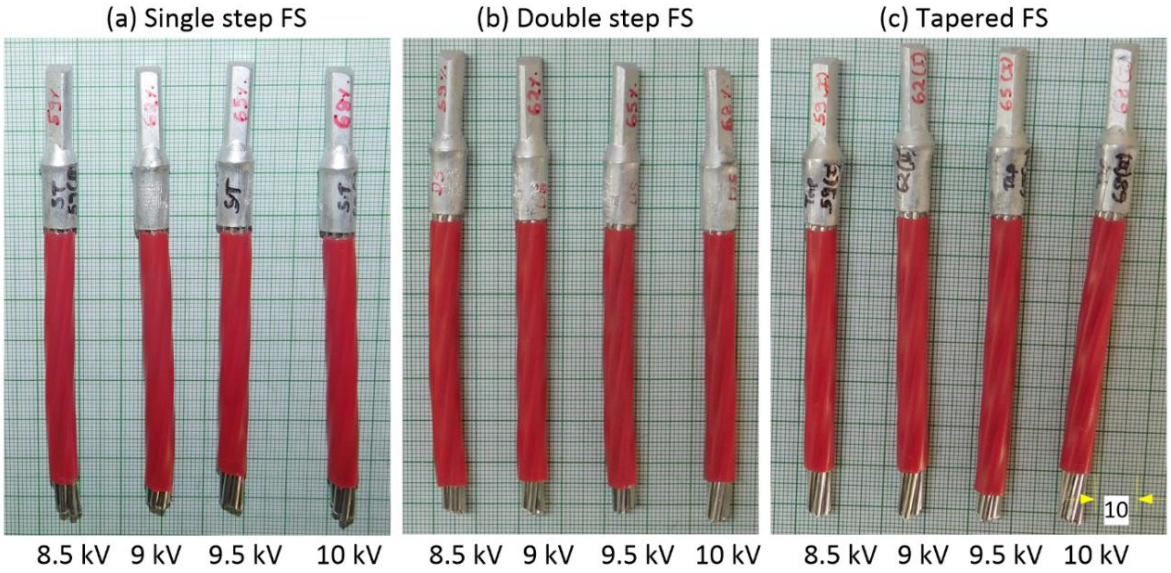


Figure 6.11 Samples crimped at different types of FS

### 6.3.2 Radial Deformation

Maximum radial deformation as per conventional crimping process can be 1.7 mm for these dimensions of the terminal to avoid dielectric and neutral phase change ("TE Connectivity," n.d.). So, the maximum change in deformation during compression was restricted to 1.70 mm.

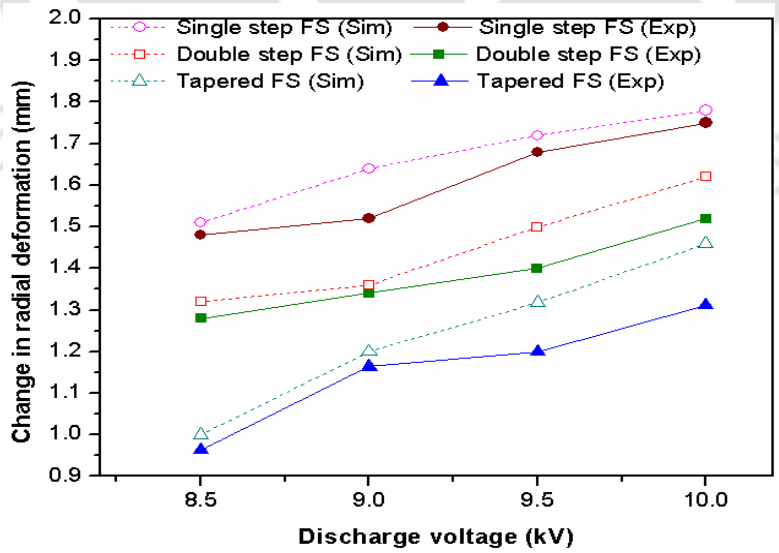


Figure 6.12 Variation of change in radial deformation for different FS geometry at different discharge voltages

The maximum radial deformation of 1.70 mm was observed for single step FS compared with 1.52 mm for double step FS and 1.44 mm for tapered FS respectively for 10 kV of discharge voltage The weight of field-shapers was measured, and it was found that single step FS has the minimum weight value of 297 gm. While double step FS and tapered FS has the weight of 435 gm and 534 gm. So, due to the lower value of mass, it resulted in lesser inductive losses. Therefore, more current density was observed over the effective working area for the single step FS compared to other two field shapers. So, higher deformation was observed for single step FS followed by double-step FS and least for tapered FS respectively. Variation of simulation and experimental data for the radial deformation with percentage error is shown in Table 6-4.

### 6.3.3 Contact Length Analysis

In terminal-wire crimping process, the gap between the terminal and the wire strands is a crucial factor because it determines the quality of the crimp joint and contact resistance as stated by Capelli et al. (2016). Cross-section analysis of the crimped samples showing radial deformation for various discharge voltages for different field-shapers are shown in Figure 6.13.

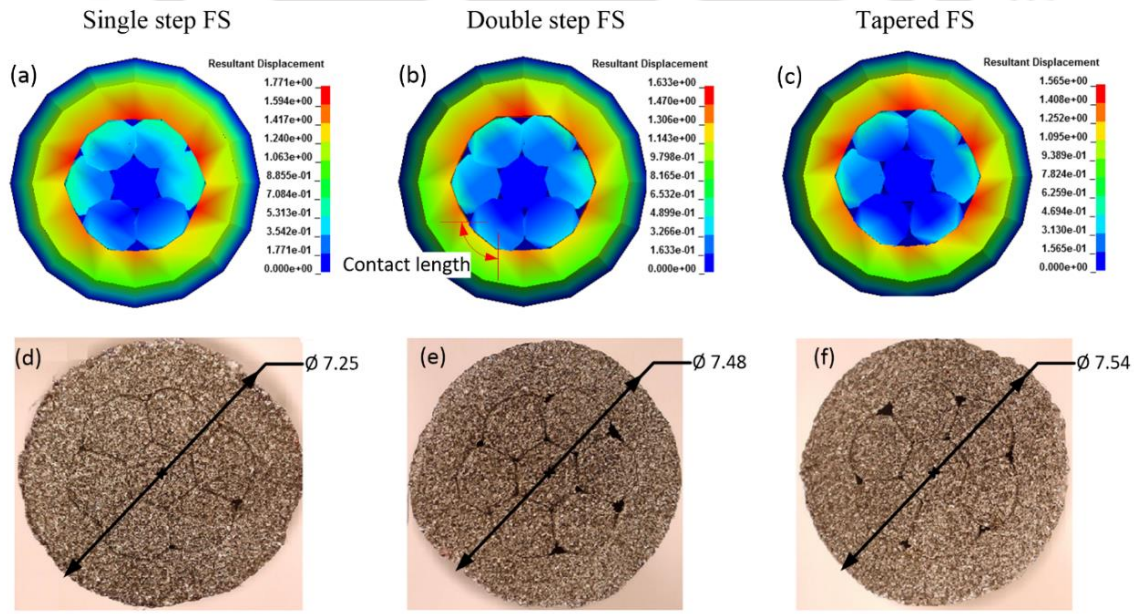


Figure 6.13 Cross-section of EM wire crimped sample for different FS at peak discharge voltage (10 kV)

It was difficult to measure the gap between the wire strands and terminal, so contact length of all the seven wire strands and terminal in contact was measured as shown Figure 6.14, by using an optical microscope. The maximum contact length of 10.45 mm was found for single step FS compared to 10.23 mm and 9.65 mm for double step FS and tapered FS, respectively. Variation of simulation and experimental data for the total contact length with percentage error is shown in Table 6-4

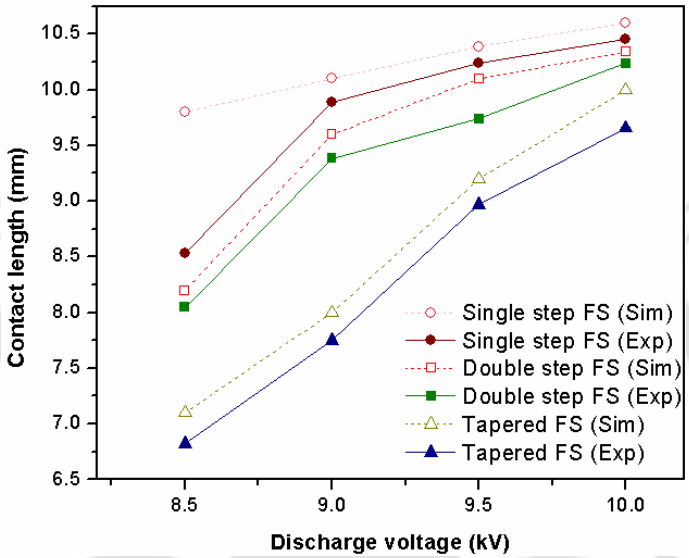


Figure 6.14 Variation of contact length between seven wire strands and the terminal for different FS

Table 6-4 Variation of simulation and experimental values

| | | Radial deformation (mm) | | | Contact length (mm) | | |
|---|---|---|---|---|---|---|---|
| Voltage (kV) | Field-shapers | Simulation | Experiment | Error % | Simulation | Experiment | Error % |
| 10 | SS FS | 1.78 | 1.75 | 1.71 | 10.74 | 10.45 | 2.77 |
| | DS FS | 1.66 | 1.52 | 9.21 | 10.34 | 10.23 | 1.02 |
| | T FS | 1.56 | 1.46 | 6.84 | 10 | 9.65 | 3.55 |
| 9.5 | SS FS | 1.72 | 1.68 | 2.38 | 10.39 | 10.23 | 1.49 |
| | DS FS | 1.5 | 1.4 | 7.14 | 10.1 | 9.74 | 3.69 |
| | T FS | 1.39 | 1.2 | 9.83 | 9.2 | 8.97 | 2.55 |
| 9.0 | SS FS | 1.64 | 1.52 | 7.89 | 10.1 | 9.89 | 2.10 |
| | DS FS | 1.36 | 1.34 | 1.49 | 9.6 | 9.38 | 2.31 |
| | T FS | 1.2 | 1.16 | 3.44 | 8 | 7.74 | 3.25 |
| 8.5 | SS FS | 1.51 | 1.48 | 2.02 | 9.8 | 8.52 | 14.9 |
| | DS FS | 1.32 | 1.28 | 3.1 | 8.2 | 8.04 | 1.87 |
| | T FS | 1.0 | 0.96 | 4.16 | 7.1 | 6.82 | 4.044 |

**SS: Single step, DS: Double step, T: Tapered**

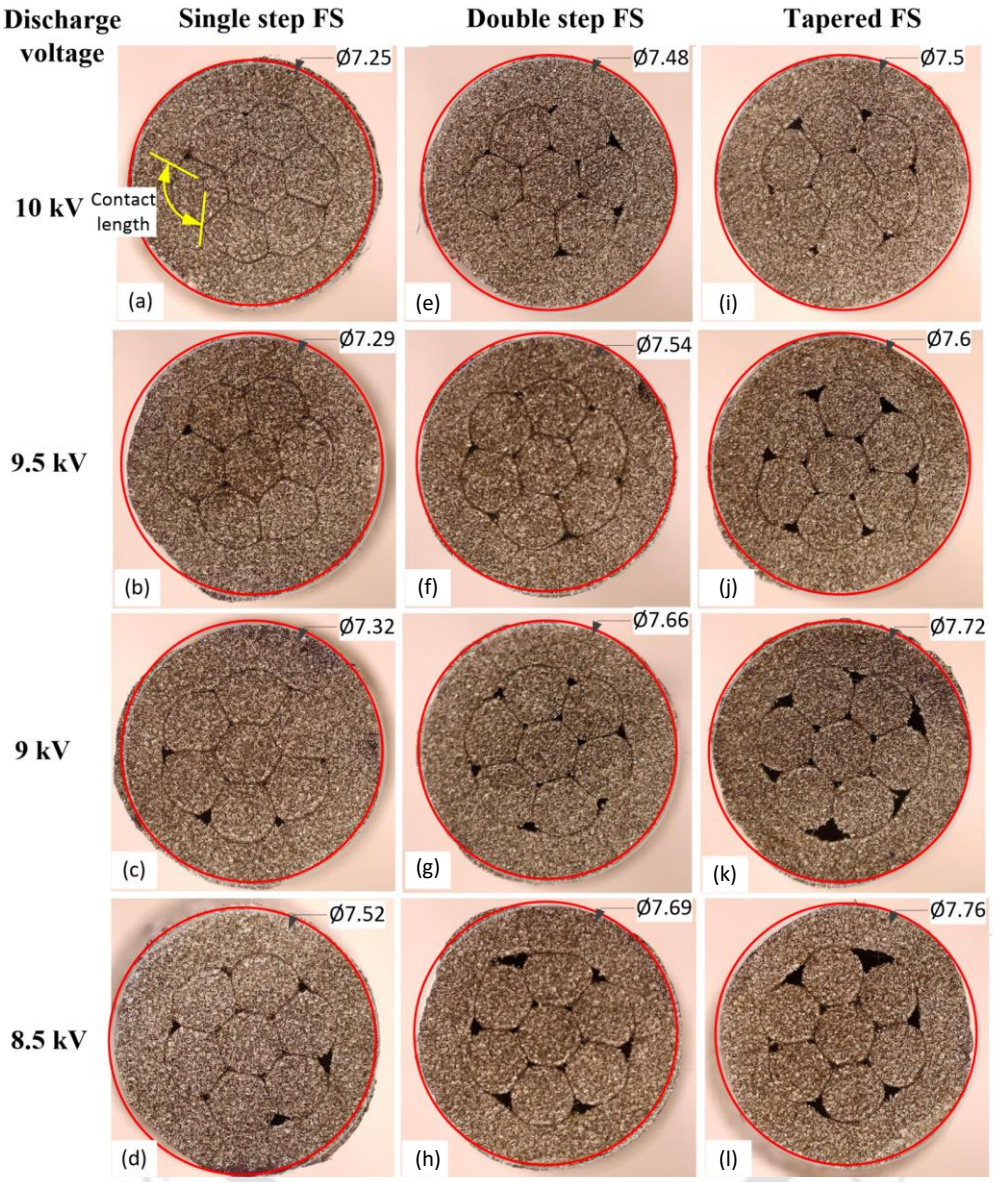


Figure 6.15 Cross-section of EM wire crimped sample carried out using different FS at various discharge voltages

With the increase in discharge voltage, terminal deformation increases resulting in a decrease in gap and increase in contact length. Maximum contact length was found to be for single step FS, followed by double-step FS and tapered FS. The main advantage of EM crimping process is no spring back of terminal due to the advantage of high strain rate deformation, which is a major issue in conventional crimping process..In wire crimping process, the gap between the terminal and the wire strands is a crucial factor because it determines the quality of the crimp joint and contact resistance. Cross-section

analysis of the crimped samples for various discharge voltages for different FS is shown in Figure 6.15. Samples crimped using single step FS a uniform radial deformation was achieved, and the gap between the wire strands and the terminal was found to decrease with increase in discharge voltage. In Figure 6.15 (a) minimum gap was observed for 10 kV discharge voltage.

This gap was found to increase at lower discharge voltages as shown in Fig. 6.15 (b,c,d). Whereas for double step FS as shown in Fig. 6.15 (e,f,g,h) the gap was found to be more compared to single step FS crimped samples. For tapered field-shaper samples as shown in Fig. 6.15 (i,j,k,l) gap between the terminal and wire strands can seen. The maximum contact length of 10.45 mm was obtained for single step FS compared to 10.07 mm and 9.65 mm for double step FS and tapered FS, respectively for 10 kV discharge voltages. Some of the cross-section cut crimped samples at lower discharge voltages can be seen in Figure 6.16. These samples show that discharge voltage less than 8.5 kV (i.e., 8 kV and 7.5 kV) is not sufficient enough to provide sufficient deformation. A significant visual gap can be seen with a non-uniform deformation of the terminal over the wire strands.

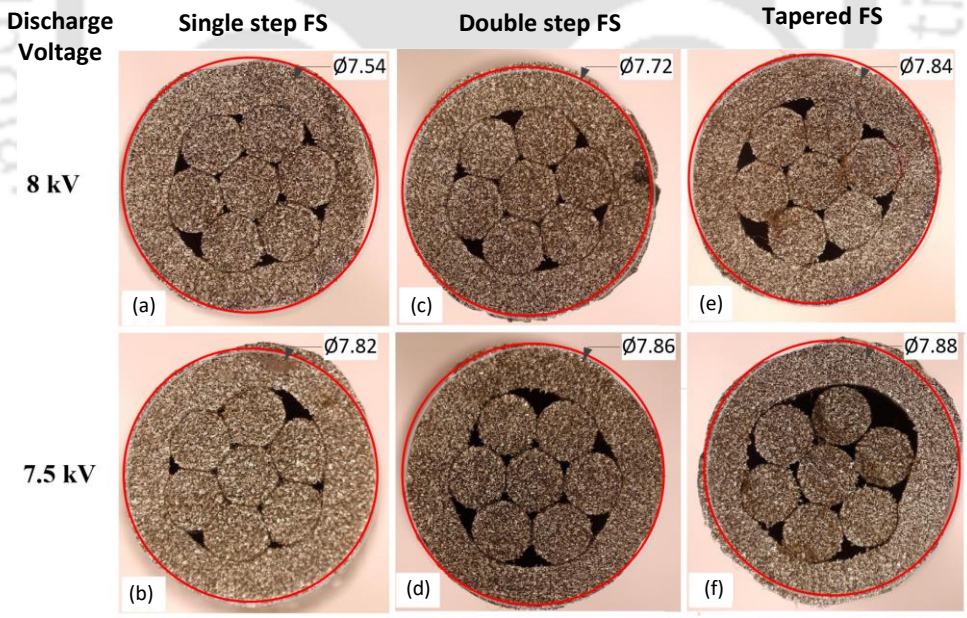


Figure 6.16 Improper crimping at lower discharge voltage

### 6.3.4 Contact Resistance

The Contact resistance of the crimped region was measured using an LCR meter. The contact resistance for samples crimped using different FS are shown in Figure 6.17.

Contact resistance is an important parameter for any wire crimped samples. On increasing the discharge voltage, the contact resistance of the crimped region decreases. It was found that samples crimped using single step FS showed a minimum resistance value of 13.4 mΩ contact resistance, while double step FS and tapered showed 14 mΩ and 14.5 mΩ contact resistance, respectively for maximum discharge voltage of 10 kV. This is because the single step FS concentrates more magnetic field on the workpiece, the most among all the three field-shapers due to the lower inductance value and its optimized design. Hence the contact resistance for a particular discharge voltage was lower for single step FS and the least for tapered FS.

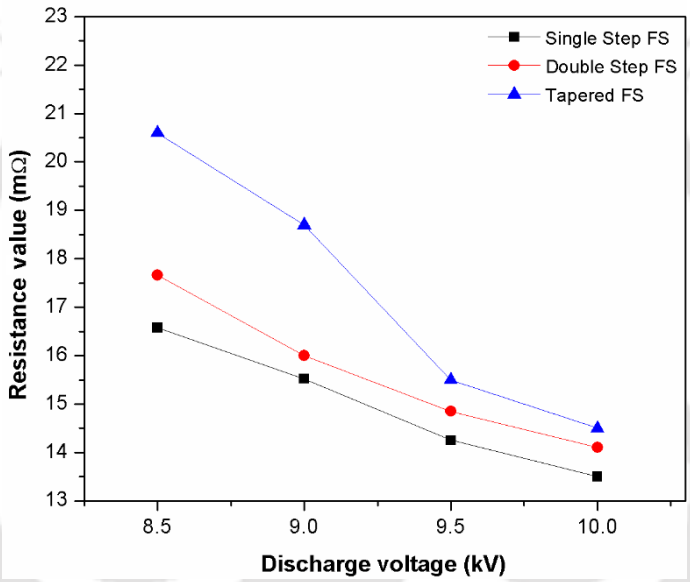


Figure 6.17 Variation of resistance over the contact area for different FS

### 6.3.5 Surface Hardness Analysis

Apart from crimping operation, the EM pressure waves on the material can be beneficial in other ways. There is a significant change in material strength and hardness which is produced by EM shock waves as claimed by Golowin et al. (Golowin et al., 2007). In actual pressure waves in EM processing is assumed to induce shock hardening due to an increased rate of dislocation accumulation and strain hardening. The hardness over the crimped terminal surface was measured by using Vickers microhardness tester, where 100-gram force was chosen as the test force in this study. As shown in Figure 6.18, the hardness values of 56 $HV_{0.1}$, 53 $HV_{0.1}$, and 48 $HV_{0.1}$ were obtained for samples crimped using single step FS, double step FS and tapered FS respectively. This is due to the surface

hardening which occurs due to the compressing of surface exposed to the high strain rate forming process. Due to maximum magnetic field concentration, surface hardening was found to be maximum for single step FS, and least for the tapered FS. This shows the advantages of this process where surface hardening can also be done with EM crimping process.

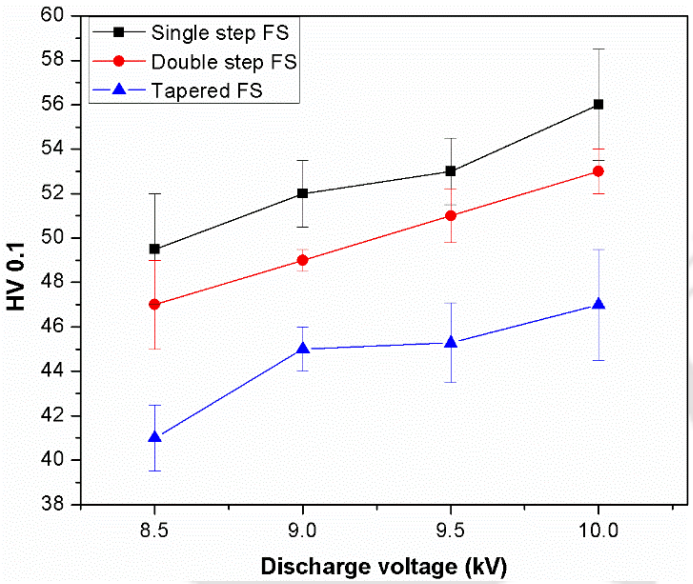


Figure 6.18 Variation of hardness over the surface for different FS

### 6.3.6 Hardness along Cross-Section

By adjusting the parameters of the EM field, compressive residual stress can be introduced along the surface to get peening effects as claimed by Golowin et al. (Golowin et al., 2007). This compressive residual stresses due to EM peening (EMP) keeps varying the thickness of the workpiece. Since the hardness is related to plastic deformation, the hardness along thickness increases with increase in discharge voltage. The variation of hardness along cross section was studied. As shown in Figure 6.19, the value of hardness increased with the increased discharge voltage. The maximum hardness value of 61 $HV_{0.1}$ was observed for single step FS, compared to 56.4 $HV_{0.1}$ and 51.2 $HV_{0.1}$ for double step FS and tapered FS, respectively at 10 kV of discharge voltage. There was an increase of 79.4 % in the hardness value compared to parent hardness value of 34 $HV_{0.1}$. One of the reasons for this increase in hardness is due to residual strain induced by the high-speed forming process.

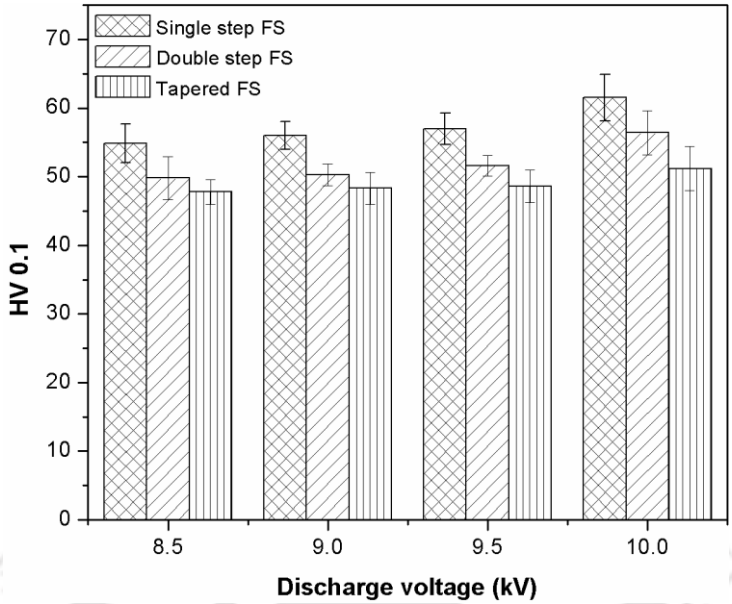


Figure 6.19 Variation of hardness over the surface for different FS along the cross-section

### 6.3.7 Pull-Out Strength

Comparison of the pull-out test was carried out using standard procedure (Connectors, 2006). Transverse speed was maintained at 50 mm/min. It was found that with an increase in discharge voltage pull-out value was found to increase as shown in Figure 6.20

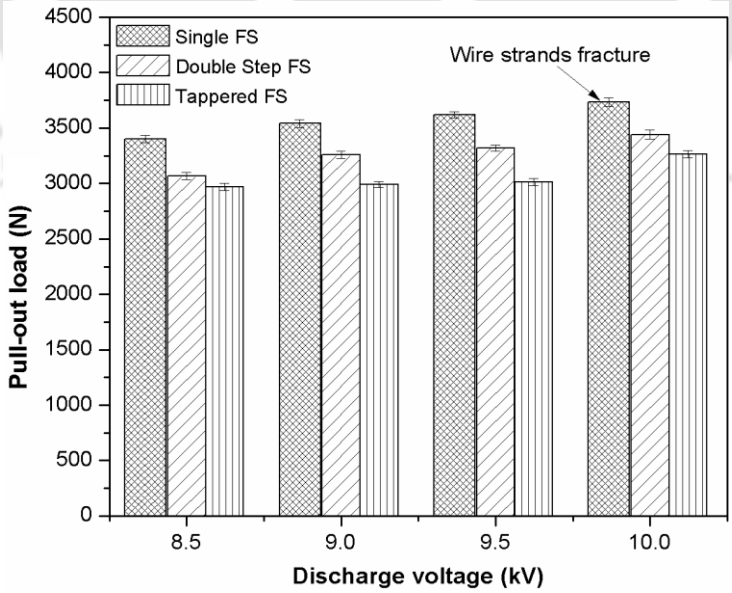


Figure 6.20 Variation in pull out strength for different discharge value for different FS

The maximum pull-out value was found to be 3.736 kN for single step FS, while for double step FS and tapered FS value was found to be 3.441 kN and 3.264 kN.. This is due to lower inductance value of single step FS which generates more concentration of magnetic field over the workpiece and more magnetic pressure leading to more deformation and contact length of the crimped junction. Since the pull out strength depends on the contact length, it was maximum in case of the samples crimped using single step FS. As shown in Figure 6.21, at 10 kV for single step FS, fracture of the terminal was observed. Scanning electron microscope (SEM) of fractured wire strands was carried showing neck formation which is a property of ductile fracture.

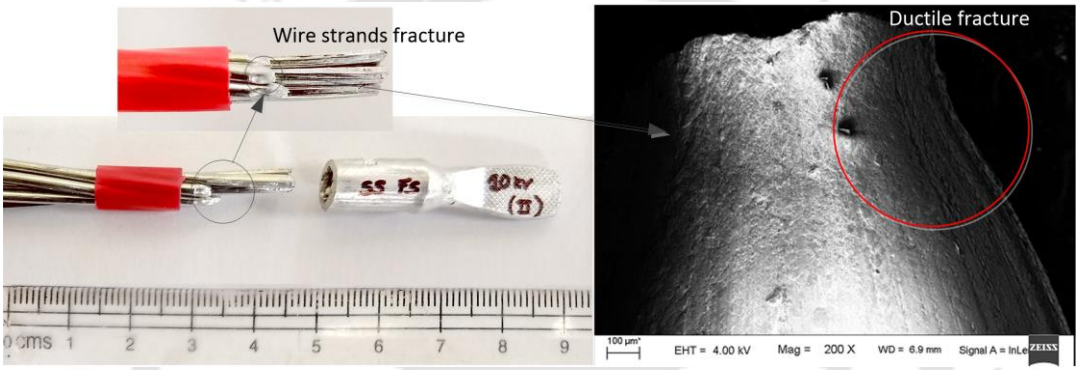


(a) (b)

Figure 6.21 Terminal fracture at 10 kV discharge voltage for single step FS

The EM terminal-wire crimping showed that the strength of the crimped sample was found to be more than the wire fracture strength which is a good measure of highest strength which can be achieved by a simple modification in the geometry of field-shapers.

## 6.4 Analytical Calculation of Field Shaper Designing

The important prospect of the FS is to concentrate the magnetic field at the effective working zone to increase the magnetic pressure over the workpiece placed inside it. Without FS, capacity of the capacitor has to be increased unnecessary to obtain the force required for forming the workpiece. For an efficient working of a FS it is important to design it with proper dimensions. Analytical calculation in the below section provides the parameters to design an optimal FS to produce a maximum magnetic pressure.

Following assumptions are made for the simplicity of the analysis:

- Outside the coil, the magnetic field is zero.
- Effect of the slit in the field shaper is neglected.
- The field skin depth is less for all the sizes of the system.

**i. Tapered FS**

Analytical calculation of the tapered FS with different dimension parameters are shown in Figure 6.22. Where $l_w$ is the length of working zone, $r_w$ is the radius of workpiece, $R$ is the outer diameter of FS, $h$ is the air gap between the workpiece and FS, and $\gamma$ is the slope angle of the FS.

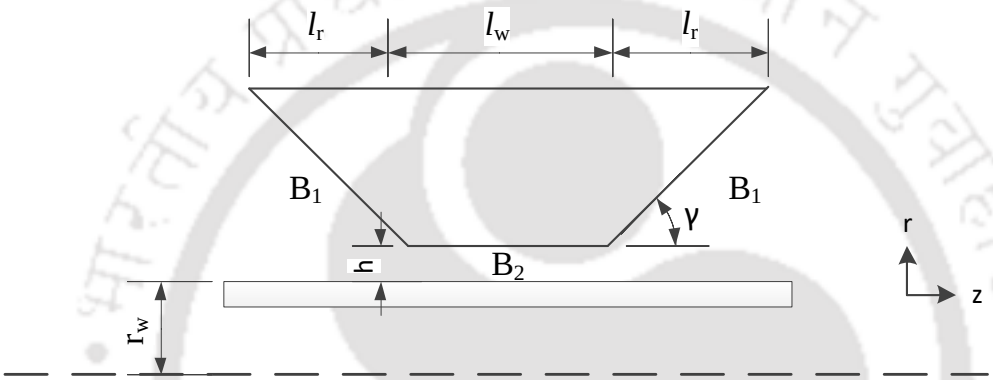


Figure 6.22 Various dimensional parameters of a tapered FS

In the end zone, magnetic field density ($B_1$) is given by,

$$B_1(r) = \frac{\emptyset}{2\pi(r - r_w)\big((r - r_w)(1 - cos\gamma) + r_w\gamma sin\gamma\big)} \tag{6.2}$$

In working zone, magnetic field density ($B_2$) is given by,

$$B_2 = \frac{\emptyset}{2\pi r_w h} \tag{6.3}$$

Integrating $B_1$ on r ∈ ( ($r_w$+$h$), $R$), taking assumption $R/r_w$ >>1, The current $i_1$ in the end zone is given by,

$$i_1 = \frac{\emptyset}{\mu_o 2\pi r_w \gamma} \ln\left(1 + \frac{r_w \gamma sin\gamma}{h\,(1 - cos\gamma)}\right) \tag{6.4}$$

While the current in the working zone $i_2$ is given as,

$$i_2 = \emptyset \frac{l_w}{\mu_o 2\pi r_w h} \tag{6.5}$$

So, the total current $i_t$ is found as the sum of the current in the end zone and the current in the working zone, i.e.

$$i_t = 2i_1 + i_2 = \emptyset \frac{l_w}{\mu_o 2\pi r_w h} \left(1 + \frac{2h}{\gamma l_w} \ln\left(1 + \frac{r_w \gamma sin\gamma}{h\,(1 - cos\gamma)}\right)\right) \tag{6.6}$$

Whereas inductance *l* of the FS is defined as,

$$l = \frac{\emptyset}{i_t} = \frac{1}{\frac{l_w}{\mu_o 2\pi r_w h} \left(1 + \frac{2h}{\gamma l_w} \ln\left(1 + \frac{r_w \gamma sin\gamma}{h\,(1 - cos\gamma)}\right)\right)} \tag{6.7}$$

i.e, inductance is a function of slope angle. Value of inductance increases with the slope angle. Efficiency of the FS can be stated as the ratio of the current over the effective working length to the total current, which is expressed as,

$$n_{eff} = \frac{i_2}{i_t} = \frac{l l_w}{\mu_o 2\pi r_w h} \tag{6.8}$$

The rate of working current to the total current approaches unity if slope angle goes to 180°. In this case inductance of the FS is equal to inductance of the working zone. Therefore the optimum field shaper is to be designed to have a slope angle of 180°. Only designing of such 180° slope angle FS is that it weakens it structural rigidity.

**ii. Single step FS**

Hence, to reinforce the protruded part FS angle can be made 90°, which can be an alternative as shown in Figure 6.23.

Calculation of the effect of the geometries parameters on the magnetic pressure. Taking assumptions like:

- Field outside the coil is zero.
- The net change of flux within the coil is also zero.

$$\pi(r_1^2 - r_w^2)B_1 = \pi(r_2^2 - r_w^2)B_2 \tag{6.9}$$

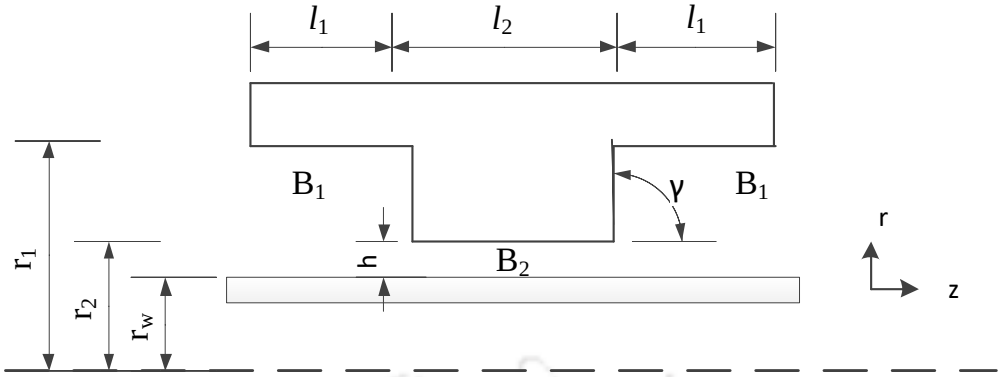


Figure 6.23 Various dimensional parameters of a single step FS

Taking line integral around complete flux path, the current in the FS is given as,

$$i_s = \frac{2B_1L_1}{\mu_o} + \frac{B_2L_w}{\mu_o} \tag{6.10}$$

The simplified magnetic pressure is given by,

$$P = \frac{B_2^2}{2\mu_o} \tag{6.11}$$

By using the principle of transformer,

$$i_cN \propto iL \tag{6.12}$$

Where $i_c$ is the coil current surrounding the FS. This also shows that, the magnetic pressure can be expressed as the function of the geometrical parameters of the field shapers. It can also be seen that by decreasing the length of the working zone, remarkable increase in the magnetic pressure can be obtained. The gap between the FS and the workpiece should be minimum for effective designing of FS.

### iii. Double step FS

Various dimensional parameters of a double step FS is shown in Figure 6.24. Similar to the above calculation current $i_d$ in the double step field shaper is given by equation (6.13).

$$i_d = \frac{2B_1L_1}{\mu_o} + \frac{2B_3L_3}{\mu_o} + \frac{B_2L_2}{\mu_o} \tag{6.13}$$

Considering the equations, it could be seen that, for any numerical value, current in the single step FS will be higher, followed by double step FS and tapered FS.

$$i_t < i_d < i_s \tag{6.14}$$

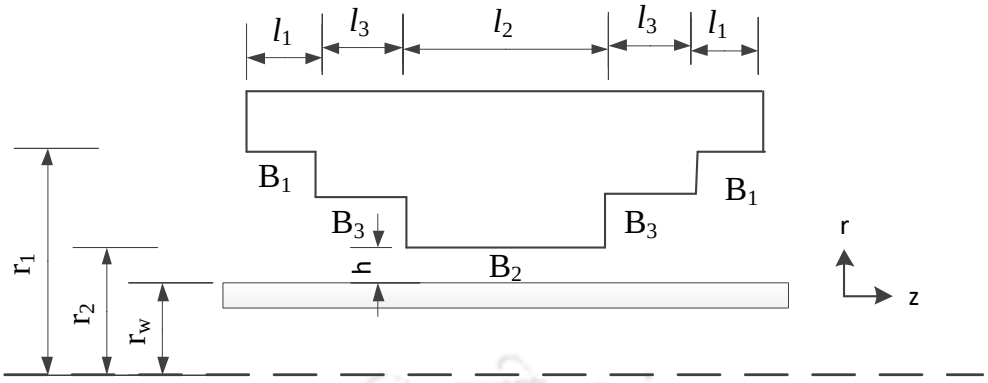


Figure 6.24 Various dimensional parameters of a double step FS

That's proves the significance of design of field shaper. That single step field shaper is more effective in terms of total current inside the field shaper.

## 6.5 Summary

In this concluding Chapter, numerical analysis and experiments were carried out on a single step, double step and tapered field-shapers, keeping the field shaper total length and working effective length constant. The following conclusions are drawn from the results.

- The current density of 14.32 kA/mm$^2$ at peak discharge voltage 10 kV was obtained for single step FS, which was 6% and 31% more, compared to double step and tapered FS, respectively over the effective working zone of the FS.
- The magnitude of the magnetic field over the terminal surface at peak discharge voltage of 10 kV for single step FS was found to be 10.84 T, whereas 10.76 T and 9.64 T was obtained for double step and tapered FS, respectively.
- Maximum Value of 199.3 N Lorentz force was observed for Single step FS, which was 11.1 N and 52.7 N more compared to double step and tapered FS, respectively.
- Impact velocity of the terminal over the wire strands of single step FS was found to be 179 m/s, whereas 170 m/s and 141 m/s were obtained for double step and tapered FS, respectively.

- The Plastic strain of terminal was found to be 0.344 for a single step, while 0.318 and 0.230 were obtained for double step and tapered FS, respectively.
- The terminal maximum radial displacement of 1.7 mm, 1.5 mm and 1.4 mm was obtained for a single step, double step and tapered FS. Experimental results are in good agreement with the numerical analysis results with an error below 5%.
- The seven wire strands and terminal interface contact length obtained for single step FS was found to 9.8 mm which was 0.8 mm and 1.1 mm more compared to double step FS and tapered FS. An error less than 6% was calculated when compared to numerical analysis results.
- Contact resistance values of crimped samples were observed to be 4.41 % lesser for single step FS compared to double step FS coil and 8.14 % lesser compared to tapered FS due to more area of contact.
- Surface hardness value reveals that by EM crimping process there is an increase in the hardness over the surface due to EM shock waves. Compared to parent hardness the value, there was an increase in hardness value by 60 %, 51.4 % and 37.1 % for a single step, double step and tapered FS.
- Hardness value along the cross-section reveals that by EM crimping process there was an increase in the hardness due to peening effect. The value of hardness was found to be 61 $HV_{0.1}$ for samples carried out by single step FS, resulting in an increase in 74.2 % hardness value compared to parent value.
- Maximum pull-out strength value was found to be 3.736 kN for single step FS, where the fracture of wire strands was observed. While a pull-out value of 3.441 kN and 3.264 kN was obtained for double step and tapered FS.
- Analytical calculation of the field shaper is carried out showing the single step FS to be more efficient followed by double step FS and tapered FS.

It was found that single step FS was found to be the most optimized FS, due to its lower inductance value, which results in improving the efficiency of the process. It is to be noted that lower inductance value may decrease the working life of the FS too due to a decrease in strength. So, proper selection of geometry is important while designing a FS for the enhancement of its working life with maximum efficiency

# Chapter 7

## 7 Conclusions and Scope of Future Work

### 7.1 Conclusions

In this thesis, research work was carried out on providing an alternative and effective way to tackle problem being faced by a conventional terminal-wire crimping process. The work carried out will be useful for cable crimping industries where cable connections are used in large numbers. Important results from the thesis work are summarised below.

i. Feasibility and optimisation of process parameters for EM terminal-wire crimping have been carried out. EM crimping of terminal wires can be an alternative to an existing conventional crimping process with many advantages like no spring-back of the terminal, lower contact electrical resistance, improved hardness properties, a contactless process resulting in no cracks or surface damage, higher pull-out strength, minimum voids between the wire strands and improved thermal property.

ii. Comparison of the threaded and plain terminal in EM crimping process show that making thread can further enhance the electrical and mechanical properties.

iii. FEM study on different cross-section helical coils geometries like trapezoidal, rectangular and circular profiles were simulated keeping the coil length and cross-section area constant. It was observed that trapezoidal cross-section profile gave a higher deformation, where high current density was observed.

iv. Helical coils were manufactured as per the dimensions obtained through numerical simulations. Experimental results were in good agreement with the simulation results. In pull-out test, fracture over the terminal crimped by trapezoidal cross-section helical coil was observed, while no fracture of the terminal was observed for sample crimped using rectangular and circular cross-section helical coil.

v. Numerical work on different field-shapers was carried out. Different geometries like a single step, double step, and tapered were simulated keeping the total field

shaper length, effective working area and slit width constant. It was observed that single step field-shaper gave more terminal deformation due to less inductance because of less mass volume resulted in lower EM losses compared to double step and tapered field shaper.

vi. Single step, double step, and tapered field shapers were manufactured, and experiments were carried out. In pull-out test ductile fracture of the wire strands crimped using single step field shaper was observed, which shows the maximum strength that can be achieved in EM terminal-wire crimping process.

vii. Compared to helical coils, field-shapers can sustain a large amount of internal pressure without getting damaged. Regarding working efficiency, single step field-shaper was found to be most efficient followed by double step, and tapered field shapers.

## 7.2 Future work

This current work was carried out in this area for the first time. There are many aspects which are not considered in this thesis work, which were taken as assumptions like in case if we increase the deformation of terminal beyond required value, may lead to weld, instead of a metallic bonding.

Many new things can be done in this area beside changing the terminal and wire material. By making use of multiple slots field shaper, it can crimp many samples in a single discharge voltage from the capacitor bank. This will not only save energy and time but will also help in increasing the production.

Some work can also be carried out on using the tapered primary coil over the single step field-shaper to study the effect of field-shaper geometries over the crimp samples, which has not been tried in this thesis due to the manufacturing issue of the tapered primary coil.

# 8 References


Akbar, S, M S Awan, M A Aleem, M N Sarwar, and M Farooque. 2015. "Effect of Field Intensity on Electromagnetic Flat Sheet Forming." *Materials Today: Proceedings* 2 (10B): 5324-5328.

Alves, Eder P, Francisco P Neto, and Chen Y An. 2010. "Welding of AA1050 Aluminium with AISI 304 Stainless Steel by Rotary Friction Welding Process." *Journal of Aerospace Technology and Management* 2 (3): 301-306.

Bahmani, M A, K Niayesh, and A Karimi. 2009. "3D Simulation of Magnetic Field Distribution in Electromagnetic Forming Systems with Field-Shaper." *Journal of Materials Processing Technology* 209: 2295-2301.

Bergmann, Jean P, Franziska Petzoldt, Rene Schurer, and Stefan Schneider. 2013. "Solid-State Welding of Aluminum to Copper—Case Studies." *Welding in the World* 57 (4): 541-550.

Capelli, F, C Abomailek, J R Riba , and J Sanllehi. 2016. "Analysis of Electrical Contact Resistance Models for Substation Connectors." *IEEE International Conference on Power System Technology (POWERCON)* 1-6.

Chaharmiri, Rasoul, and Alireza F Arezoodar. 2016. "The Effect of Sequential Coupling on Radial Displacement Accuracy in Electromagnetic Inside-Bead Forming: Simulation and Experimental Analysis Using Maxwell and ABAQUS Software." *Journal of Mechanical Science and Technology* 30 (5): 2005-2010.

Chaudhary, Himanshu, and Sachin D Kore. 2016. "Electromagnetic Forming Analysis of AA5182 at Elevated Temperatures." *International Journal of Microstructure and Materials Properties* 11 (1/2): 105-118.

Chu, Yu Yu, and Rong Shean Lee. 2014. "Effect of Field Shaper Geometry on the Lorentz Force for Electromagnetic Sheet Impact Forming Process." *Journal of Engineering Manufacturing* 227 (2): 324-332.

Connectivity, TE. 2017. *Connectors & Sensors for Harsh Environments.* Accessed 12 20, 2017. http://www.te.com/usa-en/home.html.

Connectors, E. 2006. *Cable Pull-Out Test Procedure for Electrical Connectors.*

Correia, J P M, M A Siddiqui, S Ahzi, S Belouettar, and R Davies. 2008. "A Simple Model to Simulate Electromagnetic Sheet Free Bulging Process." *International Journal of Mechanical Sciences* 50: 1466-1475.

Cui, J, G Sun, J Xu, Z Xu, X Huang, and G Li. 2016. "A Study on the Critical Wall Thickness of the Inner Tube for Magnetic Pulse Welding of Tubular Al-Fe Parts." *Journal of Materials Processing Technology* 227: 138-146.

Cui, Xiaohui, Jianhua Mo, and Fei Han. 2012. "3D Multi-Physics Field Simulation of Electromagnetic Tube Forming." *The International Journal of Advanced Manufacturing Technology* 59: 521-529.

Doley, Jyoti K, and Sachin D Kore. 2017. "Comparison of Electromagnetic Forming of Friction Stir-Welded Blanks of Dissimilar Material AA 5052-AA 6061 With Conventional Forming Process." *The International Journal of Advanced Manufacturing Technology* 93 (9-12): 3789-3797.

Faes, K, O Zaitov, and E De Waele. 2012. "Electromagnetic Pulse Crimping of Axial Form Fit Joints." *5th International Conference on High Speed Forming* 229-242.

Gary, Ji L, and J Cheng. 2009. "Multiphysics Simulation on Electromagnetic Peening of Predrilled Holes." *International Journal of Mechanical Sciences* 51 (11-12): 825-836.

Gissila, Tibebu. 2013. "Connectors and Vibrations- Damages in Different Electrical Enviroments." Department of Mechanical Engineering, Blekinge Institute of Technology, Karlskrona, Sweden.

Golovashchenko, Sergey F. 2007. "Material Formability and Coil Design in Electromagnetic Forming." *Journal of Materials Engineering and Performance* 16 (3): 314-320.

Golowin, Scott, Manish Kamal, Jianhui Shang, Jake Portier, Ahmad Din, Glenn S Daehn, John R Bradley, Keith E Newman, and Steve Hatkevich. 2007. "Application of a Uniform Pressure Actuator for Electromagnetic Processing of Sheet Metal." *Journal of Materials Engineering and Performance* 16 (4): 455-460.

Haiping, Y U, and L I Chunfeng. 2009. "Effects of Current Frequency on Electromagnetic Tube Compression." *Journal of Materials Processing Technology* 209 (2): 1053-1059.

Haiping, Y U, and L I Chunfeng. 2007. "Effects of Coil Length on Tube Compression in Electromagnetic Forming." *Transactions of Nonferrous Metals Society of China* 17 (6): 1270-1275.

Haiping, Y U, L I Chunfeng, and D E N G Jianghua. 2009. "equential Coupling Simulation for Electromagnetic–Mechanical Tube Compression by Finite Element Analysis." *Journal of Materials Processing Technology* 209 (2): 707-713.

Haiping, Yu, Li Chunfeng, and DENG Jianghua. 2009. "Sequential Coupling Simulation for Electromagnetic–Mechanical Tube Compression by Finite Element Analysis." *Journal of Materials Processing Technolgy* 209: 707-713.

Hashimoto, T, and S Kaneko. 2005. Terminal Crimping Structure for Aluminium Wire and Producing Method. Patent EP 1 503 454 A1.

Huang, Lantao, Xiaotao Han, Qi Chen, Yuanhang Niu, Zhipeng Lai, Quanliang Cao, Zhongyu Zhou, and Liang Li. 2014. "Effect of Electromagnetic Ring Expansion on the Mechanical Property of A5083 Aluminum Alloy." *IEEE Transactions on Applied Superconductivity* 24 (3): 7100104.

Hustad, T A, and A L Lindland. 2014. "Aluminium Structures Exposed to Blast Loading." Master's Thesis, Institutt for Konstruksjonsteknikk, Norway.

Ibrahim, A I, S Henschel, A C Lima, and H W Dommel. 2002. "Applications of a New EMTP Line Model for Short Overhead Lines and Cables." *International Journal of Electrical Power & Energy Systems* 24 (8): 639-645.

Jeanson, A C, François Bay, Nicolas Jacques, Gilles Avrillaud, Michel Arrigoni, and Gilles Mazars. 2016. "A Coupled Experimental/Numerical Approach for the Characterization of Material Behaviour at High Strain-Rate Using Electromagnetic Tube Expansion Testing." *International Journal of Impact Engineering* 98: 75-87.

Jiang, Yi-Hsuan, Wu-Chung Su, and Ming-Yen Wey. 2014. "Numerical Electromagnetic Analysis of a Junction Tower With Cable Arrangements." *International Journal of Electrical Power & Energy Systems* 62: 103-109.

Katou, Kazuya. 2017. Terminal Trimping Device, Terminal Crimping Tool, and Method for Producing Terminal-Crimped Electric Wire. Patent WO 2017141866 A1.

Kim, H, and J Shang. 2012. "Investigation of the Effects of the Coil Design on Electromagnetic Forming of a Thin-Walled Aluminum Tubular Material." *12th International Ls-Dyna Users Conference* 1-14.

Klauke, Gustav. 2017. *Klauke A Textron Company*. Accessed 12 20, 2017. http://www.klauke.com/electrical/technical-reports/crimping-type-hexagonal-crimps/.

Lee, Sung H, and Dong N Lee. 1994. "A Finite Element Analysis of Eectromagnetic Forming of Tube Expansion." *Journal of Engineering Materials and Technology* 116: 250-254.

L'Eplattenier, P L, G Cook, C Ashcraft, M Burger, J Imbert, and M Worswick. 2009. "Introduction of an Electromagnetism Module in LS-Dyna for Couple Mechanical-Thermal-Electromagnetic Simulations." *Steel Research International* 80 (5).

Mamalis, A G, D E Manolakos, A G Kladas, and A K Koumoutsos. 2004. "Electromagnetic Forming and Powder Processing: Trends and Developments." *Applied Mechanics Reviews* 57 (4): 299-324.

Nassiri, Ali, Chris Campbell, Greg Chini, and Brad Kinsey. 2015. "Analytical Model and Experimental Validation of Single Turn, Axi-symmetric Coil for Electromagnetic Forming and Welding." *Procedia Manufacturing* 1: 814-827.

Padmanabhan, M. 1997. "Wrinkling and Springback in Electromagnetic Sheet Metal Forming and Electromagnetic Ring Expansion." Master Thesis, The Ohio State University, Ohio.

Patel, Chandrahas, Pravin Ghatule, and Sachin D Kore. 2017. "Finite Element Analysis of Effect of Process Parameters on Electromagnetic Free Expansion of Aluminium Tube." *International Journal of Materials and Product Technology* 54 (1-3): 165-178.

Prin, G R, T Courtin, and L Boyer. 2002. "A New Method to Investigate Electrical Conduction in Crimp Joints Influence of the Compaction Ratio and Electrical Model." *Proceedings Forty-Eighth IEEE Holm Conf Electr Contacts* 10 (2): 246-251.

Psyk, V, D Risch, B L Kinsey, A E Tekkaya, and M Kleiner. 2011. "Electromagnetic Forming—A Review." *Journal of Materials Processing Technology* 211 (5): 787-829.

Quality Crimping, n.d. Handbook, Molex, USA, 1996

Rhodes, Edwin. 1946. "Electrical Contacts." *Nature Publishing Group* 158 (4019): 647-647.

Santinho, R, and B Martins. 2014. "Formability of AA1050 Sheet in High Velocity Forming." Master in Science, Department of Mechanical, Tecino Lisboa, Portugal.

Shim, J, B Kang, R LMA, and D Group. 2016. "Development of Magnetic Pulse Crimping Process for High-Durability Connection Terminal." *International Journal of Engineering Research and Application* 6 (12): 11-15.

Siddiqui, Muhammad A. 2009. "Numerical Modelling and Simulation of Electromagnetic Forming Process." Department of Mechanical Engineering, University of Strasbourg, Strasbourg.

Sobolev, A V, and M V Radchenko. 2016. "Use of Johnson–Cook Plasticity Model for Numerical Simulations of the SNF Shipping Cask DropTests." *Nuclear Energy and Technology* 2 (4): 272-276.

Song, F M, X Zhang, Z R Wang, and L Z Yu. 2004. "A Study of Tube Electromagnetic Forming." *Journal of Materials Processing Technology* 151 (1-3): 372-375.

Soulinaris, G S, C D Halevidis, A D Polykrati, and P D Bourkas. 2014. "Evaluation of the Thermal Stresses and Dielectric Phenomena in the Investigation of the Causes of Wildfires Involving Distribution Power Lines." *Electric Power Systems Research* 117: 76-83.

Suzuki, Hideo, Makoto Murata, and Hideaki Negishi. 1987. "The Effect of a Field Shaper in Electromagnetic Tube Bulging." *Journal of Mechanical Working Technology* 15: 229-240.

Tohidi, Yaser, Mohammad R Hesamzadeh, Ross Baldick, and Darryl R Biggar. 2017. "Transmission Network Switching for Reducing Market Power Cost in Generation Sector: A Nash-Equilibrium Approach." *Electric Power Systems Research* 146: 71-79.

Use, T. 2003. "Standard Test Method for Evaluation of Crimped Electrical Connections to 16-Gauge and Smaller Diameter Stranded and Solid Conductors." Accessed 12 2017, 20. https://doi.org/10.1520/B0913-05R15.2.

Vanhulsel, Peter, and Matthias V Wonterghem. 2011. "Magnetic Pulse Crimping of Mechanical Joints." Master Thesis, Department of Mechanical Construction and Production, Ghent Univerisity, Belgium. Accessed 12 20, 2017. https://lib.ugent.be/fulltxt/RUG01/001/805/512/RUG01-001805512_2012_0001_AC.pdf.

Vivek, A, K H Kim, and G S Daehn. 2011. "Simulation and Instrumentation of Electromagnetic Compression of Steel Tubes." *Journal of Materials Processing Technology* 211 (5): 840-850.

Vivek, A, S R Hansen, B C Liu, and Glenn S Daehn. 2013. "Vaporizing Foil Actuator: A Tool for Collision Welding." *Journal of Materials Processing Technology* 213 (12): 2304-2311.

W, Mc Caughey. 1973. Wire Terminal Crimping Tool. Patent US 3710610 A.

Weddeling, C. 2014. *Electromagnetic Form-Fit Joining.* Germany: PhD Thesis, Department of Mechanical Engineering, TU Dortmund University.

Weddeling, Christian, Koray O Demir, Peter Haupt, and Erman A Tekkaya. 2015. "Analytical Methodology for the Process Design of Electromagnetic Crimping." *Journal of Materials Processing Technology* 222: 163-180.

Weddeling, Christian, Volker Walter, Peter Haupt, Erman A Tekkaya, Volker Schulze, and Kay A Weidenmann. 2015. "Joining Zone Design for Electromagnetically Crimped Connections." *Journal of Materials Processing Technology* 225: 240-261.

Williams, David M, Michael E Range, Vincent C Pascucci, and J T Savrock. 2015. "Forensic Analysis of Thermally Stressed Crimp Connections." Electrical Contacts (Holm), IEEE 61st Holm Conference on. 331-337.

Yu, Haiping, Chunfeng Li, Zhiheng Zhao, and Zhong Li. 2005. "Effect of Field Shaper on Magnetic Pressure in Electromagnetic Forming." *Journal of Materials Processing Technology* 168: 245-249.

Zhang, H, M Murata, and H Suzuki. 1995. "Effects of Various Working Conditions on Tube Bulging by Electromagnetic Forming." *Journal of Materials Processing Technology* 48 (1-4): 113-121.

Zhmurkin, D V, N E Corman, C D Copper, and R D Hilty. 2008. "3-Dimensional Numerical Simulation of Open-Barrel Crimping Process." *Electrical Contacts, Proceedings of the 54th IEEE Holm Conference on Electrical Contacts.* Orlando, FL, USA. 178-184.

# 9 Publications Out of this Work

**International Journal Papers**

1. **Ashish Kumar Rajak** and Sachin D. Kore, "Experimental Investigation of Aluminium –Copper Terminal-wire crimping with Electromagnetic Process: Its Advantages over Conventional Process" Journal of Manufacturing Process, DOI: 10.1016/j.jmapro.2017.01.009
2. **Ashish Kumar Rajak** and Sachin D. Kore, "Numerical Simulation and Experimental Study on Electromagnetic Crimping of Aluminium Terminal to Copper Wire Strands" Electric Power Systems Research, DOI: 10.1016/j.epsr.2017.08.014
3. **Ashish Kumar Rajak**, Hirak Basumatary, Ramesh Kumar and Sachin D. Kore, "Numerical and Experimental Study on Effect of Different Types of Field-Shaper on Electromagnetic Terminal-wire crimping process" International Journal of Precision Engineering, DOI: 10.1007/s12541-018-0055-6
4. **Ashish Kumar Rajak** and Sachin D. Kore, "Application of electromagnetic forming in terminal-wire crimping using different types of field-shapers" Journal of Mechanical Science and Technology **(Accepted)**
5. **Ashish Kumar Rajak** and Sachin D. Kore, "Comparison of different types of coil Electromagnetic Terminal-wire crimping Process: Numerical and Experimental Analysis" Journal of Manufacturing Process **(Revision submitted Feb 2018)**

**International conferences**

1. **Ashish Kumar Rajak**, Ikshit Gupta and Sachin D. Kore, "Finite Element Analysis of Electromagnetic Terminal-wire crimping Using Different Types of Actuator at Constant Length", International Conference on Evolution in Manufacturing: Technologies and Business Strategies for Global Competitiveness, 2016, BITS Ranchi, Jharkhand, Nov 12-13. Vol. ISBN: 978-93-86256-11-9, pp 345-350
2. **Ashish Kumar Rajak** and Sachin D. Kore, "FEM Study of Electromagnetic Terminal-wire crimping Process", International Conference on Advances in Materials and Manufacturing, 2016, Osmania University, Telangana, Dec 8-10.

Vol. ISBN: 978-93-86256-19-5, pp 63-68 (**BEST RESEARCH PAPER AWARD**)